# Thermal Sprayed Aluminium for Subsea Heat Exchanger Surfaces

Effect of Temperature on Protection Current

Requirement and Calcareous Development

## Håvard Wilson

THE NORWEGIAN UNIVERSITY
OF SCIENCE AND TECHNOLOGY
DEPARTMENT OF ENGINEERING DESIGN
AND MATERIALS


# MASTER THESIS SPRING 2014
# FOR
# STUD.TECHN. HÅVARD WILSON


**THERMAL SPRAYED ALUMINIUM FOR SUBSEA HEAT EXCHANGER SURFACES –
EFFECT OF TEMPERATURE ON PROTECTION CURRENT REQUIREMENT AND
CALCAREOUS DEVELOPMENT**
**Termisk sprøytet aluminium for subsea varmeveksler overflater – Effekt av
temperatur på strømtetthet ved katodisk beskyttelse og utfelling av kalkbelegg**

## BACKGROUND
Thermal Sprayed Aluminium (TSA) is a coating that is used for components and equipment
that is exposed for long life subsea. A traditional corrosion protection system consists of
organic coating combined with sacrificial anodes to secure protection for the lifetime of the
system. However for some applications TSA combined with sacrificial anodes can be an
attractive alternative.

In the future complex process equipment will be placed subsea. This includes subsea
coolers where seawater is used as the cooling medium. One challenge is the development
of calcareous deposits due to the cathodic protection system on surfaces exposed directly to
seawater. The development of calcareous deposit depends on several parameters
including temperature. At higher temperature it is assumed that thick calcareous deposit
can develop chemically on a surface exposed to seawater. Development of a thick coating
on the heat transfer surface will reduce the efficiency of the cooling surface and the overall
efficiency of a subsea cooler. One hypothesis is that "Calcareous deposition on a TSA
coated surface is very slow compared to deposition on a steel surface".

During the last autumn the candidate has executed preliminary tests with TSA coated
samples exposed to seawater at temperatures in the range 10 to 40$^0$C. Some interesting
results have been observed through the testing, but more testing is required to get a full
understanding of the problem.

## OBJECTIVES
The <u>main objective</u> of the Master project will be to: *Quantify the effect of temperature on
development of calcareous deposit on TSA coated steel in seawater.*

## SCOPE-OF-WORK
During the project work important information about equipment design and exposure of test
specimens have been gained. This information will be the basis for a revision of the test
set-up and the test program for the Master project. The following activities will be included
(*not limited to*):

   o   Review of test set up and implementation of "best practice" from the project work

- o Review the data to be logged and implement necessary software and hardware for this
- o Execute tests with TSA coated samples – freely exposed and coupled to sacrificial anode – with internal temperature up to $90^0C$
- o Evaluation of surface condition after an exposure period (2 months and the end) including estimation of thickness of calcareous deposit
- o Evaluate the possibility of estimating the change in thermal conductivity as a result of the change in surface condition – if possible perform measurement/calculations

Three weeks after start of the thesis work, an A3 sheet illustrating the work is to be handed in. A template for this presentation is available on the IPM's web site under the menu "Masteroppgave" (http://www.ntnu.no/ipm/masteroppgave). This sheet should be updated one week before the Master's thesis is submitted.

Performing a risk assessment of the planned work is obligatory. Known main activities must be risk assessed before they start, and the form must be handed in within 3 weeks of receiving the problem text. The form must be signed by your supervisor. All projects are to be assessed, even theoretical and virtual. Risk assessment is a running activity, and must be carried out before starting any activity that might lead to injury to humans or damage to materials/equipment or the external environment. Copies of signed risk assessments should also be included as an appendix of the finished project report.

The thesis should include the signed problem text, and be written as a research report with summary both in English and Norwegian, conclusion, literature references, table of contents, etc. During preparation of the text, the candidate should make efforts to create a well arranged and well written report. To ease the evaluation of the thesis, it is important to cross-reference text, tables and figures. For evaluation of the work a thorough discussion of results is appreciated.

The thesis shall be submitted electronically via DAIM, NTNU's system for Digital Archiving and Submission of Master's thesis.

This project will be run in close cooperation with Aker Solutions (AKSO) and Force Technology.

Contact AKSO:                    Per Giltvedt
Contact Force Technology:    Jan Scheie

Co-supervisor from IPM:      Afrooz Barnoush

Torgeir Welo
Head of Division

Roy Johnsen
Professor/Supervisor

NTNU
Norges teknisk-
naturvitenskapelige universitet
Institutt for produktutvikling
og materialer

# Abstract

More and more equipment in the Oil and Gas Industry are being placed Subsea. This includes subsea coolers with high internal temperatures. With high temperatures come with challenges within material selection and corrosion. Traditional material choices like carbon steel and organic coatings with cathodic protection (CP) is not an option for subsea coolers. This is due to insulating properties to the organic coatings and the dense calcareous deposits which form on the surface of the steel.

Thermally sprayed aluminium (TSA) is known to have good corrosion resistance in seawater, and to have a small current demand under CP, which makes the probability of precipitating calcareous layer on the surface low. The surface topography for thermally sprayed aluminium is rough, which increases the total surface area for heat transfer. The rough surface also produces turbulent flow close to the surface, which may increase the heat transfer. The combination of these properties makes thermally sprayed aluminium a attractive candidate as a coating for subsea coolers.

The drawback of thermally sprayed aluminium is that there is little empirical data on its behaviour at high temperatures, especially when in contact with CP. Therefore, the purpose of this Master Thesis is to provided more documentation on the subject of the properties of thermally sprayed aluminium at high surface temperatures in seawater, with and without CP.

For providing more documentation a literature study and experiments on TSA will be carried out. The principle behind the experimental part of this project is very simple. Pipes of UNS S31245 stainless steel with a TSA coating were internally heated to different temperatures and immersed in slow flowing seawater, to simulate the conditions a subsea cooler would be subjected to. The purpose of the experiments was to find the corrosion potential, the current density requirement for TSA connected to an CP system and the corrosion rate of the freely corroding TSA. After exposure the samples was analysed to quantify the amount, if any, calcareous deposits form on TSA, and to see what effect the exposure had on the thermal conductivity of the samples.

This thesis discovered that the corrosion rate of TSA increases with temperature. Initially the corrosion rate of TSA is quite high, but it quickly decreases for all temperatures. The corrosion rate for the 90 °C internal temperature was initially 50 $\mu m/year$ but decreased to 8 $\mu m/year$ after 65 days.

The current density requirement for TSA is very low compared to steel, with a current density requirement of 3-5 $mA/m^2$ obtained in this thesis. Temperature increases the current demand slightly. Based on both the experiments and the literature it is safe to say that using the DNV recommended practice for current density requirement for TSA is acceptable, even though the recommended practice may be conservative.

Calcareous deposits form on TSA at all temperatures. For both the samples connected to an anode and the freely corroding samples, however, not as a continuous protective layer that precipitates on steel, but mostly as thin layers in small areas around intermetallic particles. The temperature affects the amount and type of calcareous deposits which form

on TSA. At high temperatures the calcareous deposits mainly consist of $Mg(OH)_2$ and at low temperature the calcareous deposits consist of both $CaCO_3$ and $Mg(OH)_2$.

Thermal conductivity measurements shows that the TSA coating and calcareous deposits are negligible when it comes to the overall thermal conductivity of the pipe. The combination of negligible effect on the thermal conductivity, low corrosion rate, and small current density requirement makes TSA a solid choice for corrosion protection of subsea heat exchangers.

# Sammendrag

Mer og mer utstyr i olje- og gassindustrien blir plassert under vann. Dette inkluderer undervannskjølere, med høye interne temperaturer. De høye temperaturene i kombinasjon med sjøvann skaper et svært korrosivt miljø. Karbonstål med organiske belegg og katodisk beskyttelse, er et klassisk valg for utstyr plassert på havbunnen. Dette er ikke et alternativ for undervannskjølere. Grunnen til det er den isolerende effekten organiske belegg, og det ette kalkholdbelegget som dannes på overflaten av karbonstål under katodisk beskyttelse. Dette vil gjøre at den totale termisk ledningsevnen minker.

Termisk sprøytet aluminium er et belegg kjent for å ha god korrosjonsmotstand i sjøvann, og for å et lavt strømbehov når katodisk beskyttet, noe som minker sjangsen for utfelling av kalkbelegg. Overflatetopografien for termisk sprøytet aluminium er ru, som øker overflatearealet og gir turbulent strømningsmønster for sjøvann i nærheten av overflaten, som øker varmeoverføringen. Kombinasjonen av disse egenskapene gjør termisk sprøytet aluminium attraktivt som belegg for undervannskjølere .

Ulempen med termisk sprøytet aluminium er mangelen på empirisk data ved høye temperaturer, særlig i kombinasjon med katodisk beskyttelse. Hensikten med denne masteroppgaven er å finne tilgjenglig litteratur og å framskaffe mer empirisk data for termisk sprøytet aluminium ved høye overflatetemperaturer i sjøvann, med og uten katodisk beskyttelse.

Prinsippet bak den eksperimentelle delen av prosjektet er enkel: Rør av UNS S31245 rustfritt stål belagt med termisk sprøytet aluminium ble plassert i sjøvann og varmet opp internt til forskjellige temperaturer for å simulere forholdene en undervannskjøler blir utsatt for. Hensikten med forsøkene er å finne strømtetthet for termisk sprøytet aluminium som er koblet til en anode, og korrosjonspotensial og korrosjonshastigheten til fritt korroderende termisk sprøytet aluminium. Deretter skal mengde og type kalkbelegg som eventuelt dannes på termisk sprøytet aluminium overflaten identifisere og den termiske ledningsevner til belegget skal måles.

Termisk sprøytet aluminium ble eksponert mot sjøvann mellom 60 og 170 dager, med innvendig temperatur fra 10 til 90 °C. Dette ga overflatetemperatur på mellom 10 og 60 °C. Korrosjonshastighet til termisk sprøytet aluminium øker med temperaturen. Opprinnelig var korrosjonshastigheten til termisk sprøytet aluminium høy, men med tid avtar den raskt for alle temperaturer. Korrosjonshastigheten for 90 °C innvendig temperatur var opprinnelig 50 $\mu m/aar$, men ble redusert til 8 $\mu m/aar$ etter 65 dager.

Strømbehovet til termisk sprøytet aluminium koblet mot anoder er svært lavt sammenlignet med stål, og ble funnet til å være 3-5 $mA/m^2$ i eksperimentene gjort i denne oppgaven. Strømbehovet øker svakt med temperaturen. Basert på eksperimentene og litteraturen er det trygt å bruke DNV anbefalt praksis for strømbehovet for termisk sprøytet aluminium, selv om anbefalingen kan være konservativ.

Kalkbelegg dannes på termisk sprøytet aluminium ved alle temperaturer, på både prøvene som er koblet til anoder og fritt korroderende prøver. Kalkbelegget som dannes er ikke et kontinuerlig belegg som det som dannes på stål, men det dannes for det meste som tynne

sjikt i små områder rundt intermetalliske partikler. Temperatur påvirker mengden og typen av kalkholdige avleiringer som danner på termisk sprøytet aluminium. Ved høy temperatur består kalkbelegget hovedsaklig av $Mg(OH)_2$ og ved lav temperatur består kalkbelegget av både $CaCO_3$ og $Mg(OH)_2$. Ved høye temperaturer dekker kalkbelegget en større del av overflaten enn ved lavere temperaturer.

Målinger av termisk ledningsevne viser at termisk sprøytet aluminium og kalkbelegget som dannes er ubetydelig når det gjelder den totale termiske ledningsevne av røret. Kombinasjonen av lite kalkutfellinger, som ikke påvirker termiske ledningsevnen i stor grad, liten korrosjonshastighet og lite strømbehov gjør termisk sprøytet aluminium til et solid valg for korrosjonsbeskyttelse av undervannskjølere.

# Preface

This thesis has been written in the course TPK4900 - Production and Quality Engineering, Master Thesis in the spring of 2014. This report is the final report of two, on a project which was begun in the course TPK 4510 Production and Quality Engineering, Specialization Project in the autumn of 2013.

The project was completed at the Norwegian University of Science and Technology, department of Production and Quality Engineering, Subsea Technology Program. Both reports, however, were written at the Department of Engineering Design and Materials.
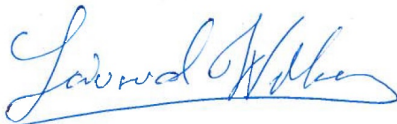
I would like to thank Mr. Nils Inge Nilsen and Mr. Børge Holen for all the advice and help with building my experimental setup and Professor Ole Øystein Knudsen for advice and help on my experimental design.

I would also like to thank Mr. Cristian Torres and Dr. Ignat Tolstorebrov for helping with the ordering of new equipment and for assistance in the laboratory.

From the industry I would like to thank Mr. Jan Scheie, Dr. Marianne Videm and Dr. John Berget from FORCE Technology for advice and help with writing my report.

I would like to specially thank my supervisor Professor Roy Johnsen for all the help and guidance, and for always being available when I needed help.

Trondheim, June 10, 2014

Håvard Wilson

# Table of Contents

# List of Tables

# List of Figures

# Abbreviations

| | | |
|---|---|---|
| Ag/AgCl | = | Silver, Silver chloride electrode |
| CP | = | Cathodic Protection |
| EDS | = | Energy-dispersive Spectroscopy |
| LPR | = | Liner Polarization Resistance |
| IPM | = | Department of Engineering Design and Materials |
| Mol% | = | Mole percent |
| OCP | = | Open Circuit Potential |
| SCE | = | Saturated Calomel electrode |
| SEM | = | Scanning Electron Microscopy |
| TLP | = | Tension Leg Platform |
| TSA | = | Thermally Sprayed Aluminium |
| NTNU | = | Norwegian University of Science and Technology |
| WT% | = | Weight percent |

# Chapter 1

# Introduction

More and more equipment in the Oil and Gas Industry are being placed Subsea. This includessubsea coolers with high internal temperatures. With high temperatures come with challenges within material selection and corrosion. Traditional material choices like carbon steel and organic coatings in combination with cathodic protection (CP) is not an option for subsea coolers. This is due to insulating properties to the organic coatings and the dense calcareous deposits which form on the surface of the steel. It is, however, very likely that subsea coolers will be in contact with a CP system, since CP is a prerequisite for all subsea installations [1]. Therefore, the material selection for a subsea cooler must take CP into account.

Thermally sprayed aluminium (TSA) is known to have good corrosion resistance in seawater, and to have a small current demand under CP, which makes the probability of precipitating calcareous layer on the surface low. The surface topography for thermally sprayed aluminium is rough, which increases the total surface area for heat transfer. The rough surface also produces turbulent flow close to the surface, which may increase the heat transfer. The combination of these properties makes thermally sprayed aluminium a attractive candidate as a coating for subsea coolers.

The drawback of TSA is lack of empirical data on its behaviour at high temperatures, especially when in contact with CP. The purpose of this Master Thesis is to provide more documentation on the subject of the properties of TSA at high surface temperatures in seawater, with and without CP.

For providing more documentation a literature study and experiments on TSA will be carried out. These activities were divided into two different courses, TPK 4510 Production and Quality Engineering, Specialization Project in the autumn of 2013 and TPK4900 - Production and Quality Engineering, Master Thesis in the spring of 2014. In the Specialization Project preliminary experiments at low temperatures were conducted, and was just as much a "proof of concept" than actually providing more documentation. Therefore, a part of the Master Thesis will be to evaluate the experimental design, and to provide suggestions for improving the design for future experiments. In this thesis the experimental design from the Specialization Project was revised and improved, and TSA was exposed

to temperatures up to 90 °C.

The literature search part of the project is presented in two chapters, Chapter 2 and Chapter 3, where the basic theory is presented in Chapter 2 and the State of the Art of TSA in seawater is presented in Chapter 3.

The principle behind the experimental part of this project is very simple: pipes of UNS S31245 stainless steel with a TSA coating was internally heated to different temperatures and immersed in slow flowing seawater, to simulate the conditions a subsea cooler would be subjected to. The purpose of the experiments was to find the corrosion potential, the current density requirement for TSA connected to an CP system and the corrosion rate of the freely corroding TSA, and to quantify the amount, if any, calcareous deposits form on TSA.

As thermally sprayed coatings are porous, corrosion products will gather in these pores, making weight loss measurement practically useless. Therefore, this project will rely heavily on electrochemical test methods, like polarization curves and Linear Polarization Resistance (LPR).

After exposure to seawater the TSA surface will be investigated in a SEM (Scanning Electron Microscope), using EDS (Energy-dispersive X-ray spectroscopy) to investigate if any calcareous deposits form on TSA.

# Chapter 2

# Basic Theory

In this chapter the basic theory required for understanding the behaviour of TSA in seawater is presented. The chapter is divided into four sub chapters al with different themes. Chapter 2.1 provides information about the application of thermally sprayed coatings and the resulting mechanical properties. In Chapter 2.2 general information about the corrosion process and the corrosion properties of aluminium and TSA is given. Chapter 2.3 shows the known effect CP has TSA in seawater, while the precipitation of calcareous deposits is presented in Chapter 2.4.

## 2.1 Thermally Sprayed Coatings

In this chapter the application and mechanical properties of thermally sprayed coating is presented. The purpose of this chapter is explain that certain coating properties like adhesion and porosity may affect phenomena like blistering or the corrosion properties of the coatings. Therefore, it is necessary to investigate these properties to fully understand what is happening to TSA immersed in seawater.

### 2.1.1 Application Methods

Thermally sprayed coatings have existed since the early 1900s [2]. The process of applying thermally sprayed coatings involves spraying a material, often in the form of powder or wire, onto a surface. The powder or wire is melted or semi melted by a heat source and sprayed onto the surface [3]. This process produces a coating with different properties, both chemical and mechanical, than it had in wire or powder form [4]. Thermally sprayed coatings have a variety of applications, but are most commonly used to enhance corrosion or wear resistance [5].

There have been developed several techniques for applying thermally sprayed coatings, like electric arc spray, flame spray or plasma spray. The different techniques produces coatings with different properties, and different techniques are used for applying different materials [3]. For applying materials with low melting temperature, like Zinc

and Aluminium, flame spraying or electric arc spraying are the most economic viable and most common application methods [2, 4, 6, 7]. Since this report is about TSA, only flame spraying and electric arc spraying will be discussed.

Flame spraying has it is name from the flame that is used as a heat source for the melting process. The flame is produced by mixing oxygen and a fuel gas in a spray gun, where it ignites, and reaches temperatures between 2700 °C and 3000 °C [8]. Normally the fuel gas is either propane or acetylene. The powder or wire is heated by the flame and transported to the surface by the force created by the ignition and by compressed gas [6, 7].

Electric arc spraying, named after the electric arc that is created during this spraying technique, is in a way similar to welding, because the heat source is an electric arc, like the one created in certain welding processes [7]. The electric arc reaches higher temperatures than flame spraying, and can be between 4000 °C and 6000 °C [8]. The arc is ignited by moving two wires of the coating material towards each other, and applying a potential between the wires. The potential difference creates an electric arc between the wires when they converge, which melts the wires, and compressed gas transports the droplets to the substrate surface [6, 7]. Figure 2.1 shows the electric arc spraying process and the resulting coating when aluminium wires are used. Electric arc spraying is a relatively simple process, with low operational costs and high efficiency [9].
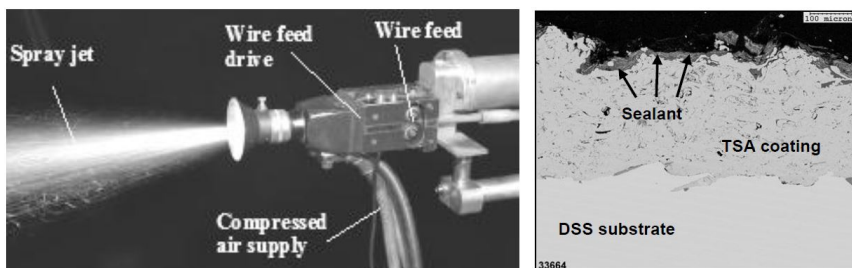


**Figure 2.1:** Electric arc spraying of aluminium and the resulting coating [10].

## 2.1.2 Coating Properties

The quality of a thermally sprayed coating is obviously dependant on the application method and the skill of the operator, however, a less obvious but just as important parameter is the quality of the substrates surface preparation. There are two parameters that determines if the quality of the surface preparation is satisfactory or not; cleanliness and surface roughness [7]. These two parameters determine the adhesion the thermally sprayed coating achieves with the substrate surface. The parameters are so important for the adhesion that there are standards for the required cleanliness and surface roughness for thermally sprayed coatings. NORSOK standard M-501 [11] specifies ISO 8503-1 [12] for surface roughness and ISO 8501-1[13] for surface cleanliness.

As with all coatings, the coating adhesion for thermally sprayed coatings to the substrate surface is important for producing a coating with good mechanical properties. There are three mechanisms which create adhesion for thermally sprayed coatings; mechanical

anchoring, metallurgical bonding and physical forces. Mechanical anchoring is a process that occurs when spray droplets hit the substrate surface. The droplets flatten and start to cool, and shrinks which creates interlocking between the coating particles and the rough substrate surface [3].

Under certain spraying processes micro-welding (localized melting of the substrate) or atomic diffusion occurs which can create intermetallic particles or solid solutions in the substrate - coating interface. This is called metallurgical bonding, and is the mechanism which creates the highest adhesion between the coating and the substrate. The third bonding mechanism, physical forces, is considered to be the least important, and consists of the weak Van-der-Waals forces [3].

Even though adhesion is important, there are other parameters than adhesion that contribute to making a high quality coating. The amount of oxidation and porosity are two other important factors [3, 14]. Porosity, for instance, may reduce the corrosion resistance of the coating [14], and it reduces both the electric and thermal conductivity of the coating. Figure 2.2 shows how a thermally sprayed coating is built up [3], and shows that thermally sprayed coatings are heterogeneous coatings that contain pores, oxides and voids [2, 3, 7].

Flame spray and electric arc spray produces relatively heterogeneous coatings, compared with other application methods, with high porosity and oxide content. Between the two application methods flame spray produces the most heterogeneous coating with higher oxide content than electric arc spraying [15]. Oxides are hard particles that increase the hardness of the coating. Too high oxide content may lead to poor cohesion in the coating, and can produce a coating with poor mechanical properties [9].
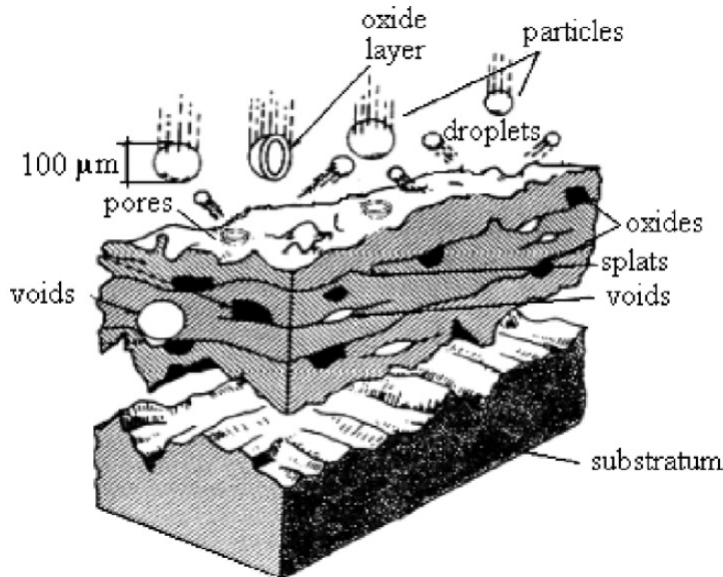


**Figure 2.2:** Schematic presentation of a thermally sprayed coating [3].

Both methods create relatively porous coatings [15]. The porosity of thermally sprayed coatings depends on the temperature, type of transport gas, particle speed, gun type and,

like adhesion, the substrate pretreatment [9, 14, 8]. Generally coatings of Zinc and Aluminium are in the range of 5-10 % [14], more specific for aluminium it is in the range of 4 to 7 % for flame spray and 1 to 6 % for electric arc spray [8]. Pores and oxides can form interconnected pathways within the coating, allowing environment to reach the substrate, so limiting the porosity is important for obtaining quality coatings [5].

The surface topography of a thermally sprayed coating will be different from solid alloys. TSA have a rougher surface and a thicker oxide layer than typical rolled aluminium with a smooth surface and thin oxide layer [16].

From Figure 2.1 it is easy to see the difference between the substrate, in this case 22Cr Duplex Stainless Steel, which is solid, and the coating with pores and oxides. Figure 2.1 also shows how the sealants fill the pores in the coating and penetrates into the coating.

### 2.1.3 Thermally Sprayed Aluminium

TSA is a thermally sprayed coating where the coating material is based on aluminium and aluminium alloys. The most commonly used material is either technically pure aluminium (99.5 % Al) or an alloy based on the 5000 aluminium series (AlMg5). AlgMg5 is an aluminium magnesium alloy with 5wt% magnesium. These alloys are commonly used due to their corrosion resistance in seawater. Both 99.5 % Al and AlMg5 are said to be seawater resistant [4, 7, 17].

TSA is commonly used in the Offshore Industry for corrosion protection, and can be applied in all offshore environments, including the splash zone, submerged zone and topside [2, 8, 18, 19, 20]. The coating is widely used due to it is many advantages over traditional organic coatings, like no curing time, long maintenance free service, more robust and higher adhesion [18, 19, 21].

Aluminium coatings protects the substrate from corrosion in two ways. The primary function is to act as a barrier to the corrosive environment, by preventing contact between seawater and the substrate, and secondary to act as a sacrificial anode in case of any coating damage [2, 8, 14]. TSA acts as an anode because aluminium coatings are lower on the galvanic series than most materials commonly used in the offshore industry. It will therefore prevent corrosion on the substrate, however, this leads to increased deterioration of the coating [2, 14, 22]. This will be further discussed in Chapter 2.3.

The mechanical anchoring mechanism explained in Chapter 2.1.2 is the most important process for adhesion for TSA. The surface cleanliness is therefore very important for TSA because the coating should interlock directly with the substrate. If the surface is covered with contaminations like grease and rust the TSA may interlock with the contaminates instead of the substrate directly. This produces a coating will poor adhesion [3, 4]. Both flame spray and electric arc spray can yield high quality coatings if the surface preparation is done sufficiently [4]. Electric arc spray tends to produce coatings with higher adhesion than flame spray, but except for that the application method does not seem to have any significant effect on the other properties, like the electrochemical properties, of TSA coatings [4, 7, 18].

To ensure the quality of the surface pretreatment, standards for the pretreatment and application of TSA have been made. Aluminium coatings can be identified as coating system No.2 in NORSOK M-501 - Surface preparation and protective coatings, and application requirements can be found there. When applying TSA for the use in the Norwegian oil

and gas industry the cleanliness of the substrate surface should be $Sa2\frac{1}{2}$ [11]. This means that the surface should be thoroughly blast cleaned, and free from visible oil, grease, dirt, rust, paint and any other foreign matter when viewed with the naked eye [13]. The surface roughness of the substrate should be of Grade Medium G ($50\mu m$ to $85\mu m$, $R_{y5}$) [11]. The "G" in "Grade Medium G" stands for "Grit", and means that grit abrasives and not shot abrasive shall be used for the blast-cleaning. "Grade Medium" indicates what roughness the surface should have, and in this case it is described by $50\mu m$ to $85\mu m$, $R_{y5}$, which means that there should be an average between 50 and $85\mu m$ between the highest and lowest points in the surface topography [12]. Table G.1 in Appendix G shows grades of cleanliness and what the requirements are in accordance with ISO 8501.

Good adhesion is important for preventing blistering of TSA in immersed conditions. Blistering is the separation of the coating from the substrate, and is a common and well-studied phenomenon in organic coatings. It does, however, also occur in TSA coatings as well [23]. Blistering tends to become more extensive with increasing temperatures, and so the quality of the coating must be high, if used at high temperatures [24]. The life time of a TSA coating is normally determined by the dissolution rate of the coating. However, if blistering occurs in TSA the lifetime of the coating is strongly reduced. The porosity in the coating might effect the blistering properties of the coating, where high porosity leads to a higher probability of blistering. This is because corrosion products accumulate in pores and at the substrate-coating interface, which might occur if the coating is permeable. This creates internal stresses in the coating and may lead to blistering [23].

Since porosity affects the quality of the coating, steps are often made to reduce the negative influence the porosity has on the corrosion resistance of TSA. A sealer is often applied to compensate for the porosity influence, and works by filling the pores and preventing corrosion attacks. A sealer is not the same as a paint, because paint adds an additional layer to the coating system, while the sealer penetrates the coating and does not necessarily add any significant thickness to the coating [4, 7]. Figure 2.1 shows a photo of a sealer applied to TSA. The figure shows how the sealer penetrates the coating and fills up the pores. The most common sealers were either Silicone-based or Vinyl-based, where the Silicone-based sealers have been reported to be of a higher quality than the Vinyl-based sealers [2, 4]. Vinyl-based sealers have now been phased out, and replaced with Epoxy-based sealers. Silcone sealers may be applied to up to 480 °C [24].

Apart from the corrosion resistance improvement, sealers have two other beneficial properties. Firstly, the sealers reduce the current requirement during CP. This is, however, linked to the corrosion resistance properties. Secondly, the sealer reduces the current output from the coating itself to the substrate, should there be any damage in the coating. The second property may not sound too beneficial, but the reduced output is enough to polarize and protect the substrate in most cases, so it prevents unnecessary deterioration of the coating [4].

A high oxide content in TSA coatings may be beneficial, because this improves the corrosion resistance, as long as the oxide content does not become so high that it affects the mechanical properties of the coating [3]. The oxide layer will generally be thicker on TSA than on solid aluminium, due to oxidation in the spraying process. Another difference between thermally sprayed and solid aluminium is the surface roughness, where sprayed aluminium will have a much rougher surface than solid aluminium [16].

## 2.2 Corrosion

In this chapter corrosion of aluminium, TSA, and electrochemical methods of finding corrosion rates are presented. This chapter is included for understanding the electrochemical properties like corrosion rate and corrosion potential of TSA when immersed in seawater.

### 2.2.1 Corrosion of Aluminium

Corrosion is an electrochemical process, with an anodic and a cathodic reaction, that occurs when metals or alloys are in contact with an aqueous solution. The electrochemical reaction dissolves the metal into metal ions. Corrosion can therefore be described as a chemical attack on a metal [22, 25].

The anodic reaction for the corrosion of aluminium is shown in Equation 2.1 [22, 25].

$$Al = Al^{3+} + 3e^-$$ (2.1)

In alkaline solutions the anodic reaction can be as shown in Equation 2.2 [26].

$$Al + 4OH^- = Al(OH)_4^- + 3e^-$$ (2.2)
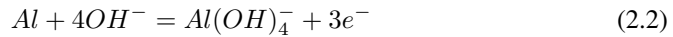
The cathodic reaction for the corrosion of aluminium may be the oxygen reaction, the hydrogen reaction, or a combination of these. The oxygen reaction and the hydrogen reaction are shown below in Equation 2.3 and 2.4 respectively [4, 21, 26, 27, 28].

$$O_2 + 2H_2O + 4e^- = 4OH^-$$ (2.3)

$$2H_2O + 2e^- = H_2 + 2OH^-$$ (2.4)
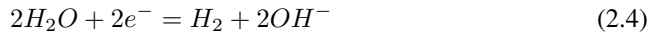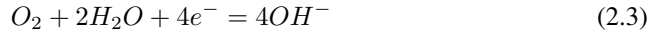
Aluminium reacts very easily with the environment, which causes an oxide layer to form on the surface of the metal. The formation of this oxide layer can be seen in reaction 2.5 [25, 29].

$$2Al + 3H_2O = Al_2O_3 + 6H^+ + 6e^-$$ (2.5)
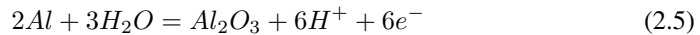
The oxide layer passivates the aluminium and makes it naturally resistant against uniform corrosion in most natural environments [4, 21, 25, 30, 31]. Aluminium should, however, theoretically corrode quite rapidly in seawater [17, 22, 25]. Figure 2.3, which a theoretical Pourbaix diagram, where the stability of the oxide is between approximately pH 2.5 and 4.2 [17], while seawater usually is close to pH 8.2 [17].

However, adding small amounts of alloying elements like Mn and Mg creates an oxidation layer which is more stable in neutral and alkaline environments. Figure 2.4 shows an experimental Pourbaix diagram, which more accurately describes the situation for aluminium alloys in seawater. The diagram is based on a aluminium 5000-series alloy [30], and will therefore reflect some of the corrosion properties as AlMg5 TSA, which is based on this type of alloy [4, 7, 17].

As can be seen in Figure 2.4, the aluminium alloy is passive in a much larger pH-range than the theoretical Pourbaix diagram indicates. This means that aluminium may
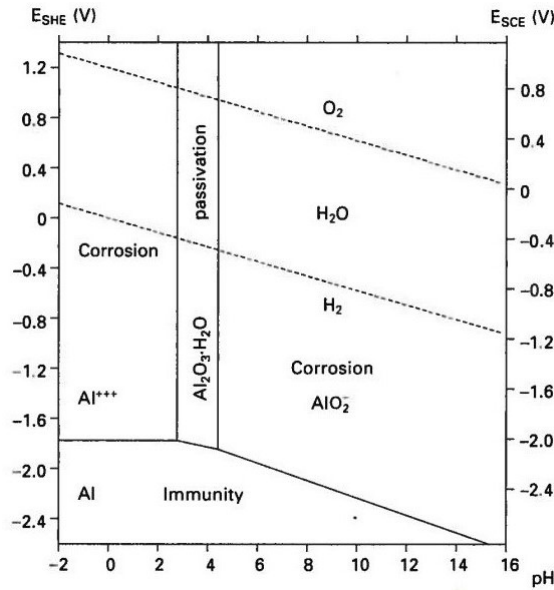
**Figure 2.3:** Theoretical Pourbaix Diagram [17].

be applicable for use in seawater. Aluminium is commonly used in seawater [32], even though seawater is a very corrosive fluid that attacks more or less all metals to some extent [33].

Even though aluminium has a passive oxide layer, it is subjected to several types of corrosion. Uniform corrosion, pitting, intergranular corrosion, and galvanic corrosion are examples of corrosion mechanisms aluminium is subjected to [22, 25]. Uniform corrosion can occur in environments where the oxide is not stable, that only is stable within a narrow pH-range, causing the oxide to dissolve. This means that aluminium is subjected to uniform corrosion in alkaline and acidic environments, where the oxide layer is unstable. [4, 21, 29, 31]. The uniform corrosion of aluminium is greatly dependant on the formation and dissolution of the oxide layer. The formation of the oxide can be seen in reaction 2.5, while the dissolution is shown in 2.6. It can be seen from the dissolution reaction that the dissolution of the aluminium oxide is a purely chemical reaction [29].

$$Al_2O_3 + 2OH^- = 2AlO^- + H_2O \qquad (2.6)$$

Uniform corrosion attack only occurs in aggressive environments, and is spread evenly on the surface of the metal and is easy to predict [25]. Figure 2.5 shows the effect pH has on the corrosion rate of aluminium. From the figure it is clear that aluminium is particularly sensitive to alkaline environments [21].

Localized corrosion mechanisms, such as pitting and intergranular corrosion, are more difficult to predict than uniform corrosion and hence more dangerous. However, intergranular corrosion is strongly tied to heat treated aluminium alloys with high copper content [34], and is therefore of less concern in this project.
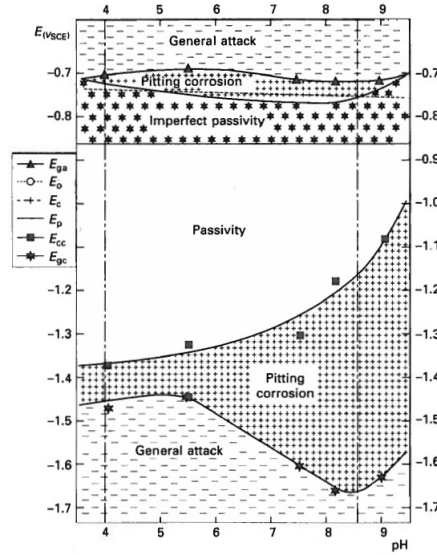
**Figure 2.4:** Experimental pourbaix diagram [30].
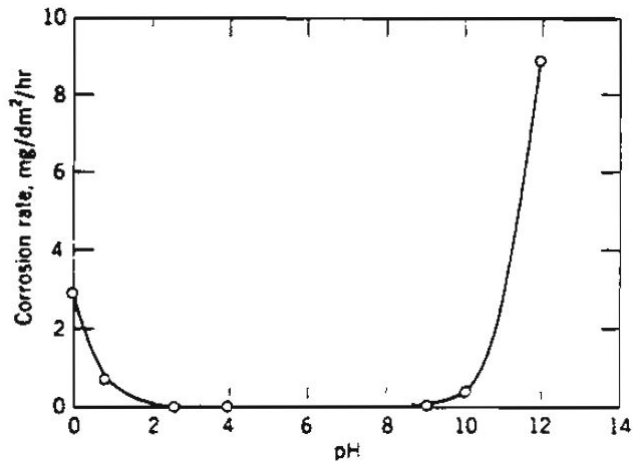


**Figure 2.5:** Corrosion rate of aluminium as a function of pH [21].
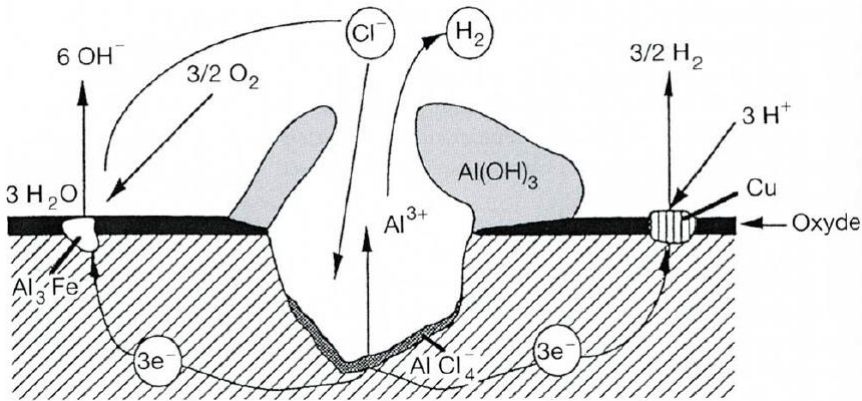
**Figure 2.6:** Schematic presentation of pitting corrosion [25].

The most common corrosion attack on aluminium is pitting corrosion [4, 35], and usually occurs in environments with a pH between 4 and 9. Pitting corrosion is a localized form of corrosion which can create narrow pits that can penetrate deep into the metal [36]. The corrosion attack commonly initiates around weak points or cracks in the oxide layer close to intermetallic particles. The particles are often iron based, and are cathodic towards the aluminium matrix. This means that the aluminium in the initiated pit and the intermetallic particle will create a galvanic coupling. The aluminium is then subjected to a form of galvanic corrosion, only on a small scale [4, 17, 31, 36]. The galvanic corrosion causes the pit to grow [17]. Inside the pit the anodic reaction (Equation 2.1) occurs, and on the particle the cathodic reaction occurs (Equation 2.3 and 2.4). This produces $Al^{3+}$ ions in the pit, which causes $Cl^-$ to migrate into the pit to equalize the electric charge the aluminium ions create. The reaction that occurs between the chloride and aluminium ions are shown in Equation 2.7 [36].

$$Al(OH)Cl^+ + H_2O = Al(OH)_2Cl + H^+ \tag{2.7}$$
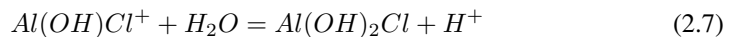
This causes the environment inside the pit to become acidic and further accelerate the corrosion rate, while outside the pit at the intermetallic particle an alkaline environment is created due to the hydroxide caused from Equation 2.1 and 2.4 [36]. Figure 2.6 shows the mechanisms behind pitting corrosion [25].

Almost all aluminium alloys are subjected to pitting corrosion in seawater. However, the severity varies. Corrosion resulting only in superficial pits are common, often referred to as micropitting. Pitting corrosion in aluminium is primarily dependant on the properties, size and distribution of the intermetallic particles, and not the matrix properties, like pitting corrosion in steel is [17].

Flow rate is another important parameter which affects the corrosion behaviour of aluminium [4, 17, 31]. High flow rates tend to favour uniform corrosion, while low or stagnant conditions favour pitting corrosion [17, 31]. Uniform corrosion rate is determined on the chemical dissolution of the aluminium oxide. At stagnant or low flow rate the water close to the aluminium surface gets saturated quite quickly, and the dissolution of
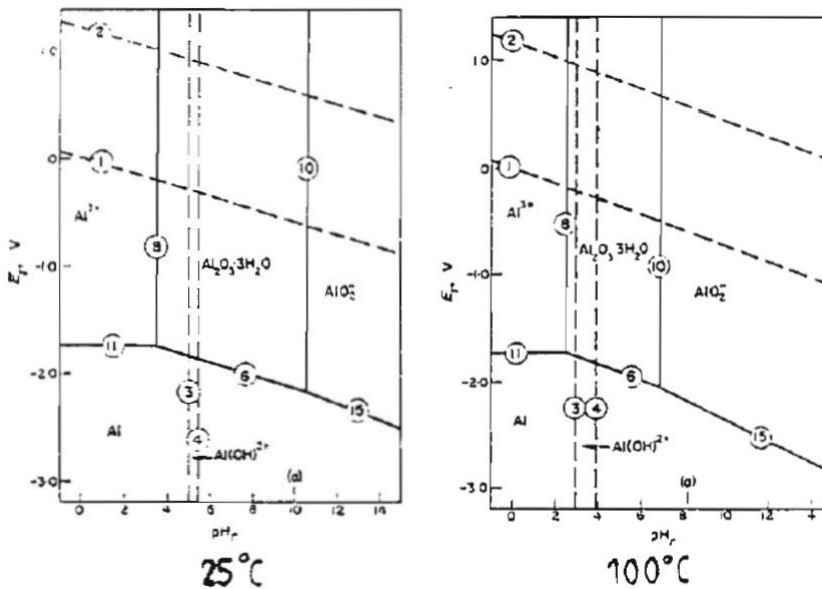
**Figure 2.7:** Theoretical Pourbaix diagram for Aluminium-water interaction at 25 and 100 °C. Adapted from [4].

aluminium oxide occurs slowly, and thus the corrosion rate is low. At high flow rates the water close to the aluminium surface is quickly replaced by fresh water, and saturation does not occur, which causes the dissolution of aluminium oxide to occur quickly, leading to a higher corrosion rate. Pitting is dependant on a localized environment to be created for the pit to grow. This does not occur if the flow rate is so high that the water inside the pit gets replaced too quickly. Therefore, pitting only occurs in slow flowing water [31].

For all chemical reactions the temperature has an effect on the reaction rate and behaviour, and the general trend is an increase in the reaction rate for most reactions when the temperature is increased [4, 21]. For the corrosion of aluminium in seawater the temperature has mainly two effects on the corrosion behaviour. Firstly, the pH-range at which the aluminium oxide layer is stable is affected. At increasing temperatures this range decreases, making the oxide less stable in neutral and alkaline environments. This can be seen from thermodynamic calculations that are illustrated in Figure 2.7 [4]. From the thermodynamic calculation the temperature seems to have an enormous effect on the stability range of the aluminium oxide. There is little empirical data on this, but there are some reports that indicate that the effect of temperature on the pH-range is not so large as the thermodynamic calculations dictates [4, 37].

The second effect the temperature has is that the corrosion potential decreases with increasing temperature [4]. Potential measurements done at elevated temperatures, however shows low potentials initially, which indicates high corrosion rates, but after a while the potential rises and stabilizes. This means that aluminium should have high initial corrosion that will decrease with time and then stabilize [4, 38]. At high temperature uniform corrosion is the dominating corrosion form, as pitting corrosion is less of a problem at high
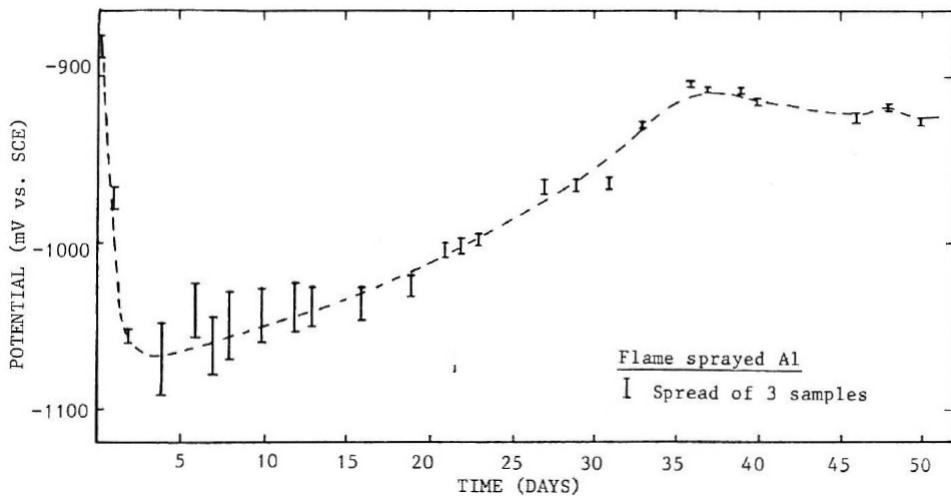
**Figure 2.8:** Corrosion potential of flame sprayed aluminium in seawater as a function of time [39].

temperatures, because the aluminium surface become passivated quickly with aluminium oxide or calcareous deposits [31].

Aluminium is low on the galvanic series. This means that the potential of aluminium in seawater is lower than most other materials, and will suffer from galvanic corrosion when in metallic contact with other metals in an electrolyte. Galvanic corrosion is a common corrosion issue for aluminium alloys in the offshore industry [22, 37].

### 2.2.2 Corrosion of Thermally Sprayed Aluminium

TSA and solid aluminium are different with regard to corrosion resistance, and corrosion behaviour. This is due to the differences in surface properties, and topography the two materials have. One difference can be seen in the dissolution rate of the aluminium oxide layer. The oxide on TSA dissolves slower than on solid aluminium [16].

The initial corrosion rate of TSA is quite high, due to corrosion around the intermetallic particles discussed in Chapter 2.2.1. After a while these particles are passivated or fall out and the corrosion rate decreases and stabilizes [4, 18] . Another factor contributing to the corrosion rate decreasing with time is that as the TSA coating corrodes the pores in the coating fills up with corrosion products and inhibits further corrosion [7]. Figure 2.8 shows how the potential of flame sprayed Aluminium in seawater changes with time, and after a while stabilizes and reaches its steady state corrosion rate. The low potential illustrates a period of high corrosion rate, while the higher potential means that the aluminium is passivated. TSA at steady state conditions in seawater at low temperatures will have a low corrosion rate [4].

As mentioned the application method and alloying elements affect the corrosion behaviour of TSA. This results in different corrosion potentials for the different coatings, which varies from -1000 to -900 mV Ag/AgCl.[40] See Table 2.1 for the corrosion poten-

tial of different aluminium based coatings [40].

**Table 2.1:** Steady state corrosion potential for different TSA coatings. Adapted from Eggen and Gartland [40].

| Coating Material | Potential [mV vs Ag/AgCl] |
|---|---|
| Arcsprayed Al | -950 |
| Arcsprayed Al sealed | -940 |
| Flamesprayed Al | -910 |
| Flamesprayed Al sealed | -950 |
| Arcsprayed AlMg | -995 |
| Arcsprayed AlMg Sealed | -970 |
| Flamesprayed AlMg | -1000 |
| Flamesprayed AlMg sealed | -1010 |
| Arcsprayed ZnAl | -995 |
| Arcsprayed ZnAl sealed | -920 |
| Flamesprayed ZnAl | -980 |
| Flamesprayed ZnAl sealed | -920 |

Table 2.2 shows the corrosion potential of TSA at three different temperatures, and from the table it looks like the potential becomes more positive at higher temperatures, after 1 month and 3 months. However, it has also been reported that higher temperatures leads to more negative potentials, with 50 mV decrease from 8 °C seawater temperature to 60 °C, after 60 days exposure [24].

**Table 2.2:** Corrosion potential of TSA at different temperatures. Adapted from Fischer et al [41].

| | Potential [mV Ag/AgCl] | | |
|---|---|---|---|
| Temperature [°]C | Initial (Day 1-2) | 1 Month | 3 Months |
| 8 (ambient) | -800 | -1000 | |
| 70 | -1040 | -970 | 945 |
| 100 | -1115 | -950 | -950 |

Another difference between solid aluminium and TSA is that solid aluminium may be painted. Painting of TSA is called a duplex coating, which is commonly assumed to give very good and long corrosion protection. If TSA is painted a process which is very similar to the acidifying process in pitting can occur, and an acidic environment is created underneath the paint. This leads to rapid corrosion and degradation of the coating system [42].

### 2.2.3 Electrochemical Methods for Corrosion Testing

As mentioned earlier it is nearly impossible to determine corrosion rate by weight loss measurements on TSA, due to the porosity of the coating [4]. However, there are electrochemical methods available that can be used to measure corrosion rates. Polarisation curves and LPR measurements are examples of methods. Polarization curves are made by
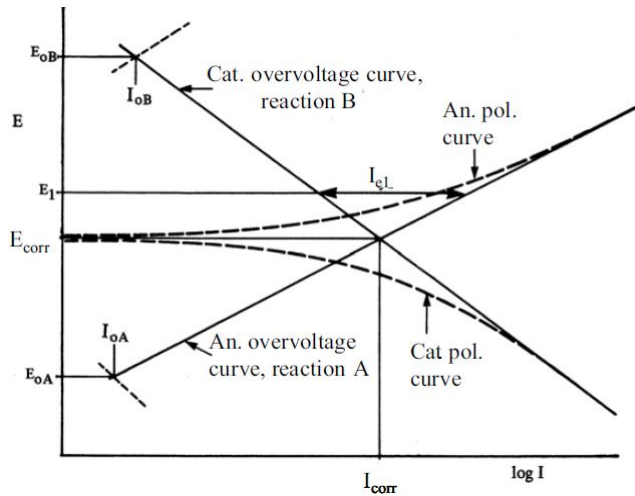
**Figure 2.9:** Polarization curves and Overvoltage Curves [22].

polarizing the metal in cathodic, then anodic direction while measuring the current. To polarize a metal means to shift the potential of the metal from the free corrosion potential. This shift of potential is what creates a net current in a direction, and it is this current that can be measured. This current is not the corrosion current, because the metal has been shifted to a potential that is different than the free corrosion potential. The purpose of obtaining Polarization curves is to get the so called Overvoltage curves, and it is from these Overvoltage curves that the corrosion rate can be estimated. Figure 2.9 shows typical Polarization curves and Overvoltage curves [22].

The overvoltage curves are, as can be seen from Figure 2.9, asymptotes of the polarization curves, and the intersection of the anodic and cathodic overvoltage curves gives the corrosion rate. From the overvoltage curves the Tafel constants $b_c$ and $b_a$ can be determined, by finding the slopes of the overvoltage curves. These constants can be used to determine the corrosion rate by using the Linear Polarization Resistance (LPR) method. This method is easier and quicker than obtaining Polarization curve every time. Figure 2.10 shows a typical Linear Polarization Curve.

Equation 2.8 shows the Stern-Geary's equation for estimating corrosion rates based on the LPR method [22].

$$\frac{dE}{dI_e} = \frac{b_a * b_c}{2.3 * (b_a + b_c) * I_{corr}} \tag{2.8}$$

Simple mathematics converts the Stern-Geary's equation to Equation 2.9 that gives the corrosion rate.

$$I_{corr} = \frac{dI_e}{dE} \frac{b_a * b_c}{2.3 * (b_a + b_c)} \tag{2.9}$$

By using the Tafel constant obtained from the Polarization Curve method, and dE
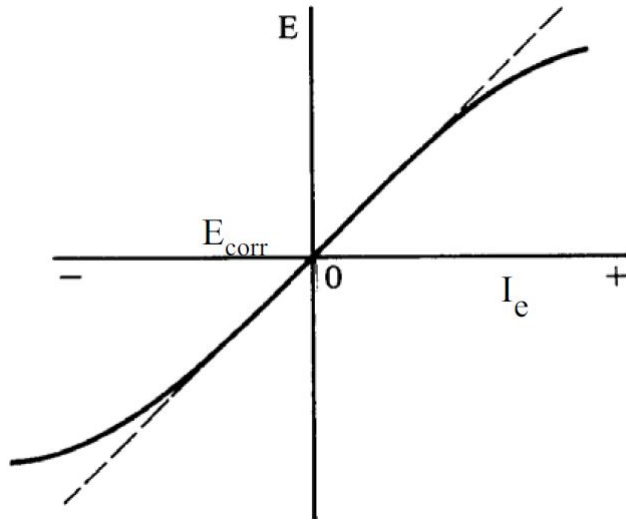
**Figure 2.10:** Typical LPR Curve [22].

and $dI_e$ measured from the LPR method, the corrosion rate can easily be calculated from Equation 2.9. This calculated corrosion rate should be compared to the graphical solution obtained from the polarization curves.

From the graphical solution and the Stern-Geary calculations a corrosion current is found. For practical purposes the corrosion current given in $A/m^2$ should be converted to corrosion rate in $\mu m/year$. Equation 2.10 shows the convertion from corrosion current to the corrosion rate.

$$Corrosion\ rate[\frac{\mu m}{year}] = \frac{i_{corr}}{F*n}[\frac{mmol}{m^2 s}] * \frac{M_{AlMg}}{\rho_{AlMg}}[\frac{m^3}{mol}] * (3.16*10^{10})[\frac{s}{year}] \quad (2.10)$$

- $i_{corr}$ - Corrosion current density

- $F$ - Faraday's constant

- $n$ - Valency number of ions

- $M_{AlMg}$ - Molar mass of the coating

- $\rho_{AlMg}$ - Coating density

## 2.3   Cathodic Protection

As mentioned in the Introduction a subsea heat exchanger may be connected to a CP system, and therefore the properties of TSA when connected to a CP system are interesting.

This chapter gives an introduction to CP, and the properties of TSA when connected to anodes. Properties like current density requirement and corrosion rate when polarized and the effect of temperature is discussed.

### 2.3.1 Cathodic Protection of Steel

CP has been in use for over 150 years, and was first introduced by Sir Humphrey Davy in 1824 [43]. It was, and still is, mainly used for protecting steel structures in seawater or soil, and is often used for corrosion protection in combination with an organic coating [22, 33]. The principle behind CP is the same as for galvanic corrosion. It is an electrochemical process that protects a metal by "sacrificing" another metal. CP is applied with anodes or the use of an impressed current system. When CP is applied by the use of anodes, the anodic reaction takes place on the anodes, often based on Aluminium, while the cathodic reaction occurs on the protected metal, often Steel [22, 33].

The cathodic reaction is the same as in a regular corrosion process, Equation 2.3 and 2.4, while the anodic reaction depends on the anode material used. If Aluminium is used, the anodic reaction will be oxidation of aluminium, Equation 2.1. From these reactions it can be seen that hydroxide is created on the surface of the metal being protected, and a localized alkaline environment is created on the metal-water interface. When steel is subjected to CP this alkaline environment causes a dense and protective calcareous layer to deposit on the surface of the steel [4, 44, 45]. The calcareous layer prevents oxygen to diffuse to the metal surface, and therefore prevents the oxygen reaction, Equation 2.3, and inhibits the corrosion reaction thus reducing the corrosion rate [45]. This means that the current demand from the CP system to the steel is reduced, since the corrosion rate on the steel is reduced. This is the reason why CP often is used in combination with a coating, to reduce the current demand from the system, and therefore reducing the amount of anodes needed [2]. NORSOK M-503 gives many guidelines and specifications for applying CP to steels.

CP is very effective on steel, and almost no corrosion occurs on the steel when CP is correctly applied. When steel is cathodically protected the steel is polarized to the area of a Pourbaix diagram called "immune". Its called that because it is said that the corrosion rate is zero, and that the steel is immune to corrosion [4, 18].

Near the surface in the Barents Sea steel has a current demand of 300 $mA/m^2$ to be polarized below -800 mV Ag/AgCl, which is the requirement for CP of steel, while in the North Sea current requirements is between 160 and 130 $mA/m^2$ and stabilized after at 70 $mA/m^2$ [46].

### 2.3.2 Cathodic Protection of Aluminium

CP is applied to aluminium for three different reasons. The first reason is that the aluminium is part of a structure where CP is applied [1], the second is to protect aluminium from pitting corrosion, and the third is to protect against galvanic corrosion [21].

When aluminium is connected to a CP system the initial current requirement is high compared to the final output, and then it stabilizes at a lower current requirement with time.

---

[1]The most likely case for subsea heat exchangers.

This is due to the same phenomena explained earlier, with corrosion around intermetalli-cal particles. When CP is applied, this is called cathodic etching,[17] and the principle is shown in Figure 2.11. The cathodic reaction occurs on the intermetallic particles and this creates a alkaline layer around the matrix. The alkaline environment makes the alu-minium oxide unstable and it dissolves, causing the aluminium matrix near the particle to corrode. Eventually all the aluminium close to the particle can be corroded away, and the particle gets detached from the aluminium matrix. In the absence of cathodic particles the aluminium is repassivated with a aluminium oxide layer, and possibly some calcareous deposits. This process will of course occur in the initial stage of the immersion, and when it is completed the current demand from the CP system will decrease significantly [47].

In practice there is no immune area for aluminium under CP as there is for steel. The corrosion rate on aluminium can be reduced by 80-90%, but not eliminated completely, and while the purpose of CP of steel is to prevent uniform corrosion, the purpose of CP is preventing pitting or galvanic corrosion [4, 18]. This means that CP of aluminium works by keeping the aluminum in the passive area of the Pourbaix diagram, Figure 2.4 [17, 48]. It can therefore be said that CP really is anodic protection when applied to aluminium [17], but in this thesis it will be referred to as CP none the less, because it is the most common term.

Since CP of aluminium works by preventing pitting corrosion, it only works when pitting corrosion is the dominating corrosion form. If uniform corrosion of aluminium is the primarily source of metal loss, the CP will not be effective. This is because uniform corrosion of aluminium is determined by the dissolution rate of the oxide, which is a purely chemical reaction, and since CP works by manipulating potentials it can not affect a chemical reaction with no potential to manipulate [17, 31].

Even though there is no "immune" area for aluminium, a potential between -1100 and -900 mV vs Ag/AgCl will keep the corrosion rate very low, due to the stability of the oxide layer at these potentials. Aluminium requires approximately one tenth of the current of steel during CP [17, 47]. The current density requirement for TSA within this potential range usually is in the magnitude of 5-10 $mA/m^2$, and if a sealer is applied the demand will be even less, down to 1 $mA/m^2$ [4]. Potential outside this range may lead to increased corrosion rates, and localized alkaline environments may occur at the aluminium/seawater interface. Potentials far below -1100 mV vs Ag/AgCl or far above -900 mV vs Ag/AgCl may cause severe corrosion rates, and a localized pH of up to 9-10 [21].

Potentiodynamic polarization curves obtained by Egtvedt [49] show that the current density requirement of TSA increases with increased polarized. This means that the lower the potential is polarized when applying a CP system, the higher the current requirement will be for TSA.

### 2.3.3 Cathodic Protection of Thermally Sprayed Aluminium at High Temperatures

TSA was used for corrosion protection for a high temperature (approximately 150 °C) pipeline in combination with a CP system. This pipeline was closely monitored, and a negative current was initially reported for the TSA coating, indicating that the coating was protecting the anodes and not the other way around, which was intended. The current
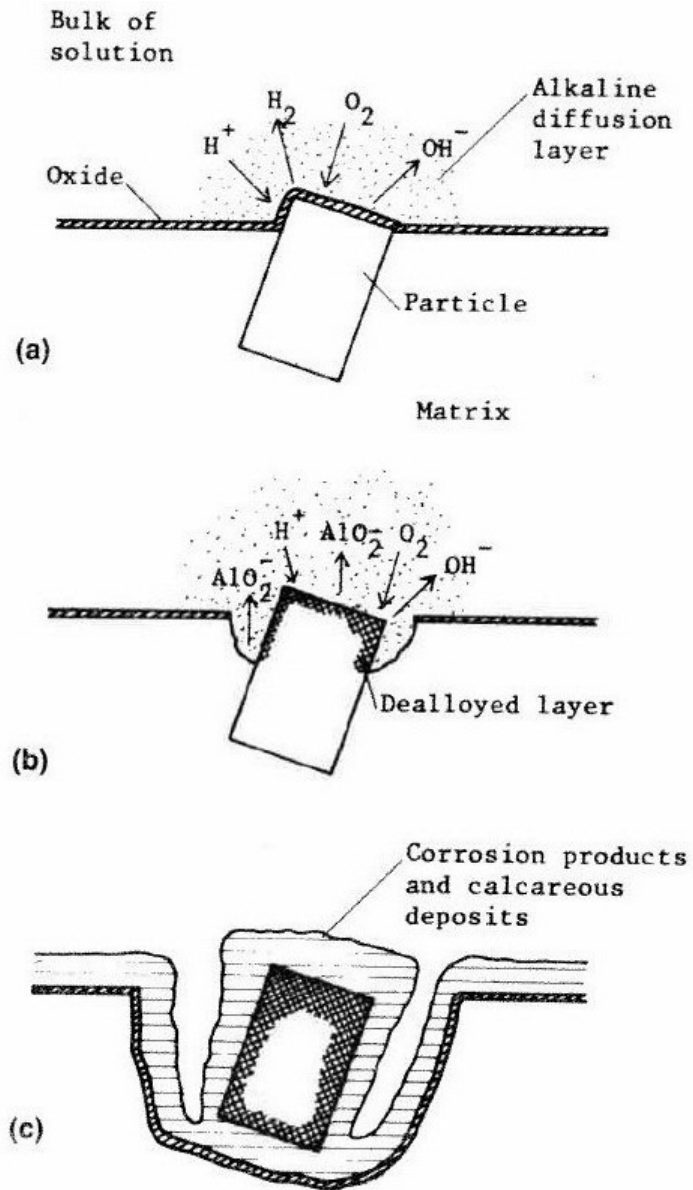
**Figure 2.11:** Cathodic protection mechanism for Aluminium [47].

shifted direction after approximately 2 months of service, and obtained a protective current density of 21.5 to 43.0 $mA/m^2$ [50].

The current density is generally expected to increase with high temperatures, while the current capacity from the anode decreases [50].

Tests performed on unsealed flame sprayed aluminium polarized to -1100 mV Ag/AgCl in seawater subjected to 70-100 °C gave a cathodic current density of 70 $mA/m^2$ after one month of exposure. After one year the current density had been reduced to 30 $mA/m^2$ [41]

The DNV standard for Cathodic Protection [51] states:

> For aluminium components, or those coated with either aluminium or zinc, a design current density of 0.010 A/m2 is recommended for initial/final as well as mean values. For internally heated components, the design current density shall be increased by 0.0002 A/m2 for each °C that the metal /seawater is assumed to exceed 25 °C.

This means that TSA at $60^2$ and 100 °C surface temperature should have a current density requirement of 17 and 25 $mA/m^2$ respectively according to the standard. The results of experiments done at 70-100 °C is presented in Table 2.3, and show that the current density after one year is 30 $mA/m^2$ for TSA at high temperatures, which is higher than the recommended current density [41]. The minimum values measured is 10 $mA/m^2$ however, which is lower than the recommended value.

**Table 2.3:** Current density for TSA at 70-100 °C. Adapted from Fischer et al [41].

| Time | Current Density [$mA/m^2$] | | |
|---|---|---|---|
| | Mean | Maximum | Minimum |
| Initial (first week) | 180 | 400 | 65 |
| 1 Month | 70 | 165 | 30 |
| 1 Year | 30 | 55 | 10 |

SINTEF carried out experiments on TSA exposed to seawater at ambient, 50 °C and 70°C surface temperature at Sealab Brattørkaia, Trondheim[3] in 2013. The purpose of the study was to examine the corrosion rates for cathodically polarized TSA in seawater and mud at elevated temperatures. TSA was cathodically polarized to -1100 mV Ag/AgCl, and the current density was monitored. The corrosion rates were measured using LPR with an assumed tafel slopes of 0.3 V/decade.

At ambient, 50 and 70 °C surface temperature the current density requirement were 3, 8 and 15 $mA/m^2$ respectively after 250 days of exposure.

### 2.3.4 Corrosion of Cathodically Protected Thermally Sprayed Aluminium

As mentioned in Chapter 2.3.2, aluminium is not immune to corrosion when cathadically polarized the same way as steel is, but gets passive when connected to a CP system. The

---

[2]60°C is mentioned because the surface temperature of the TSA in this thesis reached up to 60°C.

[3]The same laboratory as the experiments in this thesis were performed.

cathodic reaction which occurs on the TSA under CP can increases the pH locally, close to the TSA surface, moving the TSA outside of the passive area and increasing the corrosion rate.

Knudsen et al [52] found that the corrosion rate of TSA, even when cathodically polarized to -1100 mV Ag/AgCl is initially high, with a rate between 25 $\mu m/year$ for TSA exposed to ambient temperature and 55 $\mu m/year$ for TSA with a surface temperature of 70 °C. The corrosion rate decreased with time, and reached 10 $\mu m/year$ and 15 $\mu m/year$ for ambient temperature and 70 °C respectively [52].

Knudsen et al. [52] also found the corrosion rate to correlate proportionally with the current density requirement of the TSA. High corrosion rates were found when the current demand was high, and the corrosion rate decreased with decreasing current demand. This may be caused by the hydroxide production at the TSA surface due to the cathodic reaction, Equation 2.3, which activates the aluminium due to the narrow passivity pH range. Increased current demand increases the hydroxide concentration near the surface of the TSA causing accelerated corrosion rate, while decreased current demand does the opposite [52].

The reason calcareous layers form on metal surfaces is the increased pH due to the cathodic reaction on the metal surface. Knudsen et al. [52] discovered that this increase of pH may not occur on TSA due the the anodic reaction[4], occuring on TSA at high temperatures. An decrease in the pH at the TSA/mud interface from the bulk solution was actually reported, the opposite of what was expected. The reason for this was assumed to be a relatively high corrosion rate of the TSA, even when cathodically polarized. The anodic reaction for aluminium in alkaline environment is shown in Equation 2.2, and it shows that hydroxide is used in the reaction. This inhibits the accumulation of hydroxide on the TSA surface, caused by the cathodic reactions shown in Equation 2.3 and 2.4. The prevention of accumulation of hydroxides inhibits the precipitation of calcareous deposits, while causing a higher corrosion rate of the TSA [52].

The implications of the use of hydroxide in the TSA corrosion reaction is that the pH will not increase significantly above the passivity range of the TSA. Diffusion and convection in the seawater will also contribute significantly to reducing localized accumulation of hydroxide close to the TSA surface [52].

## 2.4   Calcareous Deposits

Calcareous deposits are problematic for subsea heat exchangers as it could negatively affect the heat transfer from the warm medium to the cold seawater. This chapter presents the basics of how calcareous develop on submerged metals connected to CP.

### 2.4.1   Formation

An important aspect of CP is the calcareous deposits on the surface of the protected metal. One of the most important factors for the formation of the calcareous deposit is the ability the applied current from a CP system have of changing the pH at the metal surface [53].

---

[4]Corrosion reaction for aluminium in alkaline environment, see Equation 2.2

Due to the applied current there are three stages to the formation of the calcareous layer deposition [54].

- Increase in pH near the metal surface

- Increase in carbonate ion concentration due to change in the inorganic carbon chemistry of the seawater

- Precipitation of calcareous compound when the solubility of the compound has been preceded

Temperature, seawater composition, pH, applied potential, current density, and surface finish all influence the kinetics of the steps above, and consequently the properties and morphology of the formation [33, 44, 54].

The deposits mainly consist of $CaCO_3$ and $Mg(OH)_2$ with some amount of $MgCO_3$ [55, 56]. The reactions for the precipitation of $CaCO_3$, $MgCO_3$ and $Mg(OH)_2$ can be seen in Equations 2.11, 2.12 and 2.13 respectively [28, 45, 57].

$$Ca^{2+} + HCO_3^- + OH^- = H_2O + CaCO_3 \qquad (2.11)$$

$$Mg^{2+} + HCO_3^- + OH^- = H_2O + MgCO_3 \qquad (2.12)$$

$$Mg^{2+} + 2OH^- = Mg(OH)_2 \qquad (2.13)$$
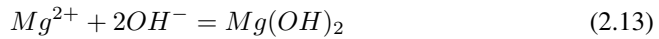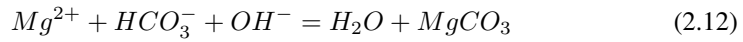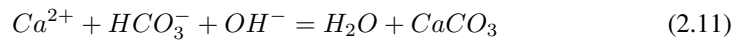
The pH at the metal/seawater interface is critical for calcareous deposits [58]. Calcareous deposits mainly precipitate between pH 8 and 10 [33]. Calcium carbonate is super-saturated in seawater near the surface, while magnesium hydroxide is under-saturated and usually does not precipitate at pH values below 9.3. Bulk seawater is around 8.2, so under natural conditions magnesium hydroxide will not precipitate, because the seawater does not reach the necessary level of alkalinity. When CP is applied, the pH at the metal/seawater interface may reach high enough values for the precipitation of magnesium hydroxide, and the calcareous deposit rate increases [44, 55, 57].

Magnesium usually deposit as $Mg(OH)_2$ with small amount of $MgCO_3$ [59]. $Mg(OH)_2$ from as thin films, only micrometers thick [55]. Formation of $Mg(OH)_2$ occurs rapidly in both cold and warm waters, but does not contribute significantly to reducing current requirements from CP systems. Only thin layers of calcareous deposits form on aluminium in seawater [49, 47].

Furthermore, the presence of $Mg^{2+}$ inhibits the formation of $CaCO_3$-based calcareous deposits, which only forms in small particles if a $Mg(OH)_2$ film is present [49]. The effect $Mg^{2+}$ has on $CaCO_3$ may cause alloys containing Mg[5] to inhibit the formation of $CaCO_3$ [44]. $Mg(OH)_2$ usually precipitate before $CaCO_3$-based deposits [56].

---

[5]Like the AlMg-TSA alloyed used in the experiments in this thesis. This is discussed in later chapters.

The different types of calcareous deposits have different microstructures. $CaCO_3$ typically form as one of two microstructures when precipitating during CP, Argonite and Calcite. Figure 2.12 shows a SEM photo of the typical Argonite structure, while Figure 2.13 show the Calcite structure [57].
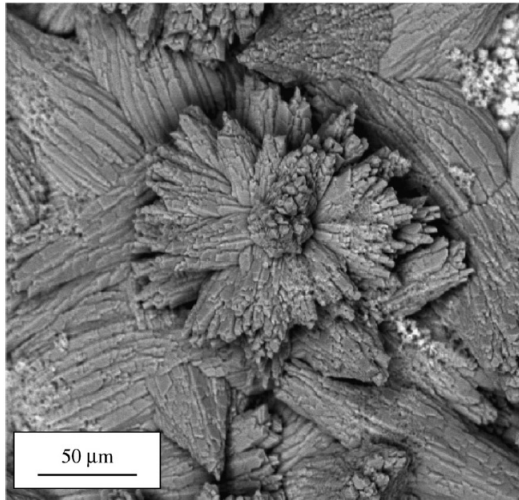


**Figure 2.12:** Photo of the Argonite structure for $CaCO_3$ formed on steel under CP [57].

Figure 2.14 show $Mg(OH)_2$ deposited on steel polarized in seawater [57]. The microstructure of $Mg(OH)_2$ on steel under CP was unfortunately not found in the literature.

Even though calcareous deposits on metal in seawater is often connected with CP, the deposits may also form without CP. According to Haraldsen [60] thermodynamically precipitation of calcareous deposits begin when the saturation ratio[6] is higher or equal to one. However, due to factors like adhesion and kintics the real saturation ratio usually needs to be higher than one for precipitation to occur. The saturation ratio of calcareous deposits is affected by the temperature, and may achieve values higher than one at high temperatures [60].

## 2.4.2 Effect of Temperature

Temperature affects the solubility of the different calcareous deposits which may deposit on metal during CP, and it also affects the CP itself, causing more current to be delivered to be protected metal. This means that temperature may affect the kinetics behind the formation of calcareous layers, but also which type of layer that may form [44].

The solubility of $CaCO_3$ decreases with increasing temperatures, which implies that calcareous deposits containing $CaCO_3$ will form more easily in warm seawater than in cold seawater [58]. The solubility of $Mg(OH)_2$ increases with increasing temperatures, implying that formation of $Mg(OH)_2$ will be inhibited at high temperatures [44].

---

[6]The ratio of actual ion product to the saturation ion product at given conductions.
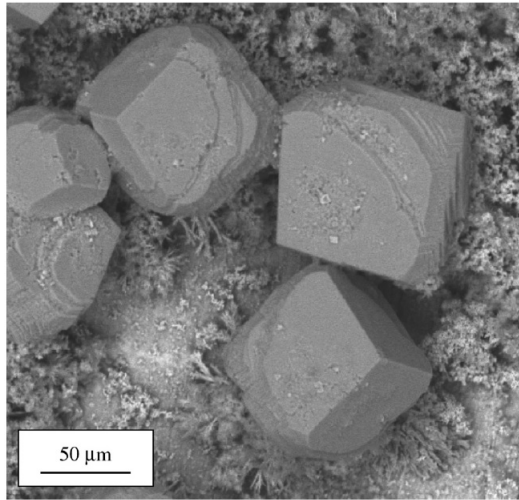
**Figure 2.13:** Photo of the Calcite structure for $CaCO_3$ formed on steel under CP [57].

However, it is has been discovered that at high temperatures, on steel, the amount of $Mg(OH)_2$ is increased. This was explained by the increased activity of the reduction of water, which can be seen in Equation 2.3. This reaction is limited by charge transfer which is accelerated by high temperatures, causing a higher pH at the water-metal interface than at lower temperature. This is crucial for the formation of $Mg(OH)_2$-based calcareous deposits [44].

Another effect temperature have on precipitation of calcareous deposits is that higher temperature require a lower saturation ratio for thermodynamic precipitation of calcareous deposits, while the saturation ratio for both $Mg(OH)_2$ and $CaCO_3$ increases with increasing temperature. The saturation dependency of temperature can be seen in Figure 2.15. The values in the graphs are based on calculation using a software called MultiScale. [60]. As can be seen the saturation ratio, and subsequently the probability of thermodynamic precipitation, increases with temperature. This means that $Mg(OH)_2$, even though it is undersaturated in seawater, might precipitate at high temperatures, without the aid of CP [60].

### 2.4.3 Sea current

Increased sea current will increase the amount of oxygen close to the metal surface, and will therefore increase the current to the metal due to higher corrosion rate. This will accelerate the $OH^-$ production close to the surface of the metal, but the high sea current it will also transport $OH^-$ quickly from the surface and prevent a high pH localized environment close to the metal surface [58].
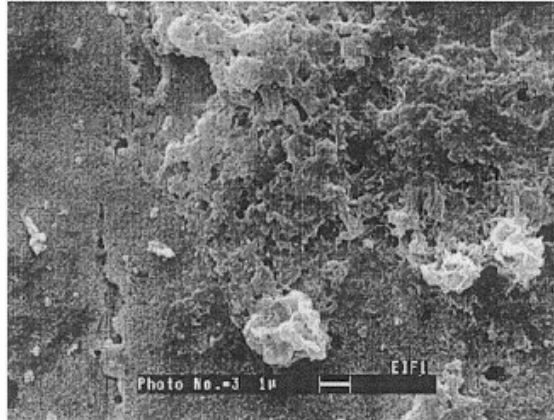
**Figure 2.14:** Photo of $Mg(OH)_2$ deposited on steel polarized to -1166 mV Ag/AgCl [55]
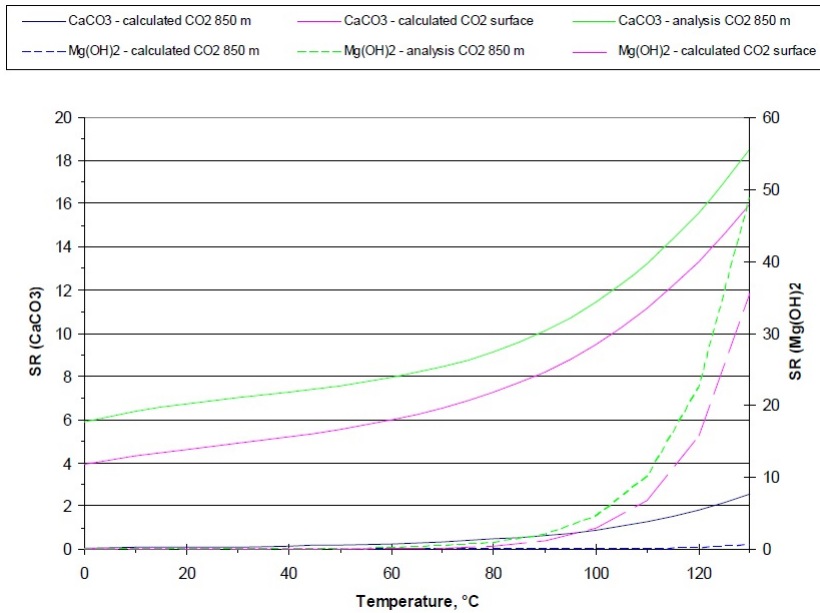


**Figure 2.15:** The effect of temperature on the saturation ratio for $Mg(OH)_2$ and $CaCO_3$ at surface conditions and at 850m sea depth [60].

# Chapter 3

# Literature Review

Very limited results from research or field experiences with TSA in connection with CP of structures in seawater has been published. In the following chapter a summery is given of the available published literature.

In 1985 Thomason [24] published an article on flame sprayed aluminium coatings used for offshore structures. Both laboratory tests and field test were conducted, and it was concluded that TSA will provide long-term corrosion protection for offshore facilities. The purpose of the laboratory test was to find the electrochemical properties of TSA coatings to determine the quality of CP the coating could deliver. Fischer discovered that TSA was sufficient to cathodically protect steel in seawater for years with up to 50 % holidays in the coating with a 200 $\mu m$ flame sprayed aluminium coating.

The same year Cooper and Vardon [61] published their experiences of using TSA as the main CP system on Hutton Tension Leg Platform (TLP). Cooper and Vardon wrote that TSA was used for on Hutton TLP due to it is satisfactory CP of steel. The TSA sufficiently polarized the steel, preventing any corrosion of the tension legs. This was done without over-polarizing it, causing hydrogen cracking problems. Fischer et al. [41] later published the results from inspection done on the TSA after 7 years, and no coating damage or significant deterioration was discovered.

From 1990 to 1993 Gartland and Eggen [4, 7, 16, 18, 21] published several SINTEF reports on the behaviour of TSA in seawater at ambient temperature based on laboratory research. Their researched included the proper way of applying TSA, their protective properties in seawater and the behaviour of TSA under CP in seawater.

Gartland [4] stated that:

> "There are no reasons to expect that Al-based coatings should behave differently than solid aluminium with respect to corrosion rates under cathodic polarization."

This means that TSA in seawater under CP won't rapidly deteriorate at low temperatures. Gartland and Eggen also mentioned that TSA has low corrosion rate, and thus a low

current demand from the CP system in seawater, with a current demand in a order of magnitude lower than steel. Thermally sprayed aluminium without CP should also have good resistance in seawater, since it is based on the 5000-aluminium series, which are known to have good corrosion resistance, at least at low temperatures.

Thomason, Cooper and Vardon found that TSA will sufficiently protect steel structures in seawater, while SINTEF found that there should be no reason to expect rapid deterioration of TSA coatings, with or without CP at low temperatures in seawater.

In 1995 Fischer [41] published an article of TSA in offshore service at elevated temperatures. Laboratory tests were conducted to discover the properties of TSA coated pipes in the splash zone, with internal temperature up to 100 °C. Both sealed and unsealed TSA was either left to freely corroding in seawater or was polarized to -1100 mV Ag/AgCl. Fischer monitored the corrosion potential, current demand and blistering behaviour of the TSA samples. The corrosion potential and current demand results of these research is presented in Table 2.2 and 2.3 respectively, and shows low current density requirements compared to steels, and steady state corrosion rate between -1000 and -950 mV Ag/AgCl. Blistering was found in the unsealed TSA samples, independent of CP.

In 1996 Wolfson [2] published a report on corrosion control of subsea pipelines using TSA. Wolfson coupled TSA coated steel and bare steel together to simulate coating holidays and exposed them to natural seawater from the Golf of Mexico for up to 12 months. The current density requirement for the holidays were recorded together with the corrosion potential of the TSA coating. Wolfson concluded that $250\mu m$ thick TSA could cathodically protect a subsea pipeline with 5% holidays up to 25 years.

In 2004 Thomason et al. [20] published more experiences with TSA used on offshore structures. The Joilliet Tension Leg Well platform had similar specification of the Hutton TLP, and was removed in 2004 after 13 years of service. Inspections of the platform legs showed no visual deterioration. The Heidrun TLP was installed in 1995 and had a combination of TSA and anodes as a CP system for the hot risers and TSA for the splash zone and atmospheric zone. After only 4 years of exposure major coating deterioration was discovered on TSA in the splash zone, with large areas of TSA completely removed from the risers. Thomason et al. [20] concluded that the cause of the deteration was fatigue due to thermal cycling, indication that TSA may not be suitable for splash zone applications with high internal temperatures.

In 2011 Egtvedt [49] published her Master Thesis on the role of calcareous deposits on TSA under CP in ambient seawater. Egtvedt polarized samples of aluminium and TSA to -1050 mV Ag/AgCl and exposed them to seawater. After exposure the samples were analysed using a SEM and EDS analysis. Egtvedt found than only thin films of calcareous deposits from on TSA during CP, and that this film does not contribute significantly to protecting the surface from corrosion as they do on steel.

Thomason, Cooper, Vardon, Gartland and Eggen discovered that the use of TSA at ambient temperature is not considered to be an issue. However, one worry was the combination of TSA and CP at elevated temperatures. The combination of CP and high temperature may cause a local alkalised environment at the surface of the aluminium coating, which will dissolve the aluminium, causing rapid deterioration of the coating. Applying a CP system to TSA at high temperatures may therefore do more harm than good. Knudsen et al [52] agreed with this and identified a overly active CP system to be a technical threat

to the use of TSA in seawater when exposed to high temperatures.

In 2014 Knudsen et al. [52] published a report on TSA in mud and seawater exposed to temperatures up to 95 °C in mud 70 °C at the water-TSA interface for up to one year. The purpose of the test were to find the corrosion rate of cathodically polarized TSA at different temperature. The current density requirements for TSA was also recorded. Knudsen et al [52] found that the corrosion rate of TSA in seawater at elevated temperature was significant, even when connected to a CP system.

# Chapter 4

# Experimental Research

In this chapter the experimental part of the thesis is described. The chapter is divided into five parts. Chapter 4.1 describes the design of the experiments conducted in this thesis. The process of building and installing the experimental design at Sealab, Braatørkaia is described in Chapter 4.2. The experimental conditions of the experiments are presented in Chapter 4.3, while the test procedures are shown in Chapter 4.4. In Chapter 4.5 the post exposure analysis is described. Prior to the experimental start up, a risk assessment of the experiment was conducted, and can be seen in Appendix I.

## 4.1 Experimental Design

The experimental design is described in this chapter. The chapter is divided into three parts because two slightly different designs were used. The first parts is called the Low Temperatures Experimental Design because this design was used only for low temperatures, between 10 and 40 °C internal temperature. The second part is called Carbon Steel Substrate Experiment because this part discribes a experiment without any heating. The corrosion potential for TSA on both a stainless steel substrate and on a carbon steel substrate was measured. This was done due to some unexpected results obtained in the low temperatures experiments. The third part is called High Temperatures Experimental Design because this design was used for temperatures between 50 and 90 °C internal temperature.

Some issues with the low temperature experiment is also discussed in this chapter, and the actions taken to improve on these issues and implementing the solutions into the high temperature experiment design.

### 4.1.1 Low Temperature Experimental Design

In this chapter the experimental design used for the three lowest temperatures (no heating, 30 °C and 40°C) is described. The first experimental design was made in the TPK4510 - Production and Quality Engineering, Specialization Project part of this project. The principle behind the experiments is simple. Test spools of UNS S31245 stainless steel

pipes with a TSA coating was exposed to seawater on the external pipe surface. The pipes were filled with oil that and heated to simulate a subsea heat exchanger that is utilizing raw seawater as a coolant. This means that the seawater is in contact with the TSA, not the steel, as it is the TSA that is being tested in this thesis. However, if the porosity in the TSA is high enough the coating may be permeable and seawater might penetrate the coating and eventually reach the steel, but it is mainly the TSA that was exposed.

For the experiments special test spools were made of each temperature. Each test spool was made out of four pipe pieces of stainless steel with TSA that were electrically isolated from each other, by polyurethane polymer parts. Two of the test pieces was be polarized by being connected to an anode, while the other test pieces was freely corroding Figure 4.7 shows a picture of two typical test pieces of UNS S31245 Stainless steel with a thermally sprayed aluminium coating. This was done to create two parallels that was cathodically protected, and two parallels that were freely corroding at each temperature. This provided more data per test than with only one test piece, making the experiments more efficient if only a single piece of TSA pipe was used.

Figure C.1 in Appendix C shows a picture of the test spools used for the three lowest temperatures. The picture also shows some of the glue spilled on the surface of the spool, which will be discussed later in this chapter.

The four different test pieces were glued together with the isolation pieces, to prevent any leakage. This production method had it's drawbacks and limitations, and problems presented itself during production of the spools and during testing. The issues that arouse during productions were connected with the gluing of the spools. May wires were connected to the pipes, and this was a problem because it was hard to keep track of them. Since there was a time limitation before the glue had before it hardened, the work was hurried and this lead to spillage of glue on the TSA surface, causing many hours of extra work on removing the glue. It also provides uncertainties regarding the true surface area of the TSA. This uncertainty of area causes the corrosion rate calculations and current requirements to be uncertain, because they are directly linked to the surface area. It is also possible that the glue penetrated the coating, and acted like a sealant. This was discussed in the Discussion chapter of the Specialization Project:

> One factor that causes uncertainty is a mistake made during manufacturing of the test spools. To produce the test spools glue was used to join the test pieces and isolating polymer pieces. During this process some glue were spilled on the TSA surface. When this was discovered the glue was tried to be removed, and most of it was, however, it proved nearly impossible to remove all the glue without damaging the TSA. Even though most of the glue was removed the corrosion area may be slightly different between the different test pieces, and thus there is uncertainties related to the corrosion rate (which is based on the area), therefore it is difficult to compare the different temperatures based on the corrosion rate.

Another drawback of using glue was that the test pieces were permanently fastened together, providing little to no flexibility in the setup. A experimental setup was requested with the possibility of separating the test pieces from each other during the experiment so that pieces may be removed during a certain amount of time, or replaced. This is not possible when the test pieces are glued together, as they had to be sawed free.

For internally heating the spools, oil, a heating element, a Mazurczak Electronic Temperature Controller and a aquarium air pump were used. The oil acted as a heating medium, transporting the heat from the heating element to the test pieces. The heating element delivered the heat to the oil, while, the Mazurczak Electronic Temperature Controller was used to control the temperature. The Mazurczak Electronic Temperature Controller used a temperature sensor to measure the temperature and apply heat when the temperature decreased below the set temperature. The aquarium pump pumped air through the spool, to circulate the oil to prevent temperature gradients within the pipe. The heat from the heating element was controlled by a temperature sensor immersed in the oil, and the power to the heating element was cut when the temperature sensor measure the set temperature. This also had some drawbacks. During the experiment at 30 ° C the air pump was by accident unplugged from it's power source, and the circulation of the oil stopped. This caused the temperature sensor, that was placed below the heating element, to be unable to register the correct temperature, and resulted in a significant temperature gradient, ultimately ruining the test. To improve this design, sand was suggested as a alternative for oil, removing the need for an air pump. New heating elements, with a longer heating zone was also purchased, to provide a smaller temperature gradient within the test spool.

The polarized potential (potential applied with the anodes), the free potential (corrosion potential of the non-polarized test spools) and the current requirement (current from the anodes to the thermally sprayed coating) were all monitored continuously. To measure the potentials mentioned above, a reference electrode has to be used. The reference electrode was connected to the seawater electrolyte through a saltbridge. During the experiment the saltbridge went dry, and potential data was lost. This was remedied in the Master Thesis by immersing the reference electrode directly into the seawater together with the test spool.

All the problems and limitations with the design mentioned above in this chapter triggered a redesign of the experimental design, which will be described in the Chapter 4.1.3. The principle of the design remained the same, where TSA coated pipes were internally heated and exposed to seawater, but some minor changes was applied.

## 4.1.2   Carbon Steel Substrate Experiment

From the specialization project it was clear that the corrosion potential for the TSA samples were lower than expected. A second experiment at no internal heating was therefore conducted. This experiment design was simpler than the others, and can be seen in Figure 4.1. Two different TSA samples was used in the experiment. One sample with UNS S31245 stainless steel substrate, and one sample with X65 carbon steel substrate, both with TSA applied with twin wire arc spraying. The purpose of the experiment was to see if the corrosion potentials from the low temperature experiments were realistic, and to see if there was any major difference based on the substrate that the TSA was sprayed onto.

V1 measured the corrosion potential of the TSA on carbon steel substrate, while V2 measured the corrosion potential of the TSA on the 254 SMO stainless steel substrate. No heating was applied to this experiment, meaning that the seawater temperatures was approximately 8 °C.
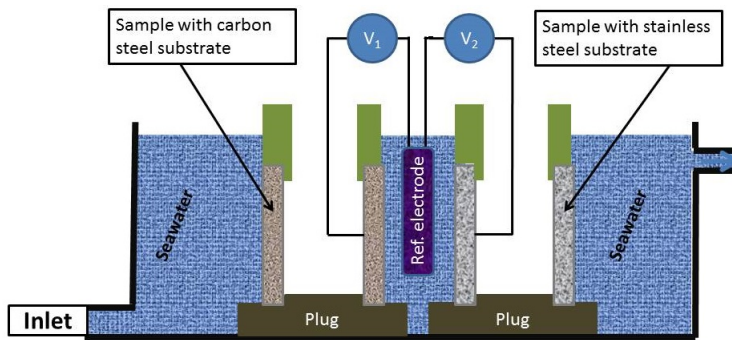
**Figure 4.1:** Experimental design for second experiment with no internal heating.

### 4.1.3 High Temperature Experimental Design

A major task in the Master Thesis was to improve on the experimental design, finding a more stable system of heating the samples, and to find a way of monitoring the temperature on the coating surface, and finding a way to be able to replace test piece during the experiment.

The old design was improved by just producing the spools in another way, by implementing O-ring gaskets instead of gluing, see Figure 4.2, and immersing the reference electrode directly into the same electrolyte, instead of counting on a saltbridge with a low reliability and by applying a new method of internally heating the spools.

The design where O-ring gaskets were used to provide sealing, was used for the higher temperature (50, 70 and 90 °C internal temperature). This had some added benefits of being able to take the test spools apart, when it was needed, and even replacing test pieces if desired. This production method was easier, and cheaper than the previous design, and is more flexible and easier to work with. The drawback of this production method is that the wall thickness of the isolation pieces must be increased to account for the pressure from the O-ring gaskets, thus reducing the inner diameter of the test spool, making it difficult to fit all the equipment in the spool. This caused some problems due to the heating elements having a larger diameter than expected, and some difficulties with fitting all the equipment into the spool.

The temperature was monitored by fastening thermocouples on the wall surfaces, both internal and external. See Figure 4.4. The thermocouple was glued to the surface in that position, with a small droplet of glue. The same was done on the internal pipe wall surface. The new design used in the Master thesis, for high temperature (50, 70 and 90 °C) is shown in figure 4.3

The new way of applying heating was done by changing the temperature control system. The reason for this was the way the Mazarczak controlled the temperature. The Mazurczak Electronic Temperature Controller shuts of all power to the heating element when the temperature rises above a set value, then applies heat until the temperature reaches the set values again. However, due to inertia in the system this caused the temperature to fluctuate around the set values, instead of holding a constant temperature.

To maintain a more constant temperature a Carroll & Meynell 1 Phase 720VA Variac,

**Figure 4.2:** Isolation piece with O-ring gaskets.
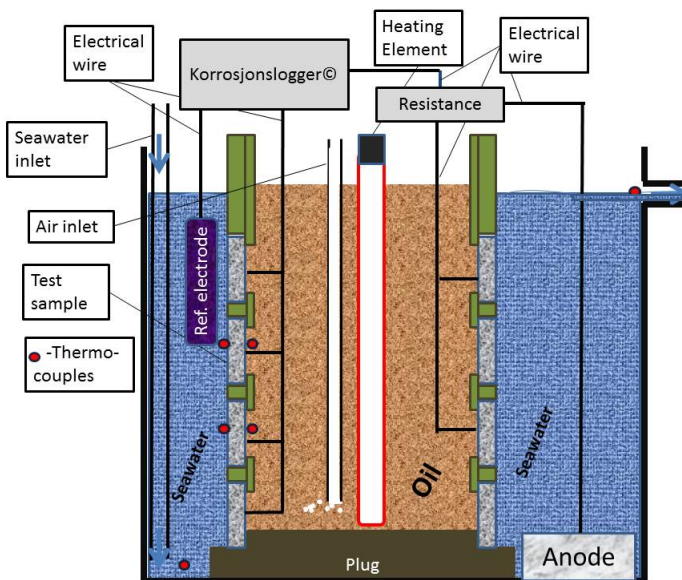


**Figure 4.3:** Schematic presentation of the experimental design used in the Master Thesis.

transformer was used. The Variac works by lower the voltage and by applying a constant ampere to the heating element. This means that the heating element applied a constant heat to the oil, instead of only applying heat in periods, as was the case with the Mazurczak Electronic Temperature Controller.

## 4.2 Experimental Set-up

This chapter describes the process of building and installing the experimental design at Sealab, Braatørkaia. The test spools were built in the corrosion laboratory in Perleporten, NTNU and at the adjacent workshop.

Pipes of steel with TSA were cut to 100 mm or 78 mm lengths. 100 mm were used for the lower temperatures and 78 mm were used for the high temperature spools. The difference in size was done purely for practical reasons, since different tanks were used in the different experiments.

Nine lengths of 1 m wire was cut, and bananas plug was fastened on one end of each wire, for each test spool. Two wires were then point welded onto the inside of each TSA test piece pipe and one wire was welded onto the anode. All the wires were marked so they could easily be identified after and during the manufacturing process, this was especially important with the old design where glue was used.

For the lower temperatures[1] bolts of polyurethane was cast at Silikonservice, using casting molds made at the IPM workshop. The polymer parts needed for the project was then machined from these bolts. The parts and the steel with TSA was glued together by Børge Holen and employees at Silikonservice in Trondheim, Norway, after wires had been welded to the steel.

For the higher temperatures[2] 1000 and 300 mm long Teflon[3] bolts with 70 and 80mm diameter respectively were ordered from Halting AS. The bolts were then machined to isolation pieces, top pieces and plugs, at the IPM Workshop. O-ring gaskets were ordered from Abra AS, and placed in the O-ring grooves machined into the Teflon pieces. The TSA test pieces were cut to 78 mm length, instead of 100 mm due to lower placement of the outlet of seawater in the tanks used for holding separate test spools.

The plug was installed on the bottom of the steel pipe that was to be the bottom pipe, and the wires from the bottom pipe were threaded through the isolation piece that was placed above the steel pipe. A new piece of pipe was place on top of the isolation piece, and a isolation pieces as added to this pipe as well. This was done until all four pieces created a test spool, and all the wires emerged from the top.

During the assembly thermocouples were glued to internal surface of two of the test pieces, so that the internal temperature could be monitored. When the test spool assembly was completed thermocouples were attached to the TSA surface of the two middle test pieces.

Figure 4.5 shows a photo of the experimental set-up for the high temperature experiments.

---

[1] No heating, 30°C and 40°C
[2] 50 °C, 70 °C and 90 °C
[3] Trade name for polytetrafluoreten.

**Figure 4.4:** Mounting of Thermocouple on TSA surface before applying glue.

To be able to do any measurements the test pieces had to be connected to the logging equipment. This was done as shown in Figure 4.6. The corrosion potential and polarized potential were measured between the test spools and a reference electrode (Ag/AgCl or SCE), and the current was measured as a function of potential over a known resistance (1 ohm).
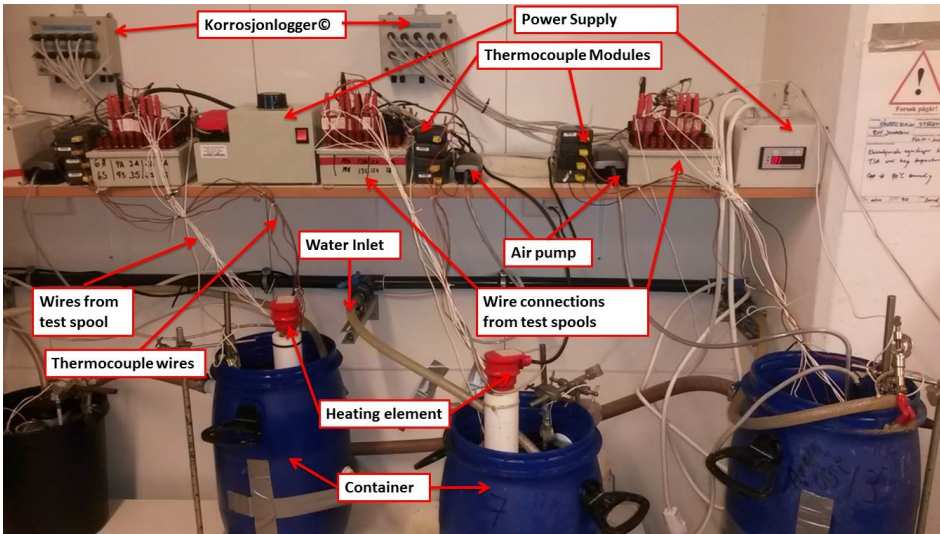
**Figure 4.5:** Photo taken of the experimental setup for the high temperature experiments at SINTEF Sealab Brattørkaia.
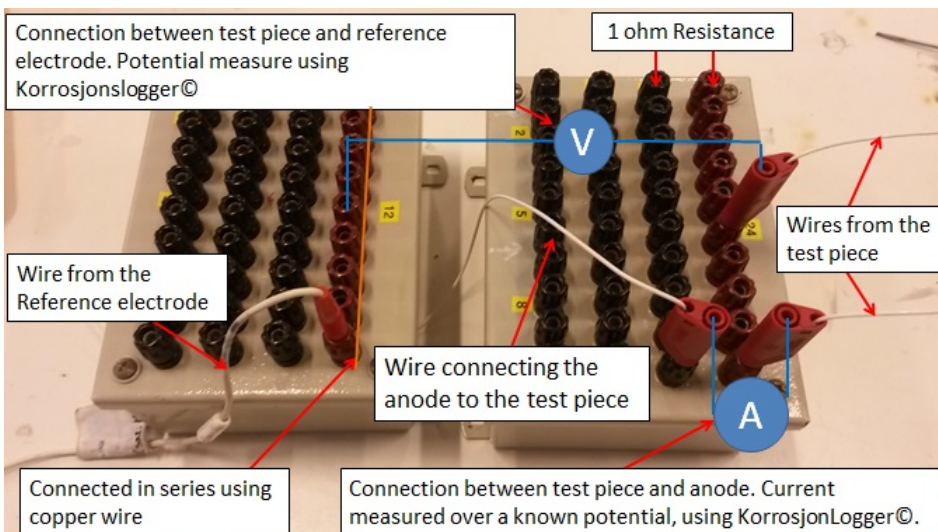


**Figure 4.6:** Picture explaining how the wires from the test pieces were connected to measure potentials and the current from the anodes.
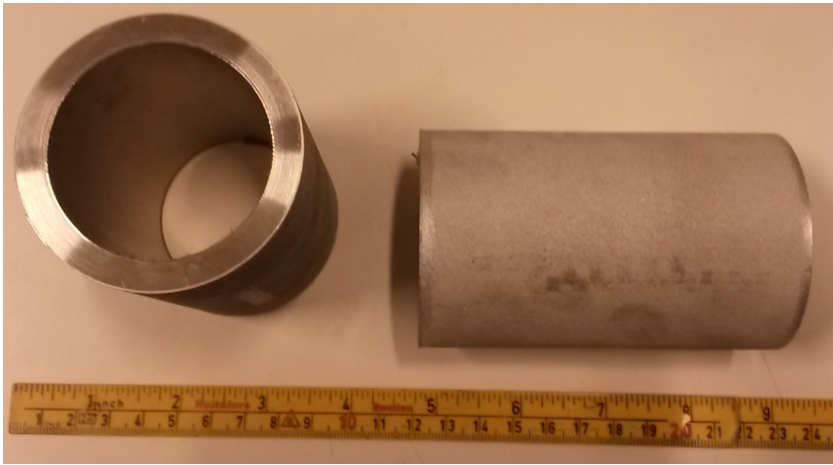
**Figure 4.7:** Picture of two typical test pieces used in this Thesis.

## 4.3 Experimental Conditions

The conditions which the TSA is exposed to during the experiments is described in this chapter.

### 4.3.1 Test Specimens

The test spools were delivered by Kvaerner Piping Technology. Two typical test pieces can be seen in Figure 4.7. The substrate is 254 SMO Austenistic stainless steel, UNS S31245, coated with AlMg5 TSA. The coating was applied at Scana, Vestby with twin-wire electric arc spray, in accordance with NORSOK M501. Before spraying the steel was blast-cleaned to Sa 3, with a roughness profile of Ra = 120 $\mu$m. The samples were hand sprayed to 200 $\mu$m, however it was reported that it was difficult to achieve a uniform thickness, so a thickness between 150 and 550 $\mu$m is to be expected.

Similar coatings have had adhesion between 15 and 25 MPa. A sealer was not applied. The test pieces were cut to 100 mm long for the three tests started in November 2013 and 78 mm for the tests started in March 2014, all pieces had a outer diameter of 61.4 mm.

Two of four TSA pieces was connected to an anode and achieved potentials close to -1050 mV vs Ag/AgCl. This is close to the potential of the anode potential, see Appendix B for technical for the anodes. The anodes used in this thesis were a Coral A-12-1 anode from Jotun, see Appendix B for technical data.

The carbon steel samples was X65 carbon steel coated with AlMg5 TSA.

All samples were washed in ethanol before exposure.

### 4.3.2 Seawater

Natural seawater from the Trondheimsfjord in Trondheim, Norway was used for this experiment. The water is pumped from 80 m depth. The seawater was slowly circulated around

the test. The inlet temperature of the seawater varied between 7 and 10 °C. The outlet temperature varied from experiment to experiment and was dependent on the internal heat of the test spool, with the higher temperatures resulting in a higher outlet temperature.

The flow rate of the seawater was not measured, but roughly estimated through some simple calculations. The inlet hose to the test containers were placed in a 2 L beaker and the time the water flow used to fill 1 L was timed. This yielded a rough estimate of the volumetric flow. The volumetric flow rate was divided on the cross section area of the container, and this gave the estimated flow rate in $m/s$. The flow rates were very low, at approximately $6 * 10^{-5} m/s$, and is the equivalent of approximately 1 L of water replaced every 5 minutes.

### 4.3.3 Temperature

Table 4.1 shows the different internal temperatures used in this experiment, and their corresponding external surface temperatures.

**Table 4.1:** Different surface temperatures obtained by the different internal temperatures.

| Internal Temperature [°C] | Surface Temperature [°C] |
|:---:|:---:|
| No internal heating | 10 |
| 30 | 15 |
| 40 | 18 |
| 50 | 25 |
| 70 | 45 |
| 90 | 60 |

The surface temperature was monitored continuously for 50 °C and up, and measured manually for the lower temperature test spools. The temperature was measured using thermocouples connected to Fluke 80TK Thermocouple Module. The thermocouple was calibrated by dipping the thermocouples in ice-water and then boiling water to get the right 0-100 °C interval.

For internally heating of the test spools three different heating mediums were tested. Oil, sand and a mix of oil and sand. In the end oil was used for all the experiments. The sand that was tested had too low thermal conductivity and ended up acting as insulation, preventing the heating element to properly heat the spools. Consequently the temperature of the heating element needed to be very high for the temperature on the specimen wall to obtain the correct temperature.

The combination of high temperature and small space within the test spool caused some problems. Thermocouples and wires came into contact with the very warm heating element leading to destroyed equipment and failed experiments. In the end all experiments were completed using oil and the heating medium.

Oil and sand did not work well because sedimentation occurred over time, and all the sand accumulated at the bottom, and only oil was on the top. This could probably work

better if the right oil/sand mixing ratio was discovered, but this was not done in this thesis, due to time restraints.

## 4.4 Test Procedure

The procedure for finding the corrosion rate, current density requirement and potential for the TSA samples are described in this chapter. The chapter is divided into two parts, were the first part is dedicated to measuring the current density requirement and the potential of the test spools. The second part is dedicated to describing the procedure for finding the corrosion rates of the spools.

### 4.4.1 Current Density Requirement and Potential Measurements

The test spools with lowest internal temperature[4] was begun in the specialization project in November 2013. Three different test spools were immersed in seawater at the same time. Initially the potentials off all the different test pieces were measured with a multimeter, the current demand from the anodes was also measured on the polarized test pieces. After it was confirmed that the test set-up was installed correctly, the KorrosjonsLogger system was connected, and continuous measurements could be conducted. The Korrosjonslogger system measured the corrosion potential, the polarized potential and the current requirement from the anodes. The Korrosjonslogger system logged the potential, current and temperature once every hour.

After one day of measuring, heating was applied for two of the spools. The one day waiting period was to ensure that the test set up was stable. One spool was heated to 30 °C and the other to 40 °C.

Initially temperature measurements were conducted at the bottom of the test spool and at the top to ensure that the temperature was equal inside the spools. Air was pumped to the bottom of the spools using a aquarium air pump. This was done to prevent temperature gradients within the spool.

Seawater temperature was continuously measured at both inlet and outlet of the container. This meant that the temperature was measured at the top of the container and at the bottom.

The spools with higher temperature (50-90 °C) were placed in separate containers. This made it possible to regulate the flow rate of the water, as a way to manipulate the temperature on the surface of the TSA. The test start-up procedures was similar for all temperatures.

### 4.4.2 Corrosion Testing

Corrosion rate measurements were done on the test pieces not connected to the anodes, i.e freely corroding. Tests were done at all temperatures, approximately once a week.

Figure 4.8 shows a schematic presentation of the set-up for the corrosion testing. $V_1$ measure a potential over a known resistance, which provides the current in the circuit,

---

[4]no internal heating, 30 and 40 °C internal temperature.
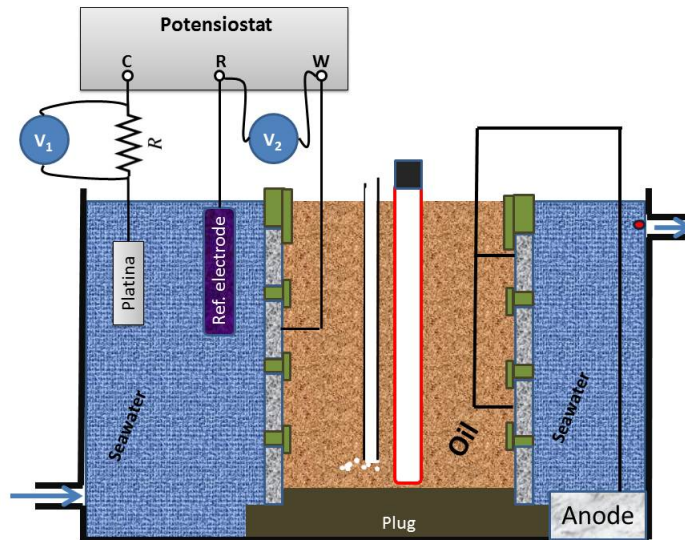
**Figure 4.8:** Schematic presentation of the test set-up for lPR and Polarization curves testing.

and $V_2$ shows the potential of the working electrode. The working electrode is one of the TSA samples in the test spool which is not polarized by an anode. $V_1$ is used for measuring the current, and $V_2$ is used for controlling the potential, so the potential of the working electrode can be manipulated so LPR measurements and polarization curves can be obtained.

LPR measurements and polarization curves were drawn to estimate the corrosion rate. The LPR measurements were obtained as following: The Open circuit potential (OCP) was first measured. Then the specimen was polarized 10 mV in cathodic direction using a potensiostat. The potential was held at 10 mV cathodic direction for 5 minutes before the current was measured. Then the potensiostat was put on stand by until the specimen stabilized back at the original measured OCP. After the specimen had stabilized the specimen was polarized 10 mV in anodic direction and held there for 5 minutes before the current was noted.

When the potential had stabilized to OCP after the LPR measurements the polarization curves were obtained. The curves were obtained by polarizing the specimen in cathodic direction in several steps. There were 6 steps total, with 3 steps of 10 mV and 3 steps of 50 mV, giving a total of 180 mV polarization in cathodic and anodic directions. The cathodic direction was obtained first. At each step the potential was held for 5 minutes before noting the current. After the cathodic direction was obtained the specimen was left to freely corrode for atleast 30 minutes for the specimen to recover to OCP. When the samples had recovered they were polarized in anodic direction using the same procedure as in cathodic direction.

The polarization curve gives a graphical solution to the corrosion rate, while the LPR gives a value for the polarization resistance of the samples. The polarization resistance and

the tafel constant, $b_a$ and $b_c$ obtained from the polarization curves are used to calculate the corrosion rate using the Stern Geary equation, Equation 2.8. The results from both tests where compared, and iterated so that the result from the polarization curves and LPR yielded the same result. This gives a corrosion rate in $mA/m^2$, and this was converted to $\mu m/year$ using equation 2.10 showed in Chapter 2.2.3. The parameters used for corrosion rate calculations are shown in Table 4.2

**Table 4.2:** Parameters used for corrosion rate calculations.

| Parameters | Value | Unite |
|---|---|---|
| Area (100m spool) | 0.0193 | $m^2$ |
| Area (78mm spool) | 0.0150 | $m^2$ |
| Molar Mass of Coating | 26.85 | $g/mol$ |
| Coating Density | 2.65 | $g/cm^3$ |
| Faraday's Constant | 96485 | $As/mol$ |
| Valency Number of Ions | 3 | |

## 4.5 Post Exposure Analysis

This chapter is dedicated to describing the post exposure analysis of the samples. Two types of analysis is performed, thermal conductivity measurements and an SEM analysis. The thermal conductivity analysis is performed to investigate if the thermal conductivity has been affected by the exposure, while the SEM analysis is done to investigate the amount and type of calcareous which precipitates on TSA during the exposure.

### 4.5.1 Thermal Conductivity Testing

Testing of thermal conductivity of the samples were preformed after the the TSA samples had been exposure to seawater. A unexposed samples was also measured to be used as a reference. The thermal conductivity was measured using Hot Disk TPS 2500 S instrument.

A sensor was placed on top of the pipe sample and covered with an insulating material that was strapped tightly to the pipe sample. This was done to avoid thermal influences from the environment.

There was a waiting period of 3 hours between each measurement, because the insulating material needed time to reach equilibrium with the lab temperature. This has to be done because the insulating material gets heated during the test.

The parameters used in the tests are shown in Table 4.3. The thermal conductivity is the mentioned in the table is the conductivity to the stainless steel substrate.

### 4.5.2 Scanning Electron Microscope

The samples were rinsed in tap-water immediately after the spool was removed from the seawater. Then the samples were cut into smaller samples that could fit into the Scanning electron microscope (SEM), and then washed in ethanol before taken to the SEM. A Hitachi S-3200N SEM was used in this thesis.

**Table 4.3:** Parameters used for thermal conductivity measurements.

| Parameter | Value | Unite |
|---|---|---|
| Thermal Conductivity of Substrate | 10 | $\frac{W}{m^\circ C}$ |
| Specific Heat | 485 | $\frac{J}{kg}$ |
| Heating Power | 1000 | $mW$ |
| Heating Time | 4 | $s$ |
| Backgrond Conductivity | 30 | $\frac{mW}{m^\circ C}$ |
| Sensor Size (Radius) | 6.65 | $mm$ |

For investigating the coating microstructure 3 samples were grinded with SiC paper with 320 grit and 2400 grit, then polished using Struers MDDac plates with diamond grain size from 3 $\mu$m to 1 $\mu$m.

To investigate if any calcareous layers were deposited on the TSA coatings, the test samples were analysed in a SEM. Energy-dispersive spectroscopy (EDS) was used to find the elements present on different points on the samples. Calcareous deposits are not electrical conductive, and therefore are only shown as white areas on pictures taken in scanning electron microscopes. These areas were particularly investigated with the EDS.

# Chapter 5

# Electrochemical Results

In this chapter the electrochemical results obtained from the test spools during exposure is shown. This includes the current density requirement, corrosion potential, polarized potential and the corrosion rate for all the different temperatures used in this thesis. The polarized potential is the potential for the TSA samples connected to an anode.

## 5.1 Low Temperature Experiments

The results from the low temperature[1] and high temperature[2] experiments are shown separately, because the results from the low temperature experiments differ from what was expected from the literature and from other experiments. However, the results are what was measured in the experiments and therefore shouldn't be discarded.

Figure 5.1, 5.2 and 5.3 show the development for the corrosion potential, the polarized potential and the current density requirement over time for the spools with no internal heating, 30 ° C and 40 ° C internal temperature respectively. The graphs are presented this way to show how negative the corrosion potential is for the TSA, which indeed is lower than the polarized potential for most of the test, leading to a negative current density requirement for most of the experiment.

A Saturated calomel electrode was used for measuring the potentials, however the results have been converted to show potentials as they would have been against a Ag/AgCl reference electrode. It is assumed that there is a constant convertion factor between a SCE electrode and an Ag/AgCl electrode. According to SI Chemical Data [62] the convertion factor is 44 mV. This means that a value of 44 mV is added to the potential values obtained in the low temperature experiments.

The spool without internal heating achieved a corrosion potential of -1150 mV Ag/AgCl, 100 mV more negative than the anode potential, but ended at -1036 mV Ag/AgCl when the experiment is ended after 170 days exposure. The potential of the samples connected

---

[1]40 °C internal temperature and below.
[2]50 °C internal temperature and p.

to an anode was approximately -1050 mV Ag/AgCl for most of the experiment for all temperatures.

The experiment with 30°C internal temperature was stopped after approximately 70 days, due to some problem with the temperature control, more on this can be found in the discussion.

The spool with 40°C internal temperature had a more positive potential than the other spools with the lowest potential registered at -1078 mV vs Ag/AgCl. The corrosion potential was around -1070 mV Ag/AgCl from day 20 to day 120, which is the major part of the experiment.
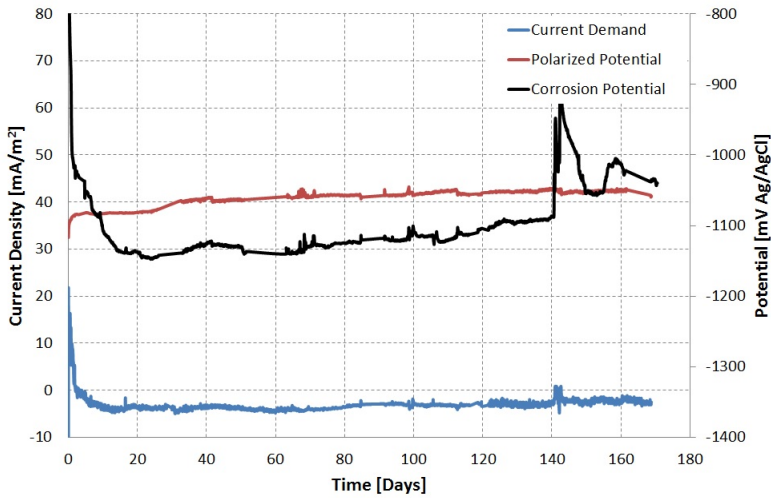


**Figure 5.1:** Current density, corrosion potential, and polarized potential development over time with no internal heating
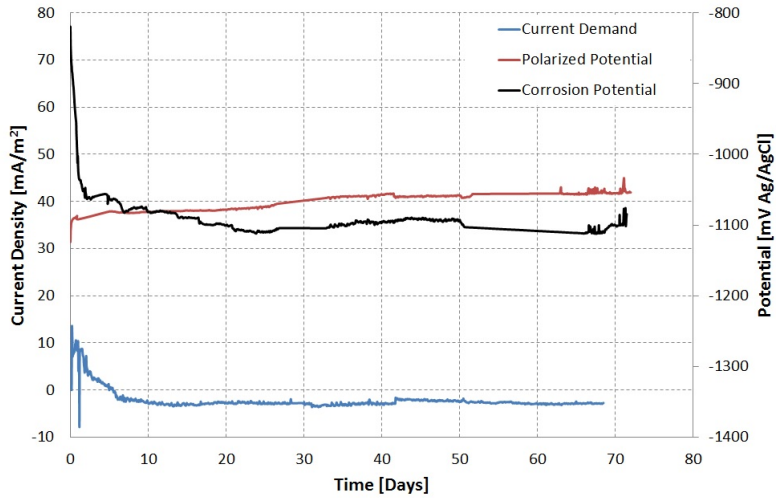
**Figure 5.2:** 30 °C Internal temperature. Current demand, polarized potential, and corrosion potential as a function of time.
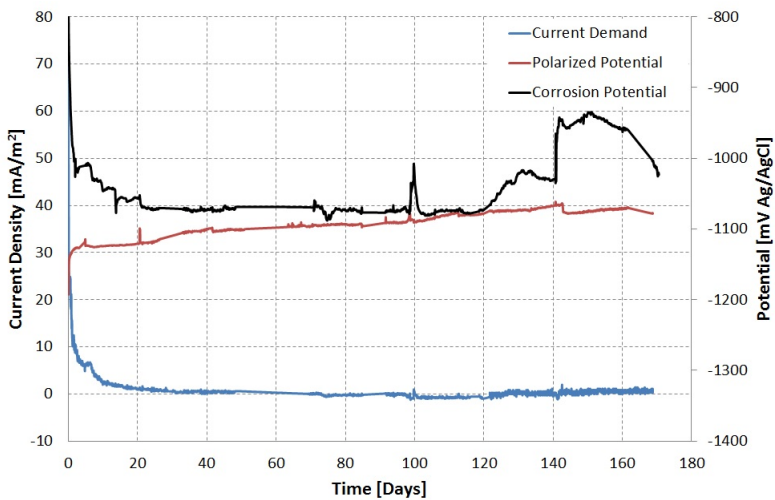


**Figure 5.3:** Current density and corrosion potential development over time with 40 °C Internal temperature

## 5.2 High Temperature Experiments

Figure 5.4, 5.5 and 5.6 shows the current density, polarized potential and corrosion potential for the high temperature experiments. The reason for presenting the results in this way is to show how the corrosion potential develops relative to the polarized potential.

A clear difference between these results and the results obtained in the low temperature is the corrosion potential and subsequently the current density requirements. As can be seen from the figures the corrosion potential is higher than the polarized potential when the tests is completed, and therefore the current density is positive.

The potential for the samples connected to the anodes is also here approximately -1050 mV Ag/AgCl for most of the experiments for all temperatures.
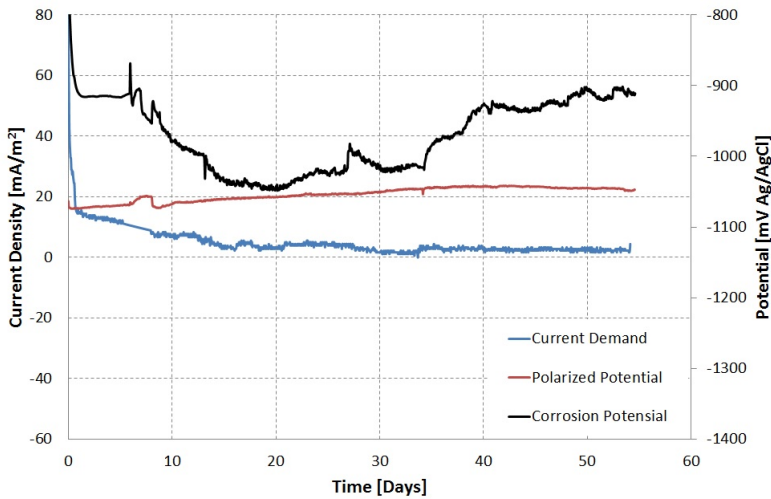


**Figure 5.4:** 50 °C Internal temperature. Current density, polarized potential and corrosion potential as a function of time.
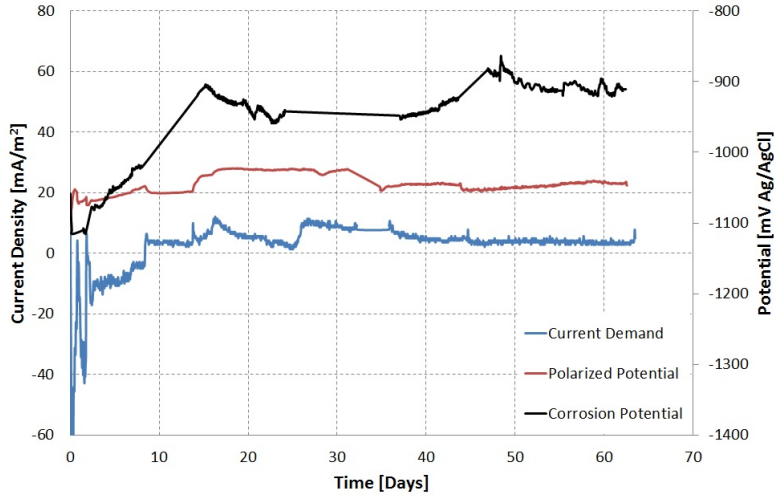
**Figure 5.5:** 70 °C Internal temperature. Current density, polarized potential and corrosion potential as a function of time.
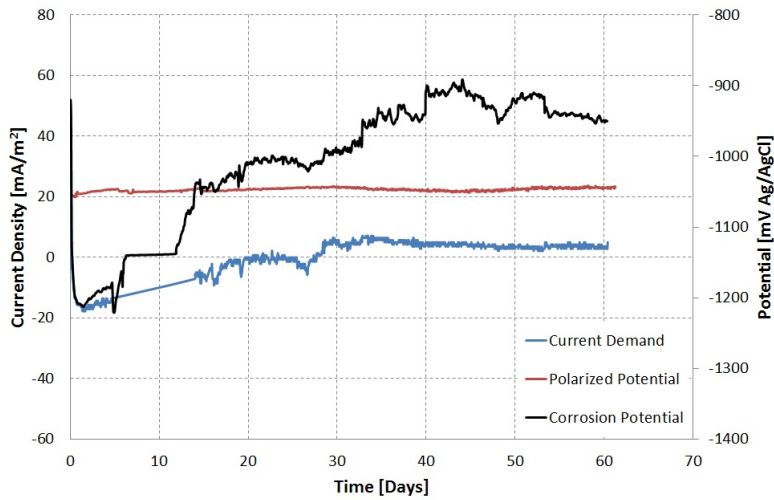


**Figure 5.6:** 90 °C Internal temperature. Current density, polarized potential and corrosion potential as a function of time.

## 5.3 Current Density Comparison

In this chapter the current density requirement for the spools connected to anodes is presented. The current density requirements for the lower and higher temperatures spools are shown separate, because it is not certain that they are comparable to the higher temperature spools due to the low corrosion potential the low temperature spool experienced.

### 5.3.1 Low Temperature

In this chapter the current density requirements for the spool without internal heating, and the spools with 30 and 40 °C is presented. Figure 5.7 shows the development of the current density for the low temperature experiments. The current density decreases rapidly and becomes negative for for spool without heating and for the spool with 30 °C internal temperature after about 5 and 10 days respectively. The spool with 40 °C internal temperature have a period of negative current density between day 70 and 120 of exposure.

The absolute current density values are small for all three spools. The spool with no internal heating had a small current density demand, with an average of -2.4 $mA/m^2$ the last week of exposure. The spool with 30°C internal temperature had an average current density demand was -2.7 $mA/m^2$ the last week of exposure. Note that the spool with 30°C internal temperature was exposed for a shorter time than the other spools, and that the values aren't directly comparable. The spool with 40°C internal temperature had an average current density demand of 0.60 $mA/m^2$ for the last week of the exposure.
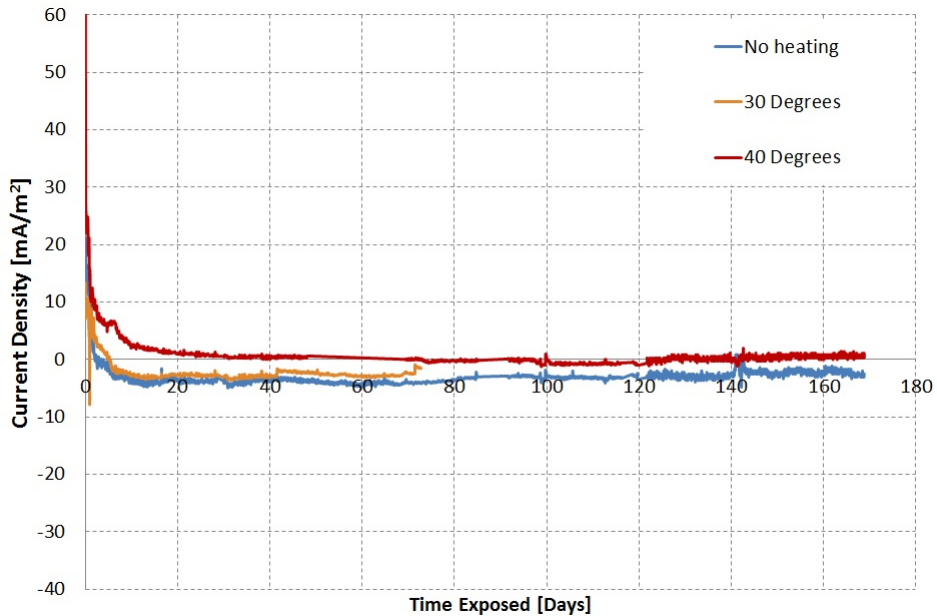


**Figure 5.7:** Current density demand development over time for TSA polarized connected to an anode with no internal heating, 30 and 40 ° C internal temperature.

## 5.3.2  High Temperature

Figure 5.8 shows the development of current demand over time for the 50, 70 and 90 ° C internal temperature. The current density requirement presented here is current from the anodes to the spools connected to the anodes. The current demand is initially negative for the 70 and 90 ° C TSA samples, but becomes positive after about 9 and 20 days respectively. The current demand stabilizes at 3, 4 and 5 $mA/m^2$ for 50, 70 and 90 ° C respectively.

The current density for the spool with 90 °C have a high negative current demand when the corrosion potential is lower than the polarized potential, and becomes higher than the 50 and 70 °C when the corrosion potential stabilizes at a more positive potential than the polarized potential.
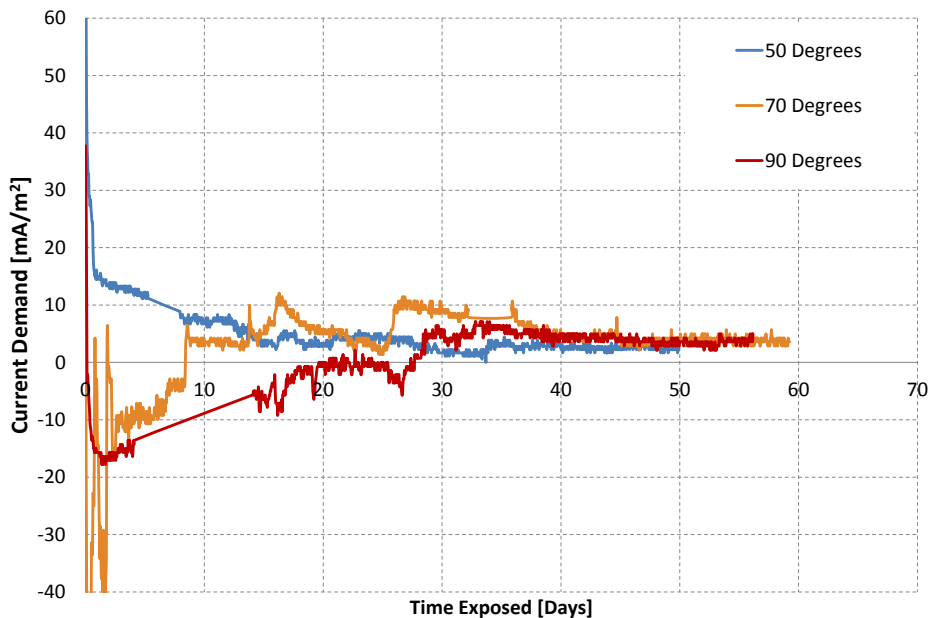


**Figure 5.8:** Current density demand development over time for TSA polarized connected to an anode with 50, 70 and 90 ° C internal temperature.

## 5.4 Corrosion Potential Comparison

In this chapter the corrosion potential for the freely corroding spools is presented. As with the current density requirement the results are divided into two parts, because of the unexpected results from the lower temperature spools.

### 5.4.1 Low Temperature

Figure 5.9 shows the development of the corrosion potential for TSA at the three lowest temperature over time. The corrosion potential rapidly falls for all temperatures and stabilized between -1050 and -1150 mV Ag/AgCl. After 140 days the potential increases and is between -1020 and -1050 mV Ag/AgCl
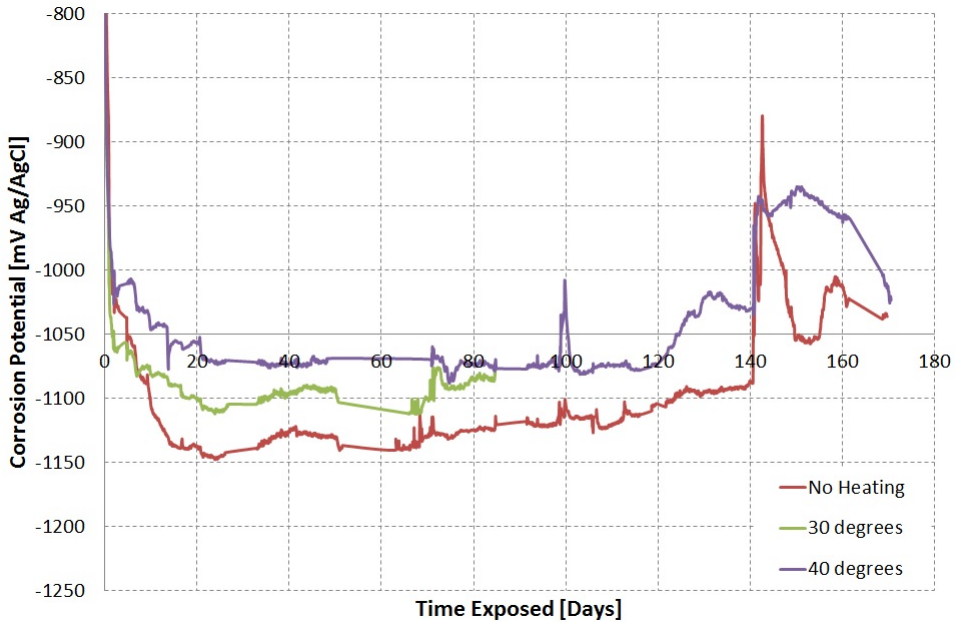


**Figure 5.9:** Development of corrosion potential of TSA exposed to seawater with no internal heating, and 30 and 40 $^\circ$ C internal temperature.

### 5.4.2 High Temperature

Figure 5.10 shows the development of corrosion potentials over time for the high temperature spools. The corrosion potential for the lower temperature spools are not shown here as it is not certain that they are comparable.

The corrosion potential is initially very low for the spool with 70 and 90 °C internal temperature with -1115 and -1207 mV Ag/AgCl. The corrosion potential of the 50 °C

internal temperature spool is not initially very low, but becomes more negative over time, reaching -1050 mV vs Ag/AgCl after 20 days.

After approximately 40 days the corrosion potentials stabilizes at approximately -990, -910 and -940 mV Ag/AgCl for 50, 70 and 90 °C internal temperature respectively.
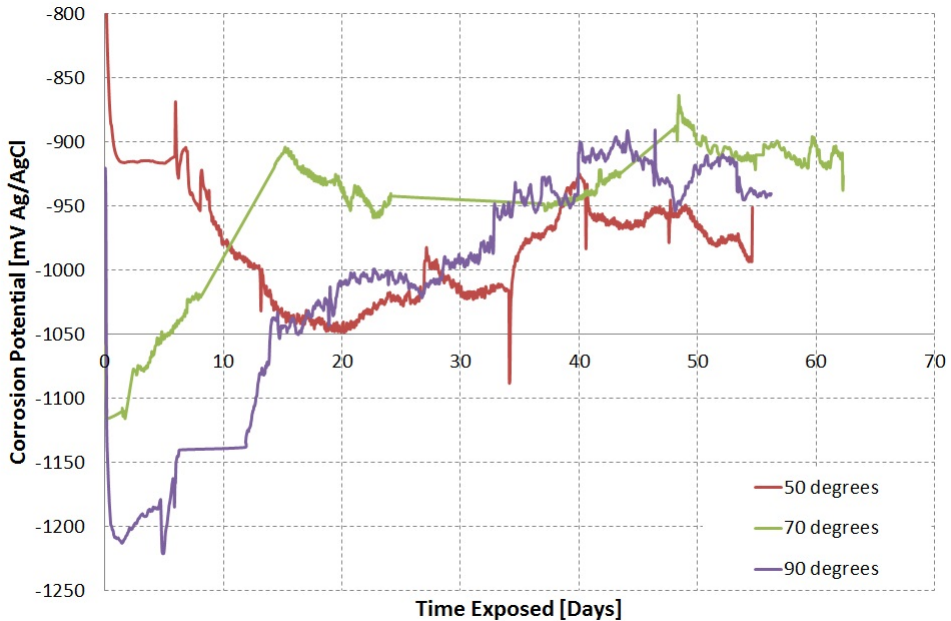


**Figure 5.10:** Development of corrosion potential of TSA exposed to seawater with 50, 70 and 90 ° C internal temperature.

### 5.4.3   Carbon Steel Substrate Experiment

Due to the low corrosion potential measured in the initial experiments at low temperatures a simple experiment was started with no heating to try to replicate the results. Two different sample were used in the test, one with UNS S31245 stainless steel substrate, and one with carbon steel substrate. The reason for the different substrates was to investigate if the substrate influenced the corrosion potential in any way. The results from this experiment can be seen in Figure 5.11. A comparison with the original corrosion rates obtained is also included.

Initially the corrosion potential of the two sample developed slightly differently, where the corrosion potential of the stainless steel sample falls faster than the carbon steel sample. However, after approximately 40 days both corrosion potentials stabilize at -1000 mV Ag/AgCl.

The corrosion potential from the original experiment without internal heated is included in Figure 5.11 to show difference in potential between the experiments.
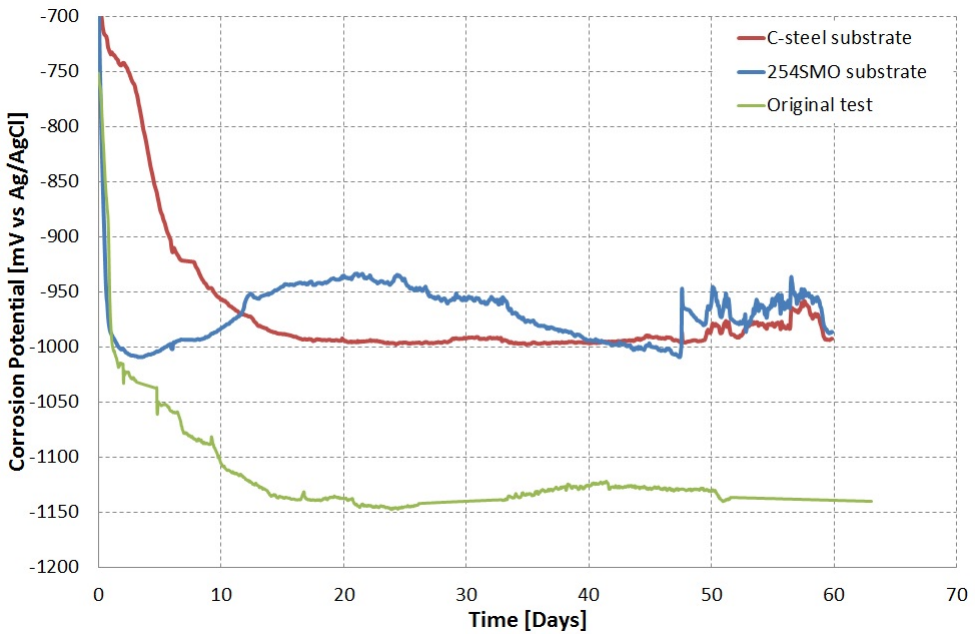
**Figure 5.11:** The development of corrosion potential over time for TSA on UNS S31245 stainless steel and X65 carbon steel without heating in seawater.

## 5.5 Corrosion Rate

The development of the corrosion rate in $\mu m/year$ over time for all the temperatures are shown in Figure 5.12. The corrosion rates have been calculated based on LPR measurements and Stern-Geary, Equation 2.8, and converter to $\mu m/year$ with Equation 2.10, shown in Chapter 2.2.3. The tafel-constants were obtained from the polarization curves obtained during the experiment, by finding the slope of the asymptotes of the polarization curves as explained in Chapter 2.2.3. The LPR values can be found in Appendix D, and the corresponding polarization curves in Appendix E.

The graphical solution from the polarization curves were compared to the results from the Stern-Geary equation. The overvoltage curves from the polarization curves were then adjusted so that the Stern-Geary equation and the graphical solution were within 10 % of each other.

Initially the corrosion rate is highest with 50, 34 and 31 $\mu m/year$ for 90, 70 and 50 °C internal temperature respectively. At the last day of exposure the corrosion rate is 8, 4 and 3 $\mu m/year$ for 90, 70 and 50 °C internal temperature respectively.

For the low temperature spools the corrosion rate is initial between 25 and 30 $\mu m/year$, and decreases to 2 $\mu m/year$ after 150 days exposure.
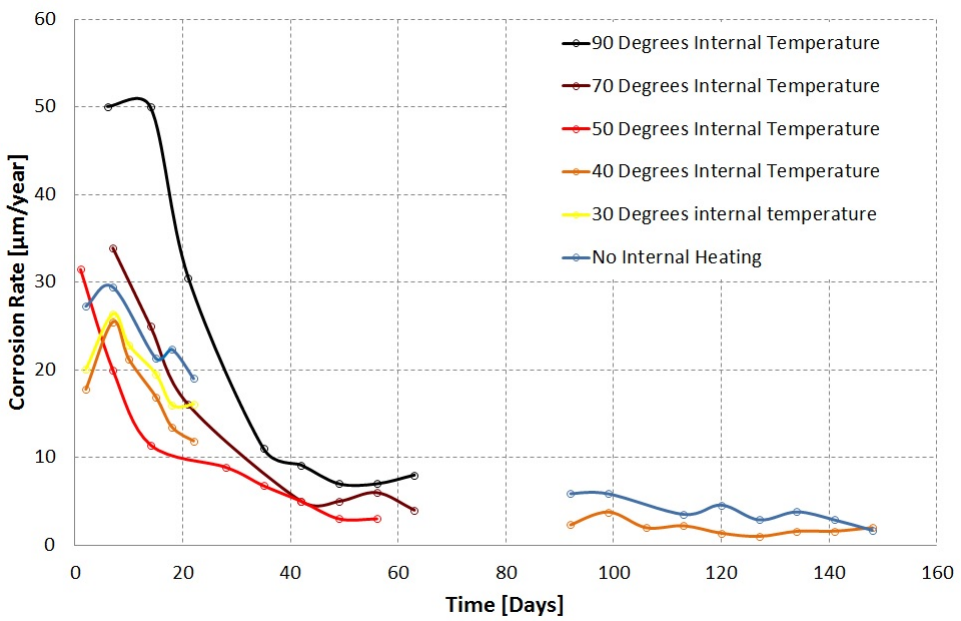
**Figure 5.12:** The development of corrosion rate as a function of exposure time.

# Chapter 6

# Post Exposure Analysis Results

In this chapter the results from the analysis done after the exposure is presented. The chapter is divided into three parts. Chapter 6.1 presents evidence of blistering in the TSA coating. Chapter 6.2 presents the evidence of calcareous deposits based on analysis done in the SEM, and Chapter 6.3 shows the results from the thermal conductivity measurements.

## 6.1 Visual Observations

On the test spool with the highest internal temperature (90 ° C) blistering was seen on one of the test spools that was freely corroding in seawater. The blisters can be seen in Figure 6.1. No other test samples experienced any blistering.



**Figure 6.1:** Photo of blisters in TSA exposed to seawater for 65 days with 90 ° C internal temperature.

Figure 6.2 shows a photo of a blister that was removed with a knife. The blister was easily removed by scraping it with the knife. This indicates poor adhesion to the substrate, and indeed it looks like the entire coating was removed exposing the substrate to the environment.



**Figure 6.2:** Photo of removed blistered on TSA exposed to seawater for 65 days 0 ° C internal temperature.

## 6.2 EDS and SEM Analysis

In this chapter the evidence of calcareous deposits are presented. The evidence is mainly based on EDS analysis of the TSA surface, and the results are shown in this chapter. The EDS spectrums can be seen in Appendix H.

### 6.2.1 Coating characterization

Table 6.1 shows the results of a EDS analysis, and is used as a reference for the exposed samples. Figure 6.3 shows a SEM photo of the unexposed sample and the area from which the EDS analysis were done. As expected there is no Ca present for the unexposed sample.

Figure 6.4 shows a SEM photo of a grinded and polished TSA surface. Table 6.2 shows the results from the EDS analysis. As can be seen from Figure 6.4 there are huge pores in the TSA coating with some intermetallic particles in a aluminium matrix.

Figure 6.5 shows a SEM photo of large pore found on a polish TSA coating sample. The pore was measured to be 67 $\mu m$ across.
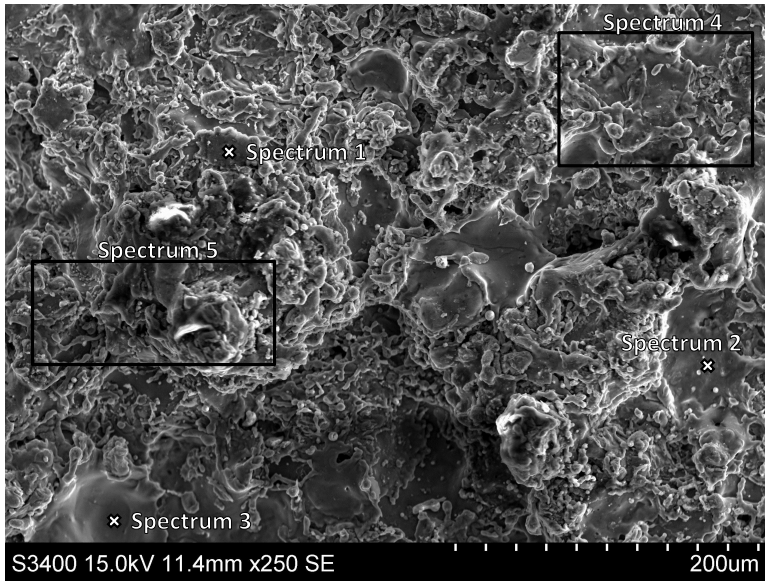
**Figure 6.3:** SEM photo of a unexposed TSA surface.

**Table 6.1:** Results of EDS from non-exposed specimen.

| Element [wt%] | Spectrum 1 | Spectrum 2 | Spectrum 3 | Spectrum 4 | Spectrum 5 |
|---|---|---|---|---|---|
| C | 8.25 | 4.87 | - | 18.42 | 31.44 |
| O | 3.5 | 2.3 | 2.72 | 7.48 | 10.21 |
| Mg | 2.93 | 2.04 | - | 2.43 | 1.86 |
| Al | 84.92 | 90.11 | 97.28 | 69.66 | 53.48 |
| Fe | 0.4 | 0.67 | - | 0.8 | 1.52 |
| Cr | - | - | - | 0.3 | 0.26 |
| Ti | - | - | - | 0.22 | 0.6 |
| Ag | - | - | - | 0.69 | 0.67 |
| Total | 100 | 100 | 100 | 100 | 100 |

**Table 6.2:** EDS analysis of grinded and polished TSA surface.

| Element [wt%] | Spectrum 1 | Spectrum 2 | Spectrum 3 | Spectrum 4 | Spectrum 5 | Spectrum 6 | Spectrum 7 |
|---|---|---|---|---|---|---|---|
| C | - | 5.24 | 6.35 | 1.93 | 6.55 | 2.32 | 4.21 |
| O | 0.70 | 1.62 | 4.59 | 0.80 | 6.18 | 1.44 | 1.95 |
| Al | 95.6 | 93.14 | 89.06 | 92.91 | 86.62 | 95.29 | 92.71 |
| Mg | 3.70 | - | - | 4.35 | 0.65 | 0.95 | 1.13 |
| Ca | - | - | - | - | - | - | - |
| Fe | - | - | - | - | - | - | - |
| Other | - | - | - | - | - | - | - |
| Total | 100 | 100 | 100 | 100 | 100 | 100 | 100 |
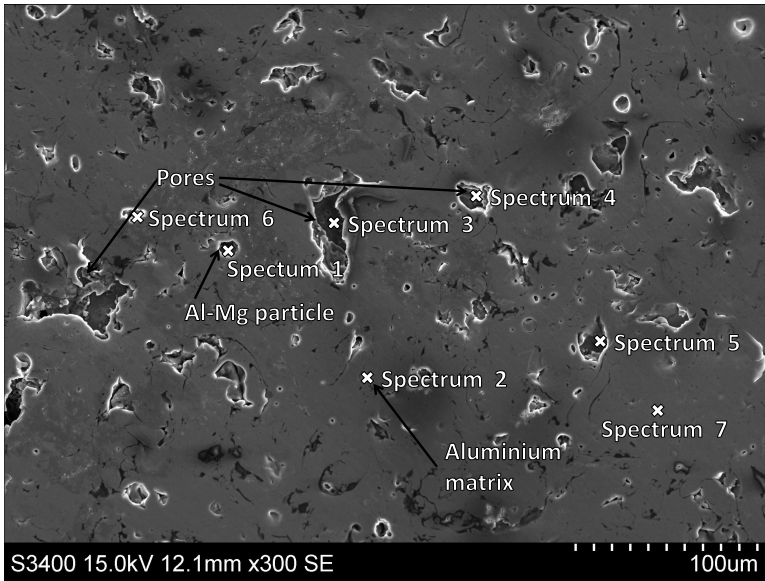
**Figure 6.4:** SEM photo of a grinded and polished TSA surface.
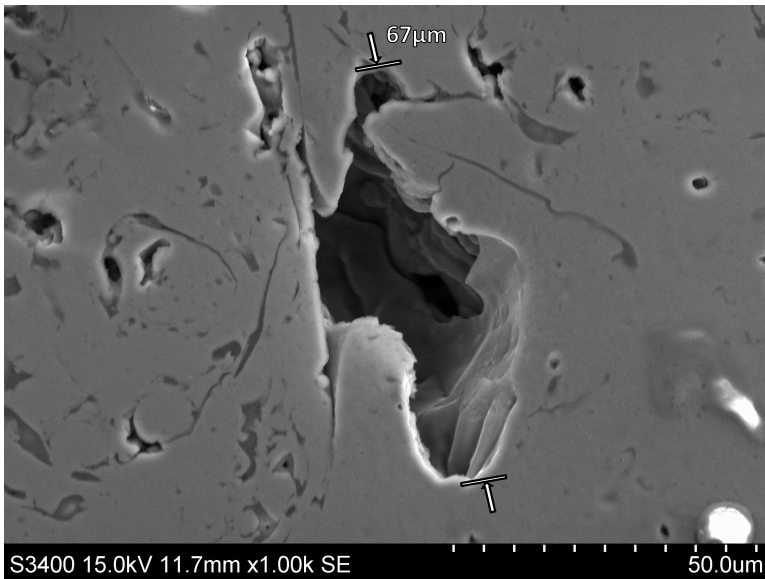


**Figure 6.5:** SEM photo of a polished TSA coating with size measurement of pore.

## 6.2.2   No Internal Heating

Figure 6.6 shows a SEM photo of TSA coating surface connected to an anode and exposed to seawater for 170 days. The positions of the EDS analysis is also shown in the SEM photo.

Table 6.3 shows the EDS results. The main difference from the non-exposed sample is the increase of Ca. The elements included in the "Other" row is trace elements like S, P, Cl, K.

Only small spots of non-conductive areas where discovered on the samples at these temperature.
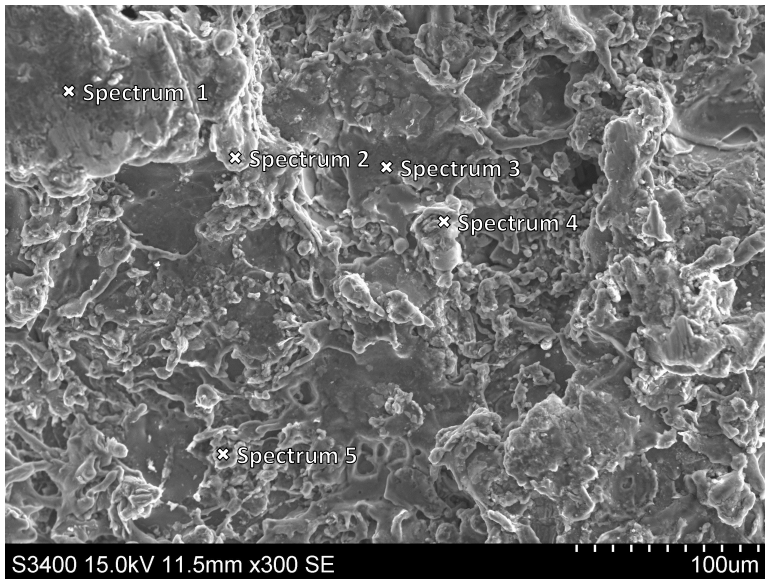


**Figure 6.6:** SEM photo of a TSA coating surface connected to an anode and exposed to seawater 170 days with no internal heating.

**Table 6.3:** Results from EDS analysis of a TSA coating surface connected to an anode and exposed to seawater 170 days with no internal heating.

| Element [wt%] | Spectrum 1 | Spectrum 2 | Spectrum 3 | Spectrum 4 | Spectrum 5 |
|:---:|:---:|:---:|:---:|:---:|:---:|
| C | 16.24 | 14.27 | 7.75 | 14.05 | 5.6 |
| O | 19.74 | 27.42 | 9.6 | 16.46 | 7.05 |
| Al | 61.12 | 53.13 | 79.63 | 66.14 | 85.09 |
| Mg | 1.15 | 2.22 | 2.77 | 2.94 | 0.75 |
| Fe | - | 0.91 | - | - | 0.8 |
| Ca | 1.09 | 1.13 | 0.25 | 0.41 | 0.71 |
| Other | 0.65 | 0.92 | - | - | - |
| Total | 100 | 100 | 100 | 100 | 100 |

Figure 6.7 shows a SEM photo of TSA exposed to seawater, freely corroding for 170 days with no internal heating. Table 6.4 shows the results from the EDS analysis of the sample. Here the iron content is shown, as well, as it is known that intermetallic particles in aluminium often contains iron. The major difference between the EDS results from the exposed sample and the reference is the high Ca and Fe amount in spectrum 2.
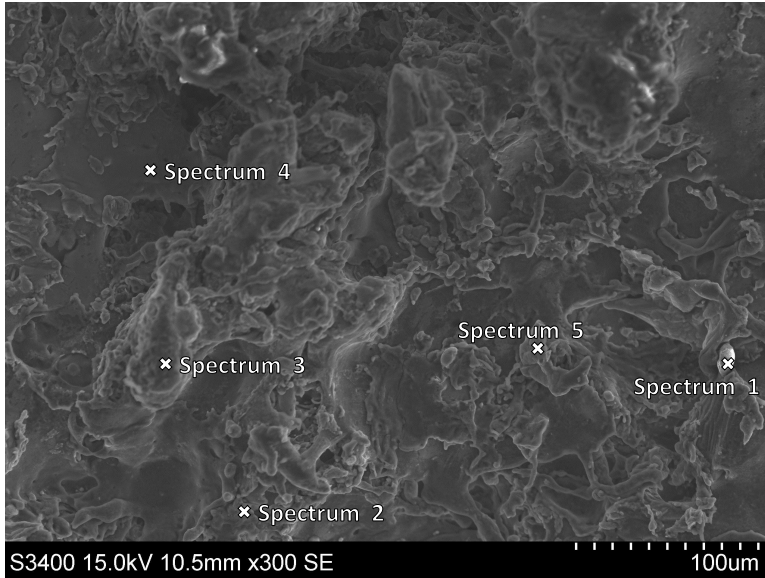


**Figure 6.7:** Sem photo of TSA surface freely corroding in seawater for 170 days with no internal heating.

**Table 6.4:** Results from EDS analysis of TSA exposed at seawater temperature for 170 days, freely corroding.

| Element [wt%] | Spectrum 1 | Spectrum 2 | Spectrum 3 | Spectrum 4 | Spectrum 5 |
|:---:|:---:|:---:|:---:|:---:|:---:|
| C | - | 6.54 | 18.74 | 6.49 | 7.63 |
| O | 37.44 | 23.58 | 24.19 | 3.75 | 7.13 |
| Al | 62.56 | 48.58 | 54.7 | 86.69 | 82.29 |
| Mg | - | 1.64 | 1.63 | 3.07 | 2.60 |
| Fe | - | 3.23 | - | - | - |
| Ca | - | 11.5 | 0.74 | - | 0.34 |
| Other | - | 4.94 | - | - | |
| Total | 100 | 100 | 100 | 100 | 100 |

### 6.2.3  30 °C Internal Temperature

Figure 6.8 shows a photo of TSA connected to an anode and exposed to natural seawater for 70 days. Table 6.5 shows the results from the EDS analysis on a sample exposed for 70 days with 30 °C internal temperature and connected to an anode. The row marked as "Other" contains traces of elements like: Cr, Ar, S, P, Ag and Ti, which is not relevant for this thesis, and is therefore not included in the table.

As with the no heating spool a higher content of calcium is found around areas of high iron content, as can be seen from spectrum 1.
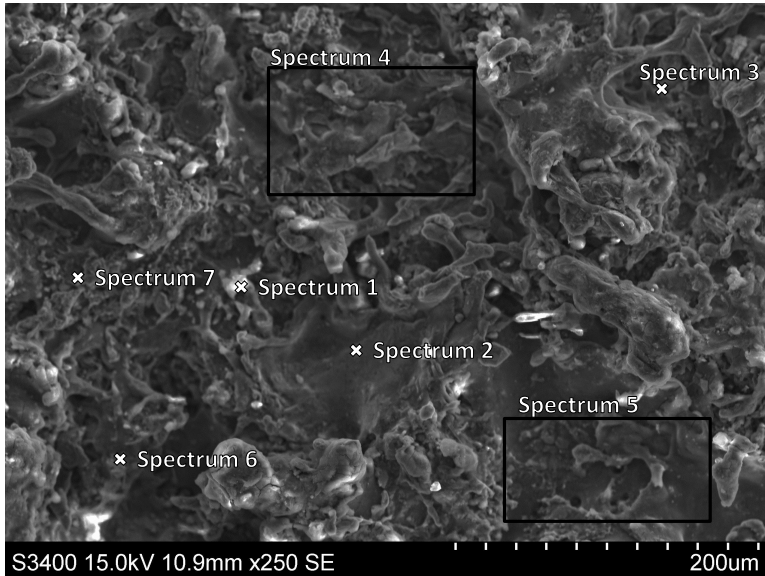


**Figure 6.8:** SEM photo TSA connected to an anode and exposed to seawater for 70 days with 30 ° C internal temperature.

**Table 6.5:** Results from EDS analysis of TSA connected to an anode and exposed to seawater for 70 days with 30 ° C internal temperature.

| Element [wt%] | Spectrum 1 | Spectrum 2 | Spectrum 3 | Spectrum 4 | Spectrum 5 |
|---|---|---|---|---|---|
| C | 26.63 | 7.63 | 13.34 | 18.38 | 24.3 |
| O | 46.58 | 5.25 | 16.58 | 28.27 | 31.89 |
| Al | 20.99 | 83.32 | 67.03 | 48.43 | 40.3 |
| Mg | - | 3.8 | 2.69 | 1.97 | 1.22 |
| Ca | 1.62 | - | 0.36 | 0.94 | 0.94 |
| Fe | 0.94 | - | - | 0.50 | - |
| Other | 3.24 | - | - | 1.58 | 1.35 |
| Total | 100 | 100 | 100 | 100 | 100 |

Figure 6.9 shows a SEM photo of TSA that freely corroded in seawater for 70 days, with 30 °C internal temperature. Table 6.6 shows the EDS results for the freely corroding test pieces with 30 °C internal temperature. From the table it can be seen that there is a relatively high calcium content where there is a high iron content. These areas of high calcium content is taken from the white area in the middle of the photo, which indicates low electrical conductivity.



**Figure 6.9:** SEM photo over TSA freely corroding in seawater for 70 days with 30 ° internal temperature.

**Table 6.6:** Results from EDS analysis for 30 °C Internal temperature test spool, corroding freely for for 70 days.

| Element [wt%] | Spectrum 1 | Spectrum 2 | Spectrum 3 | Spectrum 4 | Spectrum 5 |
|---|---|---|---|---|---|
| C | 12.06 | 9.18 | 17.61 | 10.42 | 24.06 |
| O | 44.03 | 12.96 | 41.99 | 11.64 | 30.51 |
| Al | 8.63 | 11.63 | 7.8 | 75.08 | 32.89 |
| Mg | 1.27 | 0.7 | 1.05 | 2.12 | 3.11 |
| Ca | 1.51 | 3.43 | 1.01 | - | 2.43 |
| Fe | 31.1 | 59.56 | 29.27 | 0.74 | 4.48 |
| Other | 1.38 | 2.54 | 1.27 | - | 2.01 |
| Total | 100 | 100 | 100 | 100 | 100 |

### 6.2.4   40 °C Internal Temperature

Figure 6.10 shows a SEM-photo of the surface of TSA exposed to seawater for 170 days with 40 ° C internal temperature, while Table 6.7 shows the EDS results for the TSA.

Spectrum 4 and 5 shows that the calcium content is high when the iron content is high.
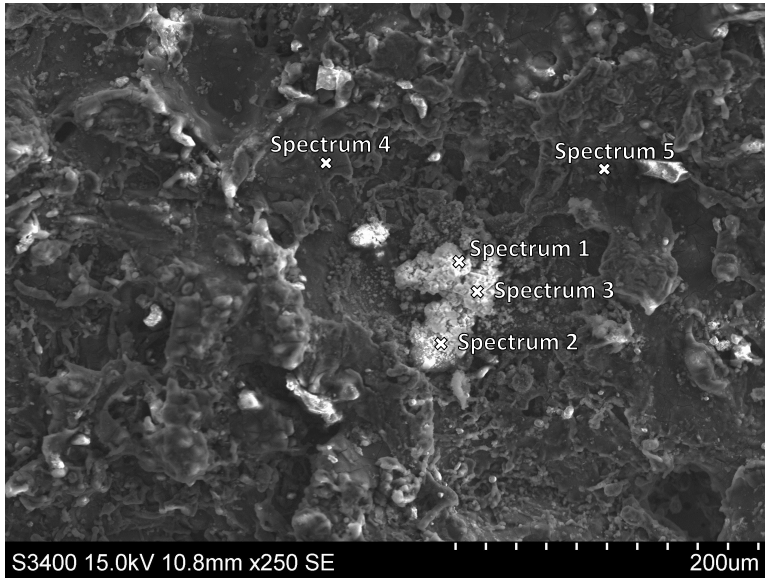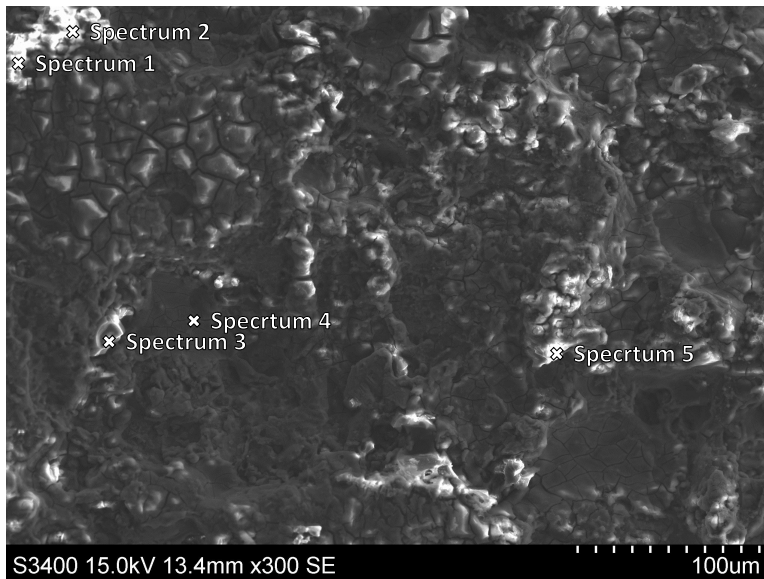


**Figure 6.10:** SEM photo of TSA freely corroding in seawater for 170 days with 40 °C internal temperature.

**Table 6.7:** Results from EDS analysis for 40 °C Internal temperature, freely corroding

| Element [wt%] | Spectrum 1 | Spectrum 2 | Spectrum 3 | Spectrum 4 | Spectrum 5 |
|:---:|:---:|:---:|:---:|:---:|:---:|
| C | 65.79 | 66.08 | 74.67 | 17.86 | 33.27 |
| O | 23.82 | 21.85 | 15.27 | 17.10 | 37.02 |
| Al | 5.53 | 6.46 | 0.75 | 53.94 | 17.87 |
| Mg | 0.67 | 0.69 | - | 0.47 | 0.75 |
| Ca | 0.27 | 0.48 | - | 5.03 | 2.43 |
| Fe | 0.43 | 0.26 | - | 3.85 | 5.19 |
| Other | 3.49 | 4,18 | 9.31 | 1.75 | 2.47 |
| Total | 100 | 100 | 100 | 100 | 100 |

Figure 6.11 shows a SEM photo of TSA connected to an anode an then exposed to seawater for 170 days 40 °C internal temperature, while Table 6.8 shows the results from the EDS analysis of the sample.

Generally the calcium content is high, especially spectrum 2.
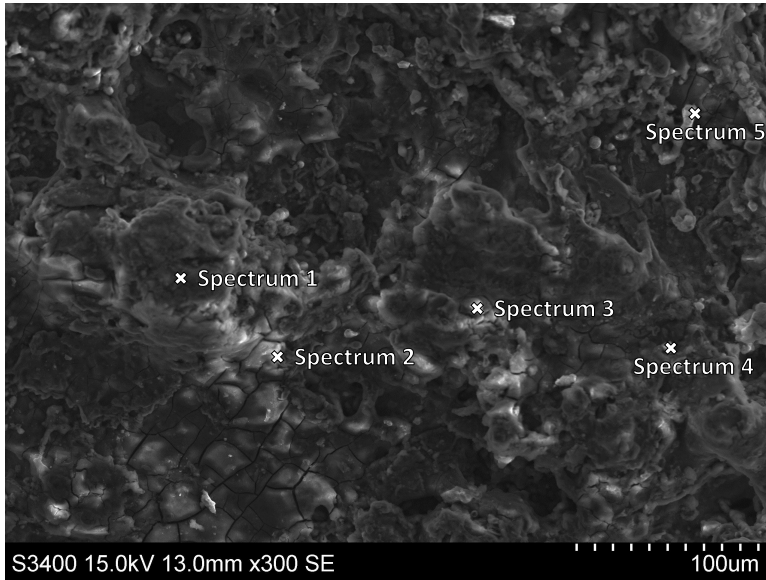


**Figure 6.11:** SEM photo of TSA connected to an anode and exposure to seawater for 170 days with 40 °C Internal temperature.

**Table 6.8:** Results from EDS analysis for TSA connected to an anode and exposure to seawater for 170 days with 40 °C Internal temperature.

| Element [wt%] | Spectrum 1 | Spectrum 2 | Spectrum 3 | Spectrum 4 | Spectrum 5 |
|:---:|:---:|:---:|:---:|:---:|:---:|
| C | 13.37 | 10.32 | 20.60 | 11.79 | 11.86 |
| O | 40.28 | 26.43 | 35.95 | 28.52 | 37.60 |
| Al | 42.89 | 17.69 | 30.96 | 23.96 | 43.33 |
| Mg | 1.74 | 0.66 | 4.92 | 1.83 | 3.47 |
| Ca | 0.54 | 27.47 | 3.20 | 1.36 | 1.73 |
| Fe | 0.39 | 15.78 | 1.63 | 31.35 | 0.60 |
| Other | 0.79 | 1.65 | 2.74 | 1.19 | 1.42 |
| Total | 100 | 100 | 100 | 100 | 100 |

### 6.2.5    50 °C Internal Temperature

Figure 6.12 shows a SEM photo of a TSA coated freely corroding in seawater for 60 days with 50 °C internal temperature, while the results from the EDS analysis is presented in Table 6.9. Sodium is included in the table due to the high concentration of it.

More white areas are present here than in the lower temperatures, and most of the spectrums that are taken in these white areas shows a relatively high content of calcium and iron.
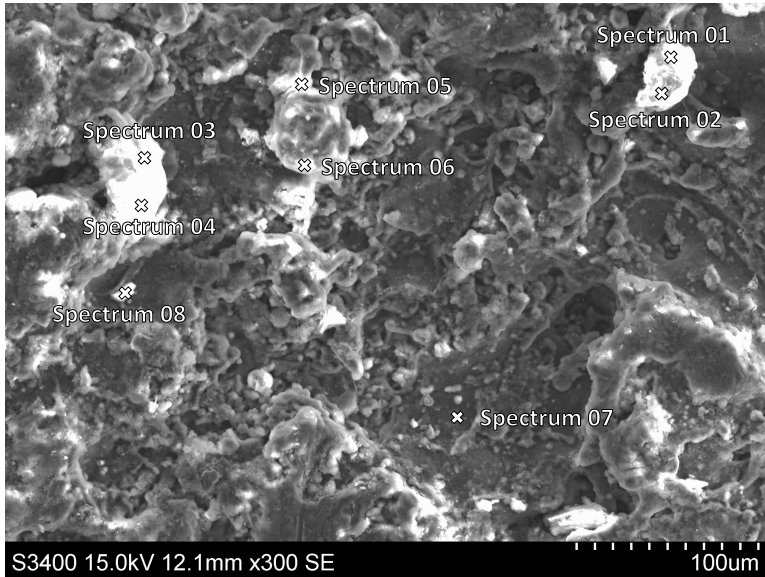


**Figure 6.12:** SEM photo of TSA surface freely corroding in seawater for 60 days with 50 °C internal temperature.

**Table 6.9:** Results from EDS analysis of TSA freely corroding in seawater for 60 days with 50 °C internal temperature.

| Element [wt%] | Spectrum 1 | Spectrum 2 | Spectrum 3 | Spectrum 4 | Spectrum 5 | Spectrum 6 | Spectrum 7 | Spectrum 8 |
|---|---|---|---|---|---|---|---|---|
| C | - | - | - | - | - | - | - | |
| O | 63.46 | 62.62 | 50.87 | 38.54 | 56.17 | 37.4 | 26.37 | 25.88 |
| Al | 20.77 | 21.7 | 38.39 | 35.92 | 30.97 | 45.49 | 71.43 | 6.53 |
| Mg | - | 0.47 | 2.32 | 3.13 | 3.49 | 3.19 | 1.13 | 6.09 |
| Fe | - | 0.86 | 1.23 | 14.08 | 3.34 | 1.67 | - | 1.38 |
| Ca | 1.00 | 0.86 | 1.88 | 2.74 | 2.36 | 5.24 | 0.54 | 59.94 |
| Na | 14.77 | 12.38 | - | - | - | 0.28 | - | - |
| Other | - | 1.11 | 5.31 | 5.59 | 3.76 | 6.16 | - | 0.18 |
| Total | 100 | 100 | 100 | 100 | 100 | 100 | 100 | 100 |

Figure 6.13 shows a SEM photo of TSA connected to an anode and exposed to seawater for 60 days with 50 °C internal temperature. The results from the EDS analysis of the sample can be seen in Table 6.10.

Spectrum 1-4, 6 and 7 are EDS analysis taken in the low conductivity areas of the sample and all show high iron and calcium content, while spectrum 8 is taken in a high conductive area and show a low content of iron and calcium, with a high amount of aluminium and oxygen.
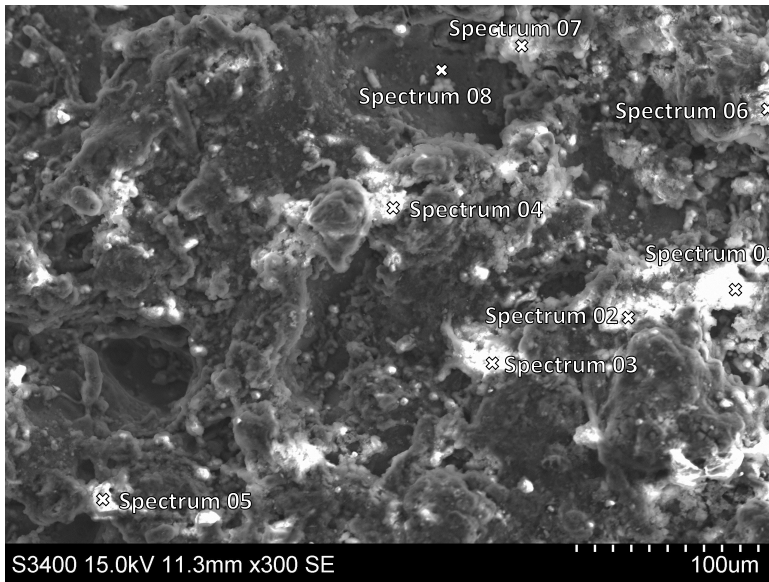


**Figure 6.13:** SEM photo of TSA connected to an anode and exposed to seawater for 60 days with 50 °C internal temperature.

**Table 6.10:** EDS results for TSA connected to an anode and exposed to seawater for 60 days with 50 °C internal temperature.

| Element [wt%] | Spectrum 1 | Spectrum 2 | Spectrum 3 | Spectrum 4 | Spectrum 5 | Spectrum 6 | Spectrum 7 | Spectrum 8 |
|---|---|---|---|---|---|---|---|---|
| C | - | - | - | - | . | - | - | - |
| O | 62.12 | 45.37 | 54.00 | 53.11 | 60.14 | 22.67 | 36.63 | 23.41 |
| Al | 29.65 | 49.35 | 38.25 | 37.47 | 25.89 | 11.72 | 46.97 | 73.80 |
| Mg | 2.57 | 2.12 | 3.34 | 2.38 | 0.44 | 1.66 | 1.99 | 2.50 |
| Fe | 2.09 | 1.68 | 2.91 | 3.12 | - | 61.99 | 10.25 | - |
| Ca | 0.99 | 0.66 | 0.58 | 1.01 | - | 0.94 | 2.34 | 0.29 |
| Na | - | - | - | - | 13.52 | - | - | - |
| Other | 2.58 | 0.81 | 0.91 | 2.92 | - | 1.04 | 1.84 | - |
| Total | 100 | 100 | 100 | 100 | 100 | 100 | 100 | 100 |

## 6.2.6  70 °C Internal Temperature

Figure 6.14 shows a SEM photo of TSA connected to an anode and exposed to seawater for 65 days with 70°C internal temperature, while Table 6.11 presents the EDS analysis results.

Nearly all the surface is covered with non-conductive material, and all the spectrums from the EDS shows a higher amount of magnesium than the EDS showed for the lower temperatures. Spectrum 6 shows a higher calcium content where the iron content was high.
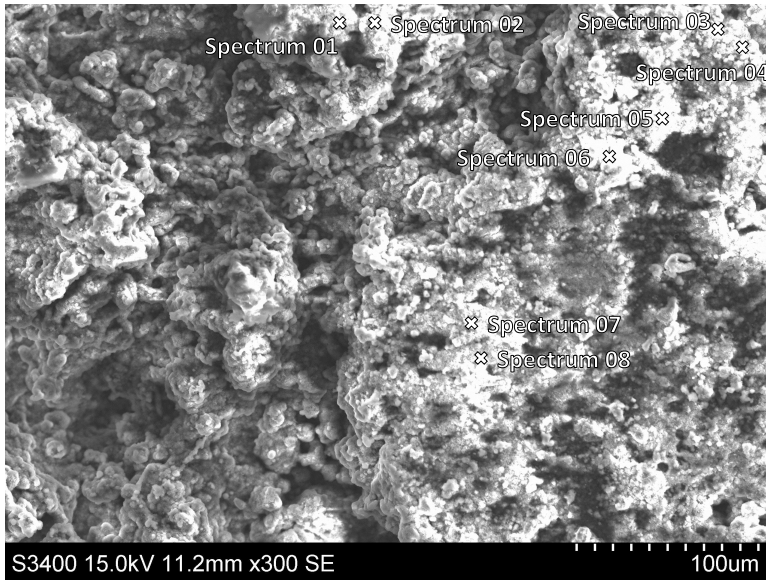


**Figure 6.14:** SEM photo of TSA connected to an anode and exposed to seawater for 65 days with 70°C internal temperature.

**Table 6.11:** EDS results for TSA connected to an anode and exposed to seawater for 65 days with 70°C internal temperature.

| Element [wt%] | Spectrum 1 | Spectrum 2 | Spectrum 3 | Spectrum 4 | Spectrum 5 | Spectrum 6 | Spectrum 7 | Spectrum 8 |
|---|---|---|---|---|---|---|---|---|
| C | 12.48 | 8.92 | 15.65 | 8.14 | 11.45 | 17.95 | 6.05 | 6.88 |
| O | 54.17 | 55.5 | 53.43 | 56.71 | 48.19 | 39.41 | 53.89 | 48.22 |
| Al | 13.82 | 15.97 | 12.44 | 16.81 | 17.01 | 16.41 | 18.79 | 26.69 |
| Mg | 17.13 | 17.25 | 16.04 | 15.82 | 18.62 | 10.97 | 18.08 | 13.49 |
| Fe | - | - | - | - | - | 10.48 | - | 0.49 |
| Ca | 0.25 | 0.17 | 0.23 | 0.14 | 0.55 | 2.15 | 0.33 | 0.9 |
| Other | 2.15 | 2.19 | 2.21 | 2.36 | 2.74 | 2.81 | 2.86 | 4.01 |
| Total | 100 | 100 | 100 | 100 | 100 | 100 | 100 | 100 |

Figure 6.15 shows a SEM photo of TSA that freely corroding in seawater for 65 days with °C internal temperature, and Table 6.12 shows the EDS results for the sample.

Most of the sample is covered with a non-conductive material. The EDS analysis shows a high magnesium and oxygen content.
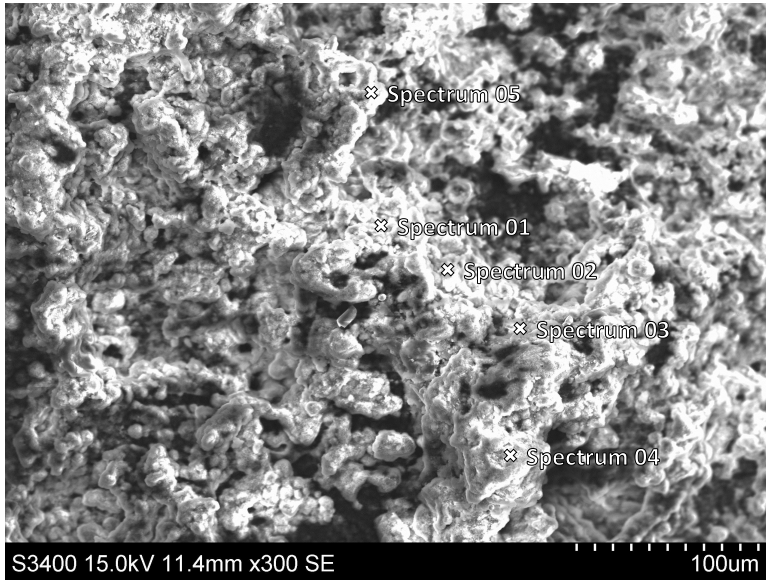


**Figure 6.15:** SEM photo of TSA freely corroding in seawater for 65 days with 70 °C internal temperature.

**Table 6.12:** EDS results for TSA freely corroding in seawater for 65 days with 70 °C internal temperature.

| Element [wt%] | Spectrum 1 | Spectrum 2 | Spectrum 3 | Spectrum 4 | Spectrum 5 |
|:---:|:---:|:---:|:---:|:---:|:---:|
| C | 7.67 | 8.47 | 9.84 | 7.23 | 8.97 |
| O | 50.3 | 53.66 | 48.29 | 53.19 | 52.27 |
| Al | 18.58 | 14.93 | 15.87 | 19.65 | 15.1 |
| Mg | 19.76 | 18.32 | 20.75 | 15.49 | 20.82 |
| Fe | - | - | 1.03 | - | - |
| Ca | 0.32 | 0.23 | 0.83 | 0.24 | 0.25 |
| Other | 3.36 | 4.38 | 4.09 | 4.2 | 2.59 |
| Total | 100 | 100 | 100 | 100 | 100 |

### 6.2.7    90 °C Internal Temperature

Figure 6.16 shows a SEM photo of TSA that was freely corroded in seawater for 65 days, and Table 6.13 shows the results from the EDS analysis. Almost the entire surface is covered with a non-conductive material.

The result from the EDS shows a even high content of magnesium than at 70 °C internal temperature, a higher oxygen content, butbarbon and calcium is absent.
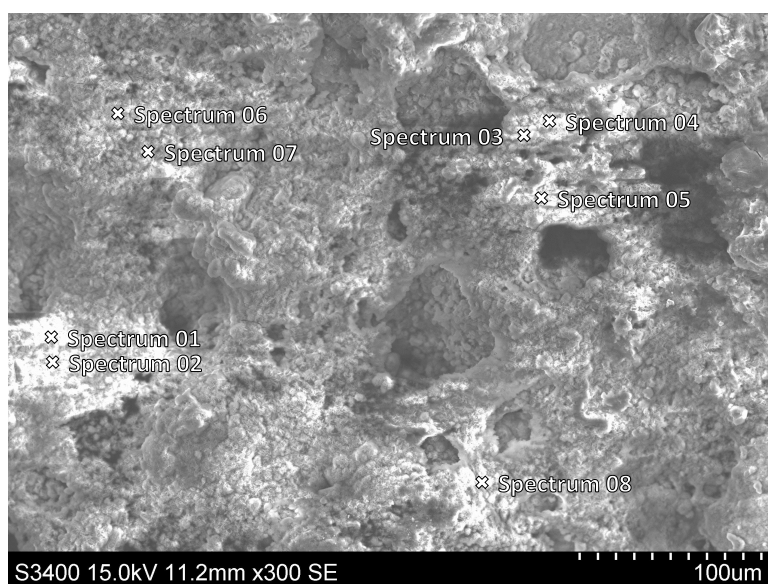


**Figure 6.16:** SEM photo of TSA that freely corroded in seawater for 65 days with 90 °C internal temperature.

**Table 6.13:** Results from EDS of TSA that freely corroded in seawater for 65 days with 90 °C internal temperature.

| Element [wt%] | Spectrum 1 | Spectrum 2 | Spectrum 3 | Spectrum 4 | Spectrum 5 | Spectrum 6 | Spectrum 7 | Spectrum 8 |
|---|---|---|---|---|---|---|---|---|
| C | - | - | - | - | - | - | - | - |
| O | 57.65 | 59.43 | 58.56 | 59.66 | 43.34 | 59.2 | 57.01 | 51.71 |
| Al | 13.3 | 11.99 | 12.33 | 12.62 | 16.9 | 12.77 | 13.26 | 14.77 |
| Mg | 27.9 | 26.11 | 26.33 | 26.66 | 34.83 | 27.06 | 28.28 | 31.71 |
| Fe | - | - | 0.36 | 0.31 | 1.99 | - | - | 0.60 |
| Ca | - | - | - | - | - | - | - | - |
| Other | 1.15 | 2.49 | 2.42 | 0.75 | 2.94 | 0.96 | 1.44 | 1.22 |
| Total | 100 | 100 | 100 | 100 | 100 | 100 | 100 | |

Figure 6.17 shows a SEM photo of TSA connected to an anode and exposed to seawater for 65 days with 90 °C internal temperature. Table 6.14 shows the results of a EDS analysis of the sample.

The magnesium and oxygen is content generally high. There is some calcium and carbon on the polarized sample that is not found on the freely corroding sample.
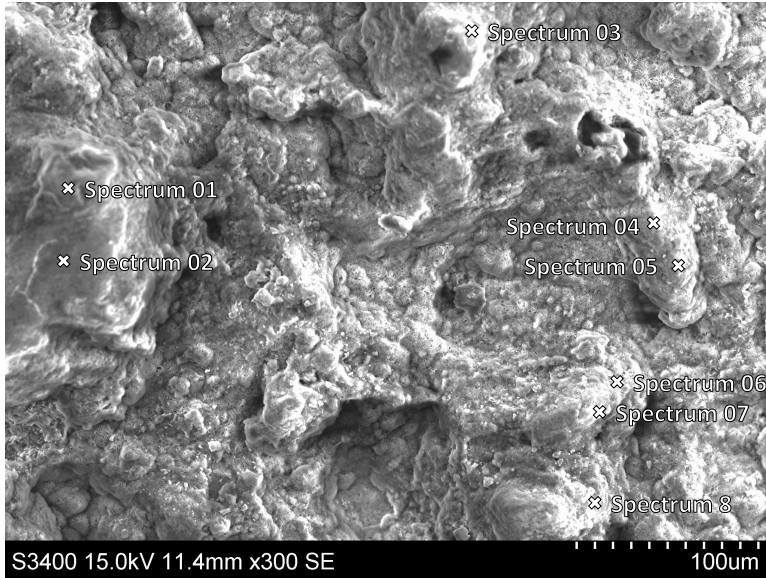


**Figure 6.17:** SEM photo of TSA connected to an anode and exposed to seawater for 65 days with 90 ° C internal temperature.

**Table 6.14:** Results from EDS of TSA connected to an anode and exposed to seawater for 65 days with 90 °C internal temperature.

| Element [wt%] | Spectrum 1 | Spectrum 2 | Spectrum 3 | Spectrum 4 | Spectrum 5 | Spectrum 6 | Spectrum 7 | Spectrum 8 |
|---|---|---|---|---|---|---|---|---|
| C | 21.64 | 16.2 | 15.16 | 10.3 | 10.1 | 7.94 | 7.29 | 13.68 |
| O | 48.77 | 52.46 | 55.64 | 58.06 | 56.83 | 57.66 | 56.38 | 53.62 |
| Al | 9.02 | 11.5 | 10.11 | 10.62 | 13.07 | 12.55 | 15.76 | 10.72 |
| Mg | 18.85 | 18.91 | 17.07 | 20.10 | 18.95 | 21.08 | 18.56 | 20.45 |
| Fe | - | - | 0.32 | 0.31 | - | - | 0.34 | 0.59 |
| Ca | 0.66 | 0.19 | 0.26 | - | 0.39 | - | 0.23 | 0.15 |
| Other | 1.06 | 0,75 | 1.45 | 0.61 | 0.67 | 0.76 | 1.43 | 0.79 |
| Total | 100 | 100 | 100 | 100 | 100 | 100 | 100 | 100 |

Figure 6.18 shows a SEM photo of the microstucture of calcareous deposits on TSA connected to an anode and exposed to seawater for 65 days with 90 °C internal temperature. The microstructure has a needle structure.
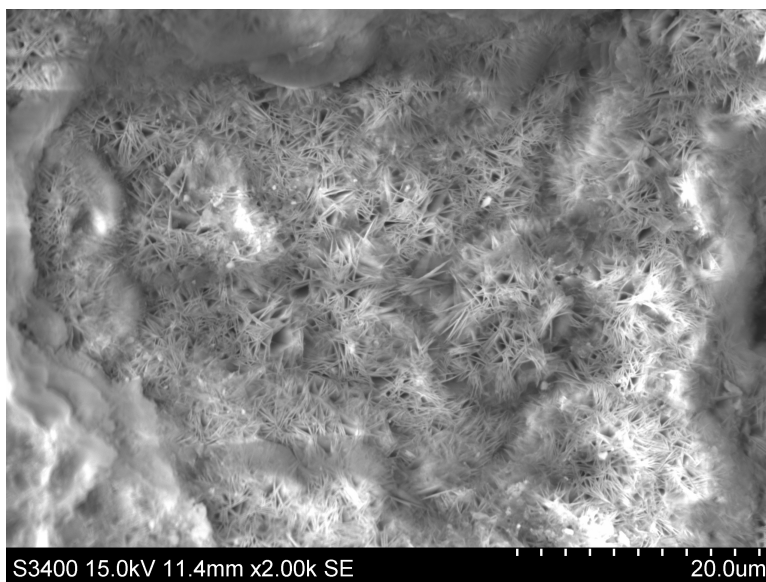


**Figure 6.18:** SEM photo of calcareous deposit microstucture of calcareous deposits on TSA connected to an anode and exposed to seawater for 65 days with 90 °C internal temperature.

## 6.2.8 Mg/Ca-Ratio

Figure 6.19 shows a presentation of the Mg/Ca-ratio in the calcareous deposits formed on TSA exposed to seawater at different temperatures. The Mg/Ca-ratio is presented for all temperatures for samples both connected to an anode and freely corroding. The data for 90 °C internal temperature freely corroding spool is not shown because no Ca was discovered, which would have given a infinite value for the Mg/Ca-ratio. The Mg/Ca-ratio does not give any indications on the amount of calcareous deposits, only the type of calcareous deposits.

The Mg/Ca-ratio is calculated from the EDS results presented in Table 6.3 to 6.17, and is an average for all the points which contains both Mg and Ca. The Mg values is then adjusted for the amount of Mg, by subtracting the amount of Mg found in the unexposed TSA sample, which is an average of 1.8. This gives an adjusted value for the weight ratio for the Mg and Ca. The weight ratio is not an appropriate value to use however, because it is the ratio of atoms of Mg and Ca that is interesting because this gives an indication of the ratio of Mg-based calcareous deposits and Ca-based calcareous deposits.

The Mg/Ca-ratio is holding more or less steady until the internal temperature reaches 70 °C, and increases from 0 to 2.3 to over 84. The ratio increases to even higher values for the samples with 90 °C internal temperature.
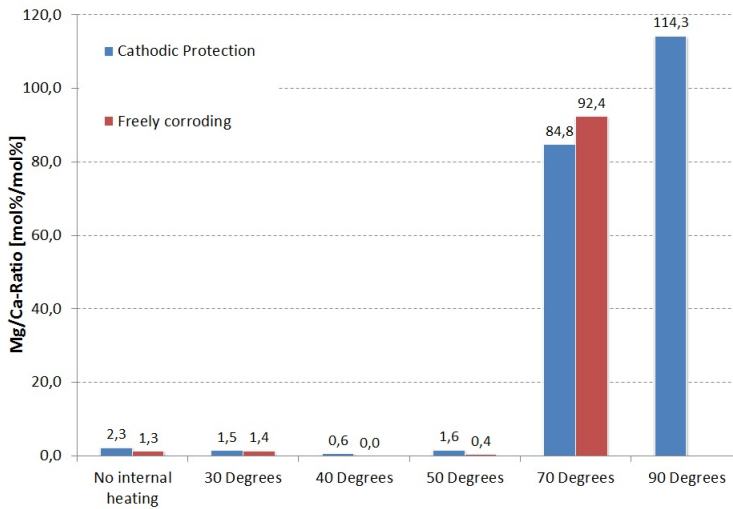
**Figure 6.19:** Graph presenting the ratio between Mg and Ca in the calcareous deposits on TSA exposed to seawater at different temperatures.

## 6.3 Thermal Conductivity

The results from the thermal conductivity measurements is presented in this chapter. Table 6.15 shows the results obtained. All the measurements are close to 10 $W/m^2K$, which is the thermal conductivity of the stainless steel pipe substrate. The standard deviation is an estimate based on several measurements on the sample not exposed to seawater.

**Table 6.15:** Results from the thermal conductivity measurements

| Sample | Thermal Conductivity [$W/m^2K$] | Standard Deviation |
|---|---|---|
| Not Exposed | 10.2 | 0.30 |
| No Heating Connected to an Anode | 10.51 | 0.30 |
| No Heating Freely Corroding | 9.87 | 0.30 |
| 40°C Connected to an Anode | 9.56 | 0.30 |
| 40°C Freely Corroding | 9.78 | 0.30 |
| 70 °C Connected to an Anode | 9.15 | 0.30 |
| 70 °C Freely Corroding | 9.65 | 0.30 |
| 90 °C Connected to an Anode | 9.99 | 0.30 |
| 90 °C Freely Corroding | 9.56 | 0.30 |

# Chapter 7

# Discussion of the Electrochemical Properties

In this chapter the results from the electrochemical testing is discussed. The chapter is divided in to four different parts. Three of the parts is a discussion of electrochemical properties, like corrosion rate, corrosion potential and the current density requirement, of the coating. The last parts is dedicated to some incidents that occurred during the experiments that caused some data to be lost.

## 7.1 Corrosion Rate

In this chapter the corrosion rate of the TSA coating is discussed, with a special focus on the effects of exposure time, corrosion potential and temperature.

### 7.1.1 Effect of Exposure Time

Based on Figure 2.8 it was expected that the TSA would have a relatively high initial corrosion potential. The corrosion potential was then expected to rapidly decrease to more negative values, and after some days stabilize at a low potential, which would indicate a relatively high rate of corrosion, since this would be close to, or in, the pitting area of the experimental pourbaix diagram shown in Figure 2.4. This is what can be seen from Figure 5.12, where the corrosion rate is initially quite high for all temperature, and is reduced with time.

The reason for the reduced corrosion rate over time may be that the active intermetallic particles gets passivated by calcareous deposits. This prevents any galvanic connection between the aluminium matrix in the coating and the particles, which reduces the corrosion rate, and enables the aluminium to passivate as well. This effect can be seen for all temperatures.

Another reason for the reduced corrosion rate might be the build up of aluminium oxide on the TSA surface, and in pores in the coating. As mentioned in the Chapter 2 the corrosion products of aluminium can fill up pores and voids in the coating which may reduce the corrosion rate by isolating the aluminium from the seawater.

### 7.1.2 Effect of Corrosion Potential

From the literature it is known that low corrosion potential is associated with high corrosion rates. This is true for all the test temperatures. It is specially clear from the 70 and 90 °C temperature experiments, but can be seen from the lower temperatures as well. The corrosion rate for the spool with no internal heatings decreased from 6 to 2 $\mu m/year$, while the corrosion potential increased with 67 mV, over a period of 50 days.

For the spool with 90 °C internal temperature the highest corrosion rate was obtained at the lowest corrosion potential. When the corrosion potential for the samples was -1200 mV Ag/AgCl the corresponding corrosion rate was 50 $\mu m/year$, the highest corrosion rate estimate in this thesis. After 65 days of exposure the corrosion potential for the sample was -950 mV Ag/AgCl with a corresponding corrosion rate of 8 $\mu m/year$.

The measured corrosion potential is lower for the spool with no internal temperature than the spool with 30 and 40°C internal temperature, and the associated corrosion rate is higher for the spool with no internal heating.

Knudsen et al. [52] found the corrosion rate of TSA polarized to -1100 mV Ag/AgCl in ambient seawater to be 10 $\mu m/year$. This is 5 times the corrosion rate that was achieved on the TSA tested in this thesis. Indicating that the potential of the sample affects the corrosion rate.

### 7.1.3 Effect of Temperature

From the lower temperatures[1] experiments it looks like the corrosion rate is reduced with increasing temperature. From the theory this is the opposite of what was expected, based on the general rule of high temperature equals high corrosion rate, so a more likely reason for this opposite trend is that a combination of a small temperature difference, and some inaccuracy in the corrosion measurements, which is explained in Chapter 7.1.4. The difference in temperature on the TSA surface is, as shown in Table 4.1, only 8 ° for the low temperature experiments.

Another reason for the opposite corrosion rate relation may be the low corrosion potential, which might be affected by other (unknown) factors than the temperature, which causes the higher corrosion rates for the spool without heating.

Alternatively, it is known that the most common attack on aluminium in seawater is pitting corrosion, and it is also known that high temperatures favour general corrosion, not pitting corrosion. It might therefore be the case that increased temperature inhibits pitting corrosion, and that this yield low corrosion rates due to a generally low uniform corrosion rate. The corrosion rates of the 40 °C samples and the no heating sample reaches the same corrosion rate at the end of the experiment.

---

[1]No internal heating, 30 and 40 °C internal temperature.

If the lower temperatures are compared with the higher temperatures[2], it is clear, especially initially, that the high temperature increases the corrosion rate significantly. However, even at the highest temperature the corrosion rate is greatly reduced from the initial corrosion rate of 50 $\mu m/year$ to below 10 $\mu m/year$, which would give the coating atleast 20 years life time, if freely corroding.

In Chapter 2.2.2 it was writen that:

> Potential measurements done at elevated temperatures, however shows low potentials initially, which indicates high corrosion rates, but after a while the potential rises and stabilizes. This means that aluminium should have high initial corrosion that will decrease with time and then stabilize.

This is exactly what is seen in this thesis. The effect of temperature is clear from the high temperature experiments. Initially the temperature gives a huge potential difference, with the highest corrosion rate on the highest temperature. The reason for the high corrosion rate at high temperature is probably due to effect the temperature has on the kinetics of the electrochemical reactions.

### 7.1.4   Sources of Inaccuracy

WThe early corrosion rate estimates for the low temperatures sppols (obtained November to December in 2013), there was a huge difference in the corrosion rates for the graphical solution and when using Stern-Geary. The Stern-Geary calculation always yielded a significant higher corrosion rate. The reason for the inaccuracy in the LPR values are probably due to way the polarization curves were obtained. The entire cathodic polarization was done first, followed by a 30 minute wait, to let the specimen adjust back to OCP. The test specimen took much longer than 30 minutes to stabilize, and did not entirely recover to OCP before the anodic polarization curves were taken. This means that the first measurement taken in anodic direction were polarized more than 10 mV from OCP, since the potential of the sample had not entirely recovered to OCP. The LPR measurements were done together with the polarization curves, meaning that the first measurement in cathodic and anodic direction were used as the LPR measurement. This means that the samples were in reality polarized more than 10 mV from OCP during the anodic polarization curves, and therefore a higher current were recorded at anodic polarization that it should. This gave a lower polarization resistance which gives a high corrosion rate.

A example of the huge difference between the corrosion rate calculated using Stern-Geary and the corrosion rate found using the graphical solution from the polarization curves is taken from 11.November from the spool with 40 °C internal temperature. The tafel constants $b_a$ and $b_c$ is the slopes of the asymptons for the anodic and cathodic polarization curves, and was found to be 499 and 342 $mV/decade$ respectively. The current at 10 mV cathodic and anodic polarization was 0.085 mA and 0.24 mA respectively. Note that the anodic current is nearly 3 times higher than the cathodic current. Using Stern-Geary, with the data obtained by the polarization curves and the LPR measurement this gave a corrosion rate of 82 $\mu m/year$. The graphical solution, using the polarization curves of the same sample gave a corrosion rate of 25 $\mu m/year$. The Stern-Geary equation gave

---

[2]50, 70 and 90°C internal temperature.

a solution that was 3.3 times higher than the graphical solution, and due to the way the LPR values were obtained, this is unrealistically high.

This means that the LPR and the corrosion rate calculated from Stern-Geary was higher than it is in reality, and should be used with caution. The corrosion currents at +/- 10mV are very small, so small deviations from reality causes a high degree of uncertainty. The corrosion rate calculations are therefore based on the graphical solution from the overvoltage curves, for all polarization curves obtained in 2013. The polarization curves are less affected by the current inaccuracy, due to the higher current outputs, and the larger range of potential at which they are recorded.

## 7.2 Corrosion Potential

In this chapter the corrosion potential for TSA in seawater exposed to different temperatures is discussed. The main focus is the effect of temperature, but the unexpected low corrosion potentials obtained in the spools with 40 °C internal temperature and below is also discussed.

### 7.2.1 Effect of Exposure Time

Figure 2.8 shows a graph of the development of the corrosion potential for flame sprayed aluminium. The corrosion potential for the flame sprayed aluminium is initially quite high, above -900 mV, then decreases rapidly with time. This is roughly the same way that the corrosion potential for TSA samples tested in this thesis developed. It is especially clear for the higher temperature spools, with internal temperatures of 50 °C and up. The reason of this is probably because intermetallic particles are passivated and the pores in the coating is filled with corrosion products. This passivates the TSA and reduces the corrosion rate, which is shown by increased corrosion potential. This process takes time, and that is why it takes days or weeks for the corrosion potential to stabilize.

### 7.2.2 Effect of Temperature

Initially the corrosion potential is more negative the higher the temperature. However, after a while the corrosion potentials for the spools with 90 and 50 °C internal temperature stabilizes between -990 and -910 mV Ag/AgCl, with no obvious temperature dependency. The corrosion potential for the sample without any heating, see Figure 5.11, does not decrease to potentials as low as the spools with heating does. However, after 40 days of exposure the corrosion potential for the spools without heating is lower than the high temperatures spools.

The effect of temperature over time is quite interesting. If the corrosion potential obtained in the experiment where TSA on carbon steel and on stainless substrates were tested, seen in Figure 5.11, is compared to the results from the 70 and 90 ° internal temperature spools the initial corrosion potential is much lower for the high temperatures. For the with 90°C the corrosion potential reached down to -1200 mV Ag/AgCl while the spools with no internal heated reached -1000 mV Ag/AgCl. However, the corrosion potential for the

heated spools stabilizes between -910 and -990 mV Ag/AgCl, when the spools without internal heating stabilized at around -1000 mV Ag/AgCl. This is also found in the literature in Table 2.2, where initially the corrosion potential was lowest for the highest temperatures, then the corrosion potential for the high temperatures stabilized at a potential above the TSA exposed to ambient temperature. The reason for this is not found in the thesis.

The low corrosion potential for the spool with no internal heating, 30 and 40°C internal temperature was not as expected, based on the literature. The corrosion potential seemed to become more negative with increasing temperature, as can be seen from Figure 5.9. The reason for this is not clear, but since the carbon steel substrate experiment did not replicate these results, the low potentials is probably not connected to the temperature, but is caused by another unknown factor. More on this can be found in Chapter 7.2.3

### 7.2.3 Unexpected Corrosion Potentials

As mentioned in Chapter 4.1 the corrosion potentials for the spools that were started in the specialization project had a lower corrosion potential than expected based on the literature. Based on Table 2.1 the corrosion potential for arc sprayed TSA is expected to be around -995 mV vs Ag/AgCl in seawater at ambient temperature. For the experiment without any heating the corrosion potential was for most of the experiment between -1150 and -1100 mV vs Ag/AgCl, which is 150 to 100 mV lower than expected.

This led to that another experiment without heating was initiated. The purpose of the experiment was to investigate if the substrate material affected the corrosion potential, and to see if the original results could be replicated. The results from this experiment, and the possible reasons for the difference in the corrosion potential for the two experiments is discussed in this chapter.

The results from the original experiments was not replicated in the new experiment, which yielded approximately 150 mV higher corrosion potentials. There was some difference in the two TSA samples initially. The rate of which the corrosion potential decreased differed from the spools, but beside from that there is not any significant difference for the two samples.

The reasons for the low corrosion potentials obtained in the low temperature spools[3] is not known. However, it is not assumed to be an measuring error, or an error with the experimental setup. The potential measured is assumed to be the actual potential of the spool. There are two reasons for this assumption. The first reason is that the potential of all the spools connected to the anodes have the same potential, which is about -1050 mV Ag/AgCl, which is close to the anode potential. This is true for all temperatures, even the high temperature experiments. The second reason is that the current goes from positive to negative approximately when the corrosion current becomes more negative than the anode potential. This indicates that the corrosion potential actually is lower than the anode potential. This means that there is a factor effecting the corrosion potential of the spools.

As mentioned the first hypothesis for explaining the low corrosion potential was that the stainless steel substrate somehow affected the corrosion potential. But the second experiments with both carbon steel substrate and stainless steel substrate did not support this hypothesis. Therefore, the reason for the unexpected low potential is not known.

---

[3]No internal heating, 30 and 40 °C

There are three differences between the low temperature experiments and the high temperature experiments.

- Different polymer used for the test spools.

- The spools for the low temperature spools were in the same container, while the high temperature spools were separated.

- Glue was used for the low temperature spools, but not for the high temperatures.

The experiment with carbon steel substrate did not use glue and used Teflon instead of polyurethane, and the samples obtained a corrosion potential closer to the values that was expected based on the literature. This might indicate that either the glue spilled on the TSA surface or the polyurethane or a combination may affect the corrosion potential of TSA.

Another explanation may be that the pipe that the low temperatures spools were created from have been treated in such a way, during storage or production that may have damage or altered the coating in say way. However, all the explanations given is this chapter is just speculations and no certain explanation was found.

### 7.2.4  Sources of Inaccuracy

When obtaining polarization curves for the corrosion rate estimates the measured corrosion potential of the spools is affected by this. This causes errors in the measurements of course, since the measured potential then could be as much as 180 mV off the real corrosion potential. This problem was mitigated by changing the measured potential during the polarization curves to the OCP measured before the polarization curves were obtained.

## 7.3  Current Density Requirement

The current density requirement for the TSA is discussed in this chapter with a special focus on the corrosion potential and the effect of temperature.

### 7.3.1  Effect of Potential

As mention the spool without any heating had a corrosion potential for most of the experiment between -1150 and -1100 mV vs Ag/AgCl, which is 150 to 100 mV lower than expected. The experiments with 30 and 40 °C internal temperature had a slightly higher corrosion potential at about -1100 mV Ag/AgCl for most of the experiments, which is 100 mV lower than expected. This caused the test with no internal heating, 30 °C, and the 40 °C to achieved corrosion potentials more negative than the polarized potential of -1050 mV Ag/AgCl. This caused the current demand to become negative, which indicates that the anodes have stopped protecting the coating, and the coating started to protect the anodes.

As explained in the theory the precipitation of calcareous deposits is dependant on locally enhanced pH to form. The increased pH is caused by hydroxide ions formed in

the cathodic reaction, which should have occurred on the TSA, as it was under CP from the aluminium anode. When the corrosion potential of the coating become lower than the protection potential from the anode, the anodic and cathodic reaction "switched" places, and the anodic reaction occurred on the coating, dissolving it. Therefore no increase in pH should have occurred on the surface of the lower temperature specimen, and therefore the CP system will not affect the deposition of calcareous deposits. Any deposits found on these spools should therefore be purely chemical deposition due to supersaturation of $CaCO_3$ in the seawater.

Potentials as low as -1150 to -1100 mV vs Ag/AgCl was not expected, and a hypothesis was that the substrate may somehow effect the potential, as no experiments have been done with TSA on a UNS S31245 substrate. However, the experiment initiated with one stainless steel sample and one carbon steel substrate sample did not replicate the low potential obtained in the initial experiments. Therefore the electrochemical results from the initial experiments begun in the Specialization Project is considered to be somewhat unreliable.

If the current density requirement for the spools with 50, 70 and 90 °C is compared to the current density requirement obtained by SINTEF [52] it is clear that the results from the experiments in this thesis are much lower than the results that they obtained. However, SINTEF polarized their specimen to -1100 mV Ag/AgCl, which is 50 mV more negative than in this thesis. Furthermore Egtvedt [49] found that the current demand will increase with increased polarization. This might explain why the current demand in this thesis is somewhat lower than the current demand obtained by SINTEF.

### 7.3.2  Effect of Temperature

The most obvious difference between the spool with 50 °C internal temperature and the highest temperatures, 70 and 90 °C internal temperature, is the initially negative current demand. This is due to the low initial corrosion potential caused by the high temperatures. The current demand stabilizes after approximately 40 days for the spools with 50, 70 and 90 °C internal temperature, between 3 and 5 $mA/m^2$. These low current demands and the small difference in current demand was not expected based on the research of Egtvedt [49] and Knudsen et al [52]. However, since Etgvedt only performed experiments at ambient temperatures, and Knudsen polarized the TSA 50 mV more negative than in this thesis there is little to no directly comparable experiments in the literature. It is therefore probably not possible to precisely conclude anything when comparing the results in this thesis to the literature.

The current density requirements for the high temperature experiments are very low, compared to the DNV recommended practice[51]. DNV recommend a current density of 17 $mA/m^2$ with a surface temperature of 60 °C. This is approximately 3 timers higher than the current demand obtained by current demand with 90 °C internal temperature, which had a surface temperature of 60 °C.

As was seen from the SEM-photos of the 70 and 90 °C internal temperature samples a thin film of $Mg(OH)_2$ precipitated on the surface. This might have contributed to reduced the current demand from the anodes, due to it is protective abilities. The precipitation of calcareous deposits be further discussed in Chapter 8.1.

CP of TSA is based on preventing pitting corrosion, however at high temperature pitting corrosion is less of a threat. This means that the current demand may be low due to

low pitting corrosion activity. Another explanation may be the low seawater flow rate. A low flow rate will replace the water close to the test spools at a slow rate, causing the seawater close to the TSA to be oxygen depleted. This makes the oxygen reaction, Equation 2.3 diffusion limited, which is a slow process. This is known from the literature to cause a low corrosion rate, thus a low current demand. The current density requirement results may therefore be reasonable, even though that they are quite low.

## 7.4 Loss of data

During the experiment four different incidents caused loss of data, and is discussed in this chapter. All experiments were affected, however, the severity differed. The four incidents were:

- Dry saltbrigde

- Computer crash

- Blown fuses

- Water inlet stopped

For the low temperature experiments the reference electrode was not placed directly into the seawater together with the test spools, but in a separate container with a saltbridge to connect the seawater and the reference electrode container. Seawater was sucked into a silicon tube to create the saltbridge, however this tubing lost it is seawater a couple of times, and the data between 07.11.14 to 09.11.14 and 01.12.13 to 07.12.13 was lost before it was permanently fixed. The loss of data does not effect the experiment however, only the measurements, and because the experiments on lower temperatures have been exposed for so long, the loss of data for some days is not critical for the experiments, only annoying.

During the Christmas holidays the computer at Sealab crashed and was turned off. The Korrosjonslogger program stopped working and data between 26.12.13 and 06.01.14 was not recorded. The Korrosjonslogger program has since been replaced by a newer program.

Due to a blown fuse, all data between 19.03 to 24.03 were lost because the heating elements lost power and couldn't heat up the interior of the pipe.

For some reason the inflow of water stopped on the 70 °C internal temperature experiment. This caused the water to evaporate and the water level in the tank sank. The water level decreased below the reference electrode and the connection between the reference and the test spools was lost. During this a layer of salt also formed on the test spool, which caused weird potential measurements, probably due to the resistance through the layer of salt. The salt layer was dissolved within one day when the water inflow was opened again.

The measurements affected by these incidents have been deleted when presented in the results. All data, included the data that was deleted, can be seen in Appendix F.

The test spools in this thesis was made up of four pipe pieces, this mean that the pipe piece were stacked on top of each other. This obviously means that the distance between the water level and the pipe differed. The reason for this was to get two parallels of both freely corroding samples and samples connected to anodes at all temperatures.

For the high temperatures[4] only the measurements for one parallel of freely corroding sample and one parallel for the samples connected to an anode was presented in the results. This was because only the top two samples showed the same temperature. For the lower spools there were a temperature gradient, meaning that the lower spools had a lower external temperature than the higher spools. Therefore only one parallel was used when current density requirement, corrosion potential and polarized potential was presented in the results. The results from the two highest pipe pieces was used. The author decided to present it this way, because it was assumed that this gave a more accurate presentation of the actual properties of TSA at the different temperatures.

The temperature gradient was probably caused by the cool seawater that entered the tank from the bottom. The seawater was warmed when flowing upwards, providing less cooling to the top of the test spool. The experiments were completed as specified in Chapter 4, meaning that the internal and external surface temperatures are as shown in Table 4.1 but only the two top pipe pieces. Therefore results from one freely corroding sample and one samples connected to an anode is presented in the results. However, the results from all the samples are presented in Appendix F.

---

[4]50°C and up

# Chapter 8

# Discussion of the Post Exposure Analysis

In this chapter the results from the post exposure analysis is discussed, which includes the results from the SEM and EDS analysis, the thermal conductivity measurements and the blistering found in the TSA coating.

## 8.1 Calcareous Deposits

The results from the SEM and EDS analysis is discussed in this chapter. Firstly the EDS analysis is used to identify the different types of calcareous deposits which form on the TSA, then the effects of CP and temperature is discussed. The thickness of the deposits and any sources of inaccuracy is also discussed.

### 8.1.1 Identifying the Calcareous Deposits

Based on the SEM photos alone it is impossible to identify the calcareous deposits, and the EDS results is the only thing that can be used for identifying the calcareous deposits. Therefore an assumption based on Egtvedt's master thesis was made.

As Egtvedt noted in her Master Thesis [49], areas of white in the SEM photos might represent calcareous deposits. Therefore the EDS-analysis were focused on these spots, and a high amount of Ca, Mg, O and C were found in them. This indicates that the spots are calcareous deposits, because the calcareous deposits are made up of these elements, and these elements is not found in these amounts in the EDS analysis of the unexposed TSA surface. Another discovery was the amount of iron in some of these white areas, and as mentioned in Chapter 2, intermetallic particles are often iron based, and the corrosion of TSA is focused around these particles.

The white areas on the SEM photos are not electrically conductive, and therefore can not be viewed in the SEM. Therefore, due to the electrical isolation properties of calcare-

ous deposits, these white areas are assumed to be indications of calcareous deposits. This strengthen the assumption of these areas being calcareous deposits.

As mentioned in Chapter 2.4 three types of calcareous deposits may precipitate on metal surfaces when exposed to seawater, $CaCO_3$, $Mg(OH)_2$ and $MgCO_3$. To identify what type of calcareous deposits that formed on the the ratio between Mg and Ca is used, and can be seen in Figure 6.19. Obviously an increase of the amount of Mg or an decrease of the amount of Ca causes the Mg/Ca-ratio to increase. This means that a high Mg/Ca-ratio is indications of a Mg-based calcareous deposits of either $Mg(OH)_2$ or $MgCO_3$, or a combination of both, while a low Mg/Ca-ratio is an indication of Ca-based calcareous deposits, meaning $CaCO_3$.

Differentiating between $Mg(OH)_2$ and $MgCO_3$ for spools with a high Mg/Ca-ratio can somewhat be done by looking at the carbon content from the EDS analysis. High carbon content might indicate some $MgCO_3$, while a low or absent carbon content might indicate $Mg(OH)_2$ deposits. Figure 6.18 shows the microstructure of the calcareous deposits on the spool with 90 °C internal temperature. From the EDS analysis of the area it is high in Mg and O, while low in carbon. It is clear by comparing Figure 6.18 with the photos of Argonite and Calcite, Figure 2.12 and 2.13 that the microstructure found on the sample is not Argonite and Calcite, which is based on $CaCO_3$. The unknown microstructure combined with the high Mg and O may indicate $Mg(OH)_2$, which is not surprising since the literature indicates that $Mg(OH)_2$ might precipitate at high temperatures.

## 8.1.2 Effect of Cathodic Protection

For both the polarized and freely corroding sample areas of calcareous deposits were discovered at all temperatures, however no continuous film is seen in the photos. For the freely corroding samples the formation of calcareous deposits close to intermetallic particles is expected, due to the galvanic corrosion that occurs around these, which increases the local pH near to these particles. Several EDS spectrums at low temperatures show that a high Ca content has a corresponding high Fe content. This is an indication that the calcareous deposits form on and close to intermetallic particles. This might explain why only small spots of calcareous deposits are found on the freely corroding samples at low temperatures.

The Mg/Ca-ratio varies little for the sample connected to an anode and the freely corroding sample within each temperature, and there is no significant difference between them. There is not for example a higher Mg/Ca for all the freely corroding samples, but it varies for the different temperatures. However, the Mg/Ca-ratio is very low, compared to the 70 and 90 °C spools.

The reason for there not being a significant difference between the polarized and freely corroding spools might be the initial negative current density requirements and then the small density requirements that was delivered from the anodes. See Chapter 7.3 for more details. The negative current for the spools with no heating, and 30 and 40 °C internal temperature provides no hydroxide production on the TSA, which means that no localized alkaline environment is created. This may mean that the CP does not contribute significantly to the calcareous deposit formation at low temperatures.

From Figure 6.19 it can be seen that the spools with 50 °C internal temperature or lower has a Mg/Ca ratio close to one. This indicates that the calcareous deposits are

Ca-based, or atleast parts of the deposits are Ca-based. This was expected based on the literature. The reason for this is that the CP system did not create a alkaline environment close to the TSA-seawater interface, because of the negative currents achieved due to the low corrosion potentials. This means, as mentioned in Chapter 7.3.1, that the calcareous deposits formation is probably a purely chemical precipitation due to the supersaturation of $CaCO_3$ in seawater, or that the deposits form only on intermetallic particles. The intermetallic particles are higher on the galvanic series than the aluminium matrix, and will therefore receive a protective current from the aluminium matrix, creating a alkaline environment at the particle-seawater interface.

It was assumed that more calcareous deposits should be formed at the polarized samples, however due to the low corrosion potential the roles of anode and coating switched and the anodic reaction, Equation 2.1, occurred on the TSA coating and therefore no pH increase at the water-metal interface occurred. The means that any calcareous deposits should precipitate in a similar way to the samples that was not polarized, and only spots of calcareous deposits should be found around intermetallic particles.

For the spool with 50 °C the current density requirement was positive the entire exposure time, and therefore the CP might effect the precipitation of calcareous deposits. Based on the SEM-photos there was not an obvious difference in the amount of the areas covered with calcareous deposits, both samples had spots of calcareous deposits on the surface, and no continuous film. This indicates that the CP did not contribute significantly to the precipitation, however the a difference is seen in the Mg/Ca-ratio.

There is small different between the samples connected to an anode and freely corroding samples at the two highest temperatures. The calcareous deposit does not seem to be concentrated around certain areas, as which the lower temperatures. From the SEM photos and the experiences done when doing the SEM analysis seem to indicate that more or less the entire surface of the samples with the highest temperatures is covered by calcareous deposits. This indicates that the calcareous deposits does not solely precipitate on and around intermetallic particles, not on the aluminium matrix as well. However, the spools with 70 and 90 °C also had a period of negative current demand, and has a low current density requirement when it becomes positive, with order of magnitudes lower than steel has. This indicates that the calcareous deposits formation may not have been very dependent on the CP.

### 8.1.3   Effect of Temperature

At low temperatures, 40 °C internal temperature and lower, there is not much difference between the different temperatures in regard to the amount of calcareous deposits. From the SEM photos it may be possible to see a slight increase in the amount of calcareous deposits, based on how much of the photos is covered with white areas. For the spools with 50 °C internal temperature and lower the Mg/Ca-ratio is between 0 and 2.3, and it is hard to conclude if any specific calcareous deposit is more dominating than any other from these values, as there is not any clear trend, therefore it is not unreasonable to assume that a more or less equal amount of $CaCO_3$ and $Mg(OH)_2$ is precipitated.

For 50 °C internal temperature and below, the white non-conductive areas generally have a high amount of carbon, oxygen, calcium magnesium and iron. This might indicate that $CaCO_3$ and $Mg(OH)_2$ or $MgCO_3$ calcareous deposits form around iron-based

intermetallic particles.

If the entire temperature range is considered however, an obvious trend appears. The Mg/Ca-ratio increases considerably from 25 °C surface temperature[1] to 45 and 60 °C external surface temperature[2].

On high temperatures, 70 and 90 °C internal temperature, the carbon and calcium content has been reduced dramatically, and is replaced by a very high Mg/Ca-content and oxygen content. This might indicate that the $CaCO_3$ deposits have been replaced by $Mg(OH)_2$ deposits. A difference between the polarized samples and the freely corroding samples may be seen in the amount of carbon and calcium detected in the EDS analysis. The freely corroding samples generally have a smaller amount or no carbon at all and a smaller amount of calcium in the EDS analysis while the polarized samples have some amount of carbon in it and a generally a higher amount of calcium. From the 90 °C internal temperature samples this is particularly clear.

This might indicate that small amount of $CaCO_3$ precipitate on the sample with CP in combination with $Mg(OH)_2$, while only $Mg(OH)_2$ formed on the samples freely corroding.

As mentioned in the theory the pH increase needed from depositing calcareous layers will be inhibited by the corrosion reactions occurring on TSA during CP, and this will likely prevent any significant built up of pH close to the TSA surface, preventing formation of calcareous deposits on TSA during CP.

From the SEM photos it looks like the surface of the TSA at high temperatures is more or less covered with calcareous deposits. This assumption of a more homogeneous precipitation on the high temperature spools is strengthened by the fact that all the EDS analysis taken on the surface of the TSA showed similar results, with high amount of Mg and O. This again indicates that the precipitation of calcareous deposits is not dependent on any galvanic connected that produces hydroxide through the cathodic reaction and creates and alkaline environment, but it purely driven by the high temperatures. Therefore the precipitation on the two highest spools may be dominated by thermodynamic precipitation as mention could be possible by Haraldsen [60] at high temperatures, in Chapter 2.4. This indicates that precipitation of calcareous deposits on TSA is more dependent on temperature than on CP.

### 8.1.4 Calcareous Deposit Thickness

For the lower temperatures[3] calcareous deposits mainly formed in small areas around and on intermetallic particles, and was not visual by the naked eye on the surface. This means that the area of the sample which was examined in the SEM was chosen randomly, and some searching had to be done to find the areas with calcareous deposits on it. When this was done for the cross-section of the specimen nothing was found.

For the two highest temperature the deposit is most likely $Mg(OH)_2$ which is know to be difficult to observe because it forms as a very thin layer. All in all there was very little calcareous deposits formed on the surface of the TSA, therefore this thesis was not

---

[1]The surface temperature of the spool with 50 ° internal temperature.
[2]The surface temperature of the spool with 70 and 90 ° internal temperature respectively.
[3]50 °C and lower

able to accurately quantified the thickness of the calcareous deposits with the equipment and techniques available.

It may, however, be possible to roughly estimate of the coating thickness, or atleast find what order of magnitude the thickness of the calcareous deposits are. All the EDS analysis performed in this thesis had atleast traces of aluminium in spectrum. This may be because the EDS analysis penetrated through the calcareous deposits and into the coating below. EDS analysis usually, depending on the test material and the power of the electron beam, penetrates between 2 and 6 $\mu m$ into the sample according to Goldstein et al [63]. It might therefore be reasonable to assume that the thickness of the calcareous deposits is no more than 6 $\mu m$, and probably 2 $\mu m$ or less.

### 8.1.5   Sources of Inaccuracy

Due to practical limitations only a small area of the TSA samples could be analysed in the SEM. It is is therefore not certain that the areas of examination is representative for the entire sample.

A fairly high amount of carbon was detected in the unexposed sample. This was unexpected, because there is no obvious carbon sources, as there is no obvious reason for it to be there. A source of the carbon might be the ethanol that is used to clean the samples before taken to the SEM, which might have penetrated the coating and gathered in the pores of the coatings. As a precaution the other samples were washed in distilled water and then dried using a hair drier, as a means to remove most the ethanol

The TSA used in this thesis is alloyed with Mg, which obviously may lead to a naturally higher Mg content than would be expected from the exposure alone. This means that the Mg/Ca-ratio might be higher than it should be. The Mg/Ca ratio for the two highest temperatures however is so high, that the amount of Mg alloying elements can be neglected. For the other temperatures however, these might cause some uncertainties with accurately determining the ratio of Mg and Ca.

The exposure time was not equal for all the experiments. The lower temperature[4] spools was started in the Specialization Project in November 2013, while the higher temperature[5] was started in March 2014. The reason for the difference in exposure time is purely practical. A lot time was used for redesigning the experiment, building the experiment, ordering parts and so on. The different exposure times may cause the results from the low temperatures and the high temperatures is not directly comparable due to the exposure time difference.

## 8.2   Thermal Conductivity

Due to the fact that no there was no significant difference in thermal conductivity between the different spools makes it impossible to say what effect temperature and cathodic protection had on the conductivity of TSA. Since the thermal conductivity was similar to the thermal conductivity of the stainless steel substrate, it might indicate that the TSA coating, calcareous deposits and oxides does not affect the conductivity of the pipe significantly.

---

[4]40°C internal temperature and below.
[5]50, 70 and 90°C internal temperature.

The reason for the calcareous deposits not affecting the conductivity may be due to the thickness of the deposits, which is very thin compared to the thickness of the pipe wall.

The sensor size used for the experiments had to be relatively large, because the surface of TSA is rough and uneven. This however, causes the experiments to measure the conductivity of a larger volume than smaller sensors would. The indications of this is that the thermal conductivity of the entire pipe wall is being measured, not only the TSA coating.

## 8.3  Blistering

As mentioned in Chapter 2 blistering might occur in TSA coatings when immersed in seawater at high temperatures. Unsealed TSA is especially prone to blistering. This was seen in spool freely corroding with 90 °C internal temperature, which is not surprising as the TSA tested in the thesis was unsealed. In the coating characterization huge pores were found, this combined with high temperature is known to increase the chances of blistering. This is what probably occurred with the 90 °C internal temperature spool. The high corrosion rate quickly filled the huge pores in the coating, which created internal stress in the coating which caused it to crack and blister.

Applying a sealer that fills the pores might prevent corrosion products from accumulating in the pores, and this might prevent blistering. A sealer will also cause a lower corrosion rate, which will atleast cause blistering to occur after a longer time than without the sealer.

# Chapter 9

# Conclusion

- The corrosion rate of TSA increases with temperature. Initially the corrosion rate of TSA is quite high, but it quickly decreases for all temperature. The corrosion rate for the 90 °C internal temperature was initially 50 $mm/year$ but decreased to 8 $mm/year$ after 65 days. The corrosion rate for the spool with no heating has initially 27 $mm/year$ but decreased to 2 $mm/year$ after 150 days.

- The current density requirement for TSA is very low compared to steel, with a current density requirement of 3-5 $mA/m^2$ obtained in this thesis. Temperature increases the current demand slightly. Based on experiments done in this thesis and the literature it is safe to say that following the DNV recommended practice for current demand for TSA is acceptable, even though the recommended practice may be conservative.

- High temperatures will initially cause TSA to have very low corrosion potentials, but the potential will increase over time. These initial low corrosion potential will cause negative current demands at high temperatures, meaning that the coating is cathodically protecting the anodes. After sometime the corrosion potential of the TSA increases and the current demand comes positive, and the anodes starts protecting the coating.

- High temperatures may cause blistering in TSA coatings, which might significantly reduce the life time of the coating. Applying a sealer might mitigate this problem and should be applied if the TSA should be exposed to high temperatures.

- Calcareous deposits form on TSA at all temperature on both polarized and freely corroding samples, but not as a continuous protective layer on TSA as with steel. Precipitation of calcareous deposits on TSA seems to be undependable of a CP system. At low temperature calcareous deposits mainly precipitation in small areas around intermetallic particles. At higher temperature the calcareous deposits form mostly as thin layers in on the surface by thermodynamic precipitation. The temperature effects the amount and type of calcareous deposits which form on TSA. At

high temperature the calcareous deposits mainly consist of $Mg(OH)_2$ and at low temperature the calcareous deposits mainly consist of $CaCO_3$.

- Thermal conductivity measurements shows that the TSA coating and calcareous deposits is negligible when it comes to the overall thermal conductivity of the pipe.

- The combination of negligible thermal conductivity, small corrosion rate and small current demand makes TSA a solid corrosion protection choice for subsea heat exchangers.

# Chapter 10

# Recommendations for Further Study

- Finding techniques to accurately measure the thickness of the very thin calcareous deposits which form on TSA may be useful, if the precisely determining the thickness of these layers is important.

- More experiments, especially at lower temperatures should be conducted to find the actual corrosion potential and thereby the correct current density requirement. The protection potential applied to the TSA should be approximately -1050 mV Ag/AgCl, so the results can be compared.

- Finding a way to accurate measure the pH development over time at the TSA-water interface during the exposure would make it possible to give a more accurate presentation of the precipitation of calcareous deposits on TSA.

- Investigations of other possible coatings, which is not prone to rapid deterioration when overly protected by a CP system at high temperatures may be beneficial.

# Bibliography

[1] K.P. Fischer. Field testing of cp current requirements at depths down to 1300m on the norwegian continental shelf from 63 to 67° n. In *NACE International*, Sandefjord, Norway, 1999.

[2] S.L. Wolfson. Corrosion control of subsea piping systems using thermal sprayed aluminium coatings. *NACE International*, (560), 1996.

[3] R.S.C. Paredes, S.C. Amico, and A.S.C.M. d'Oliveira. The effect of roughness and pre-heating of the substrate on morphology of aluminium coatings depoisted by thermal spraying. *Surface & Coatings Technology*, 200:3049–3055, 2006.

[4] P.O. Gartland. Protective properties of al-based coatings in seawater. Number STF34 F91106. SINTEF Corrosion Center, 1991.

[5] S.D. Berti, B.A. Shaw, and W.W.S. Shaw. Corrosion evaluation of aluminium sacrificial coating applied by various sprayed metal techniques. *NACE Internatinal*, 2002.

[6] O. Doeble and G. Pryde. Use of thermally sprayed aluminium in the norwegian offshore industry. Technology Publisher Company, 1997.

[7] T.G. Eggen. Thermal sprayed coating of al and zn - surface preparation and application. Number STF34 F91085. SINTEF Corrosion Center, 1991.

[8] R.M.H.P. Rodriguez, R.S.C. Paredes, S.H. Wido, and A. Calixto. Comparison of aluminium coatings deposited by flame spray and by electric arc spray. *Surface Coatings and Technology*, 202:172–179, 2007.

[9] V.R.S. Sá Brito, I.N. Bastos, and H.R.M. Costa. Corrosion resistance and characterization of metallic coatings deposited by thermal spray on carbon steel. *Materials and design*, 41:282–288, 2012.

[10] D. Harvey, S. Shrestha, S. Paul, and C. Lee. Thermally sprayed aluminium coatings for the mitigation of corrosion and environmentally assisted cracking of welded duplex stainless steel at elevated temperature. *NACE International*, (2621), 2013.

[11] NORSOK Standard. Surface preparation and protective coating. *NORSOK M-501*, 2012.

[12] European Standard. Preparation of steel substrates before application of paints and related products - surface roughness characteristics of blast-cleaned steel substrates. *ISO 8503-1*, 2012.

[13] International Standard. Preparation of steel substrates before application of paints and related products - visual assessment of surface cleanliness. *ISO 8501-1*, 2007.

[14] M-S. Han, Y-B. Woo, S-C. Ko, Y-J. Jeong, S-K. Jang, and S-J. Kim. Effects of thickness of al thermal spray coatings for sts 304. *Transactions of nonferrous Metals Society of China*, 19:925–929, 2009.

[15] M.D.F. Harvey, S. Shrestha, and A.J. Sturgeon. Coatings for offshore applications by high velocity wire flame spraying. *NACE International*, (05011), 2005.

[16] T.G. Eggen and J.M. Drugli. Sea water corrosion of thermal sprayed aluminium. Number STF34 F93108. SINTEF Corrosion Center, 1993.

[17] K. Nisancioglu. *Corrosion behaviour and protection of copper and aluminium alloys in seawater*. Number 50. Woodhead Publishing Limited, 1 edition, 2007.

[18] P.O. Gartland and T.G. Eggen. Thermal sprayed aluminium coatings in sea water with and without cathodic protection. SINTEF Corrosion Center, N-7034 Trondheim, Norwa, 1993.

[19] T. Rosbrook, M.A.M Swidzinski, and C.J. Houghton. Thermal spray aluminium past, present and future. *NACE International*, (616), 1999.

[20] W.H.Thomason, S. Olsen, T. Haugen, and K. Fischer. Deterioration of thermal sprayed aluminium coatings on hot risers due to thermal cycling. *NACE International*, (04021), 2004.

[21] P.O. Gartland and T.G. Eggen. Aluminium arc spray for riser couplings. Number STF34 F91097. SINTEF Corrosion Center, 1990.

[22] E. Bardal. *Corrosion and Corrosion Protection*. Tapir Akademiske Forlag, 3 edition, 1994.

[23] Y.G. Kweon, R.W. Chang, Y.M. Yang, and S.M. Lee. Blistering behaviour of thermally sprayed aluminium metallic coatings in seawater. *The International Society of Offshore and Polar Engineers*, 1992.

[24] W.H. Thomason. Offshore corrosion protection with thermal-sprayed aluminium. *Offshore Technology Conference*, 1985.

[25] C. Vargel. *Corrosion of Aluminium*. Elsevier Ltd Oxford England, 1 edition, 2004.

[26] R.D. Armstrong and V.J. Braham. The mechanism of aluminium corrosion in alkaline solutions. ”*Corrosion Science*, 38(9):1463–1471, 1996.

[27] C. Deslouis, P. Falaras, O. Gil, V. Maillot M. Jeannin, and B. Tribollet. Influence of clay on calcareous deposit in natural and artificial sea watere. *Electrochimica Acta*, 51:3173–3180, 2006.

[28] C. Deslouis, D. Festy, O. Gil, S. Touzain G. Ruis, and B. Tribollet. Characterization of calcareous deposits in artificial sea water by impedance techniques – i. deposits of caco3 without mg(oh)2. *Electrochimica Acta*, 43:1891–1901, 1998.

[29] S.M. Moon and S.I. Pyun. The corrosion of pure aluminium during cathodic polarization in aqueous solutions. *Corrosion Science*, 39(2):399–408, 1997.

[30] Ph. Gimenez, J.J. Rameau, and M.C. Reboul. Experimental ph potential diagram of aluminium for sea water. *NACE International*, (12), 1981.

[31] K. Nisancioglu and T. Wenn. Corrosion and cathodic protection of aluminium in flowing sea water. In *12th Scandinacion Corrosion Congress and Eurocorr 92*. NTH Institt for teknisk elektrokjemi, N-7034 TRONDHEIM and SINTEF, Korrosjonssentret, N-7034 TRONDHEIM, NORWAY, 1992.

[32] K. Nisancioglu, O. Lunder, and H. Holtan. Improving the corrosion resistance of aluminium alloys by cathodic polarization in aqueous media. *CORROSION*, 41:247–257, 1985.

[33] D.A. Shifler. Understanding material interactions in marine enviornments to promote extended structural life. *Corrosion Science*, 2005.

[34] G. Svenningsen. *Intergranular Corrosion of AA600-series Aluminium Alloys*. PhD thesis, Norwegian University of Science and Technology, 2005.

[35] J. Birn and I. Skalski. *Corrosion behaviour and protection of copper and aluminium alloys in seawater*. Number 50. Woodhead Publishing Limited, 1 edition, 2007.

[36] Z. Szklarska-Smialowska. Pitting corrosion of aluminium. *Corrosion Science*, 41:1743–1767, 1999.

[37] A. Bjørgum, H. Sigurdsson, and K. Nisancioglu. Corrosion of commercially pure al 99.5 in chloride solutions containing carbon dioxide, bicarconate, and copper ions. *NACE International*, (7), 1995.

[38] K.P. Fischer, W.H. Thomason, and J.E. Finnegan. Electrochemical performance of flame sprayed aluminium coatings in seawater. *NACE International*, (360), 1987.

[39] P.O. Gartland. Cathodic protection of aluminium-coated steel in seawater. *NACE International*, (299), 1986.

[40] T.G. Eggen and P.O. Gartland. Termally sprayed coatings of al and zn - long time testing of al, almg and znal-coatings in sea water. Number STF16 F87063. SINTEF Corrosion Center, 1989.

[41] K.P. Fischer, W.H. Thomason, and J. Murali. Performance history of thermal-sprayed aluminium coatings in offshore service. *Materials Performance*, 34:27–35, 1995.

[42] Ole Øystein Knudsen and Trond Rogne. Rapid degradation of painted tsa. *NACE International*, (04023), 2002.

[43] J.L. Solis and J. Genesca. Effect of calcareous deposits on galvanic anode cathodic protection of steel in seawater. *NACE International*, (09520), 2009.

[44] C. Barchiche, C. Deslouis, P. Refait O. Gil, and B. Tribollet. Characterization of calcareous deposits by electrochemical methods: Role of sulphates, calcium concentration and temperature. *Electrochimica Acta*, 49:2833–2839, 2004.

[45] W. Sun, G. Liu, L. Wang, and Y. Li. A mathematical model for modeling the formation of calcareous deposits on cathodically protected steel in seawater. *Electrochimica Acta*, 78:587–608, 2012.

[46] K.P. Fischer, W.H. Thomason, and S. Eliassen. Cp in deep water: The importance of calcareous deposits and the environmental conditions. *NACE International*, 1996.

[47] R. Gundersen and K. Nisancioglu. Cathodic protection of aluminium in seawater. *CORROSION*, 46:279–285, 1990.

[48] K. Nisancioglu and H. Holtan. Corrosion of aluminium in aqueous chloride media. Norwegian Institute of Technology, Laboratories of Industrial Electrochemistry, N-7034 Trondheim-NTH, Norway, 1975.

[49] Solveig Egtvedt. *Thermally Sprayed Aluminum (TSA) with Cathodic Protection as Corrosion Protection for Steel in Natural Seawater.* Master thesis, NTNU, 2011.

[50] M. Surkein, S. Leblanc, S. Richard, and J.P. La Fontaine. Corrosion protection program for high temperature subsea pipeline. *NACE International*, 2001.

[51] DNV RECOMMENDED PRACTICE. Cathodic protection design. *DNV-RP-B401*, 2010.

[52] O.Ø. Knudsen, G. Clapp, J.V. Bokhorst, and G. Duncan. Corrosion of cathodically polarized tsa in subsea mud at high temperature. *NACE International*, 2014.

[53] S.C. Dexter and S.H. Lin. Calculation of seawater ph at polarized metal surfaces in the presence of surface films. *NACE International*, 1991.

[54] A. Neville and A.P. Marizot. Calcareous scales formed by cathodic protection – an assessment of characteristics and kinetic. ” *Journal of Crystal Growth*, 243:490–502, 2002.

[55] C. Deslouis, O. Gil D. Festy, V. Maillot, S. Touzain, and B. Tribollet. Characterization of calcareous deposits in artificial sea water by impedences techniques: 2.deposit of mg(oh)2 without caco3. *Electrochimica Acta*, 45:1837–1845, 2000.

[56] C. Deslouis, A.Doncescu, D. Festy, O. Gil, V. Maillot, S. Touzain, and B. Tribollet. Kinetics and characterisation of calcareous deposits under cathodic protection in natural sea water. *Materials Science Froum*, 289-292:1163–1180, 1998.

[57] H. Möller. The influence of mg2+ on the formation of calcareous deposits on a freely corroding low carbon steel in seawater. *Corrosion Science*, 49:1992–2001, 2007.

[58] H.P. Hack and R.J. Guanti. Effect of high flow on calcareous deposits and cathodic protection current denisty. *NACE International*, (38), 1988.

[59] NACE: The International Corrosion Foum. *Calcareous Deposits deposits on metal surfaces in sea water - a critical review*, NACE: Anaheim, California, 1983.

[60] Kristian Haraldsen. Subsea cooling project. factors affecting external scale formation. Hydro Oil & Energy Internal Report, 2007.

[61] M.T. Cooper and J.D.C. Vardon. Hutton tlp:innovative corrosion control systems for a new generation platform. *Offshore Technology Conference*, 1985.

[62] G.H. Aylward and T. Findlay. *SI Chemical DATA*. John Wiley & Sons Austrailia, Limited, 6 edition, 2008.

[63] J.I.Goldstein, C.E. Lyman, D.E. Newbury, E. Lifshin, P. Echlin, L. Sawyer, D.C. Joy, and J.R. Michael. *Scanning Electron Microscope and X-Ray Microanalysis*. Kluwer Academic/Plenum Publisher, New York, 3 edition, 2003.

# Appendices

# Appendix A

# Equipment

Table A.1: Equipment used for making the test spools.

| Equipment | Vendor | Quantity |
|---|---|---|
| 78mm Pipe with Thermally sprayed aluminium coating | Aker Soluton | 4 |
| Teflon Isolation Pieces | Hatling AS | 3 |
| Teflon Plug | Hatling AS | 1 |
| Teflon Top Piece | Hatling AS | 1 |
| O-Ring Gaskets | Abra AS | 6 |
| PTFE 19/0.2 White Wire | RS Components | 10 m |
| Banana connector | RS Components | 9 |

Table A.2: Equipment needed for electrochemical measurements.

| Equipment | Vendor | Quantity |
|---|---|---|
| Anode Coral A-12-1 | Jotun | 1 |
| Ag/AgCl Reference Electrode | | 1 |
| Resistance Box | | 2 |
| Multimetre | Fluke | 2 |
| Potensiostat | | 1 |

**Table A.3:** EEquipment used for heating the spools during the experiment.

| Equipment | Vendor | Quantity |
|---|---|---|
| Heating Element | Jens Gundersen A/S | 1 |
| Carroll & Meynell 1 Phase 720VA Variac | RS Components | 1 |
| Mazurczak Electronic Temperature Controller | Jens Gundersen A/S | 1 |
| Thermocouples | RS Components | 6 |
| Thermocouple Module | RS Components | 6 |
| Aquarium Air Pump | Tropehagen Zoo | 1 |
| Oil | | 2 L |

# Appendix B

# Technical Data for Coral A Anode

# *TECHNICAL DATA*

## *CORAL A*
### *HIGH GRADE*

### *Al-In-Zn alloy*

Chemical composition according to NORSOK specification no. M-503, rev. 2 and certified according to DnV Type Approval program, IOD-90-TAI, November 1982.

The chemical composition and performance data of CORAL 'A' High Grade allloy are as follows:

| **Elements** | **Analysis (% by weight)** |
|---|---|
| Zn | 3,5 – 5,0 |
| In | 0,015 – 0,025 |
| Cu | max. 0,003 |
| Fe | max. 0,09 |
| Si | max. 0,10 |
| Others (each) | max. 0,020 |
| Al | Remainder |

## **Specific gravity**

2,78 $kg/dm^3$ (theoretically)

## **Performance data in ambient sea water**

| | |
|---|---|
| Capacity | 2585 Ah/kg |
| Consumption rate | 3,39 kg/A.yr |
| Closed circuit potential | -1,09 volt v.s. Ag/AgCl/sea water |

## **Performance data in sea bottom sediments (mud)**

| | 0-20$^o$C | 40$^o$C | 60$^o$C | 80$^o$C |
|---|---|---|---|---|
| Capacity (Ah/kg) | 2400 | 1750 | 1150 | 600 |
| Consumption rate (kg/A.yr) | 3,65 | 5,00 | 7,62 | 14,6 |
| Closed circuit potential (volt v.s. Ag/AgCl/sea water | -1,05 | -1,03 | -1,01 | -1,00 |

# Appendix C

# Pictures of the test spools
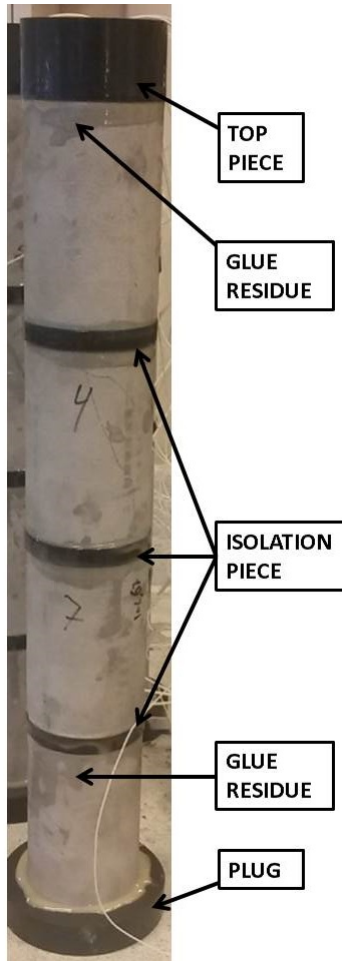
**Figure C.1:** Picture of spool used for no heating, 30 $^\circ$C and 40 $^\circ$C.
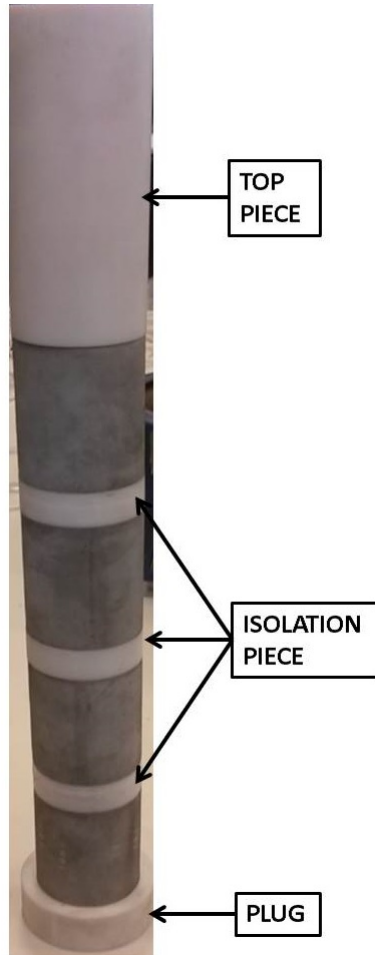
**Figure C.2:** Picture of spool used for 50, 70 and 90°C internal temperature.

# Linear Polarization Resistance Values

| Date | No heating | | 40 °C | | 50 °C | | 70 °C | | 90 °C | |
|---|---|---|---|---|---|---|---|---|---|---|
| | Cathodic [mA] | Anodic [mA] | Cathodic [mA] | Anodic [mA] | Cathodic [mA] | Anodic [mA] | Cathodic [mA] | Anodic [mA] | Cathodic [mA] | Anodic [mA] |
| 04.02.2014 | 0,02 | 0,02 | 0,02 | 0,01 | - | - | - | - | - | - |
| 11.02.2014 | 0,02 | 0,02 | 0,02 | 0,015 | - | - | - | - | - | - |
| 18.02.2014 | - | - | 0,01 | 0,01 | - | - | - | - | - | - |
| 25.02.2014 | 0,01 | 0,01 | 0,01 | 0,01 | - | - | - | - | - | - |
| 04.03.2014 | 0,02 | 0,015 | 0,005 | 0,01 | - | - | - | - | - | - |
| 12.03.2014 | 0,013 | 0,015 | 0,005 | 0,005 | - | - | - | - | - | - |
| 18.03.2014 | 0,015 | 0,014 | 0,005 | 0,005 | - | - | 0,07 | 0,07 | 0,09 | 0,063 |
| 25.03.2014 | 0,02 | 0,014 | 0,005 | 0,005 | 0,05 | 0,05 | 0,04 | 0,03 | 0,08 | 0,09 |
| 01.04.2014 | 0,008 | 0,003 | 0,005 | 0,003 | 0,035 | 0,025 | 0,04 | 0,02 | 0,04 | 0,043 |
| 15.04.2014 | - | - | - | - | 0,035 | 0,01 | 0,01 | 0,01 | 0,04 | 0,014 |
| 22.04.2014 | - | - | - | - | 0,025 | 0,01 | 0,012 | 0,006 | 0,02 | 0,02 |
| 29.04.2014 | - | - | - | - | 0,02 | 0,017 | 0,014 | 0,01 | 0,02 | 0,02 |
| 06.05.2014 | - | - | - | - | 0,008 | 0,01 | 0,01 | 0,011 | 0,012 | 0,007 |
| 13.05.2013 | - | - | - | - | 0,018 | 0,017 | 0,013 | 0,014 | 0,01 | 0,006 |

**Table D.1:** Values obtained by LPR during the exposure of TSA.

# E | Appendix

# Polarization Curves

## E.1 Curves No Internal Heating
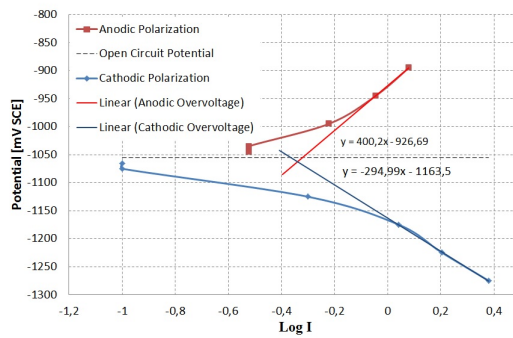


**Figure E.1:** Polarization Curve of thermally sprayed aluminium with no internal heating, obtained 06.11.13
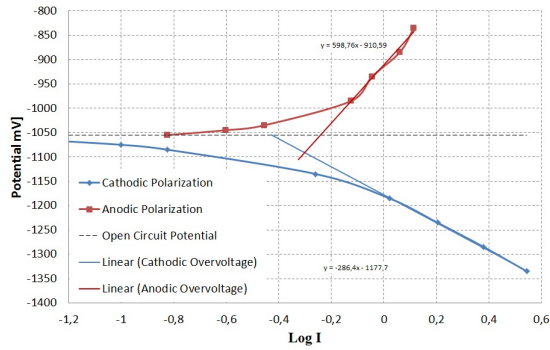
**Figure E.2:** Polarization Curve of thermally sprayed aluminium with no internal heating, obtained 09.11.13
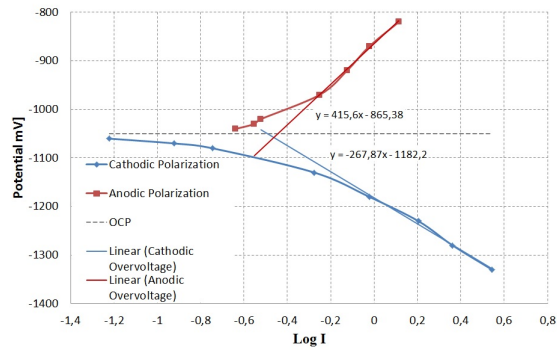


**Figure E.3:** Polarization Curve of thermally sprayed aluminium with no internal heating, obtained 11.11.13
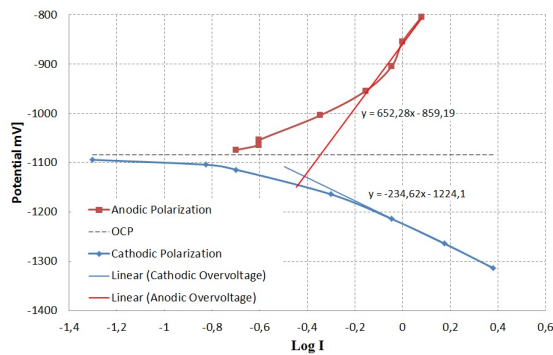


**Figure E.4:** Polarization Curve of thermally sprayed aluminium with no internal heating, obtained 14.11.13
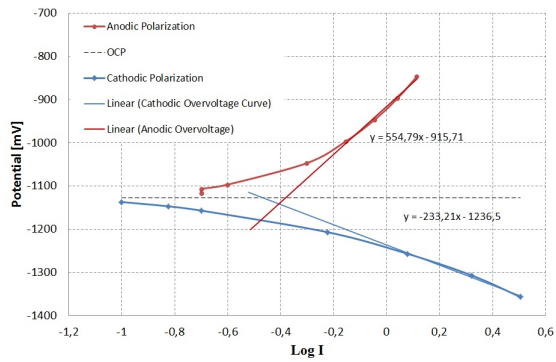
**Figure E.5:** Polarization Curve of thermally sprayed aluminium with no internal heating, obtained 18.11.13
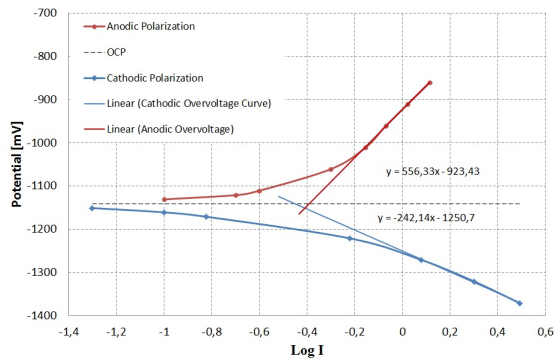


**Figure E.6:** Polarization Curve of thermally sprayed aluminium with no internal heating, obtained 21.11.13
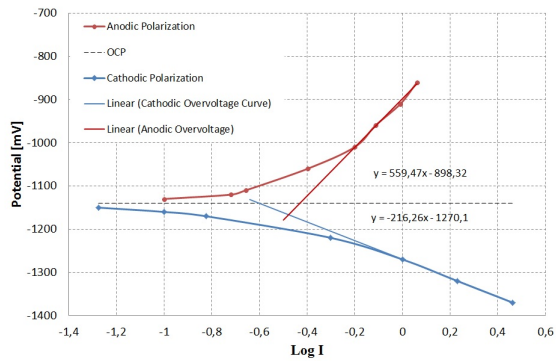


**Figure E.7:** Polarization Curve of thermally sprayed aluminium with no internal heating, obtained 25.11.13
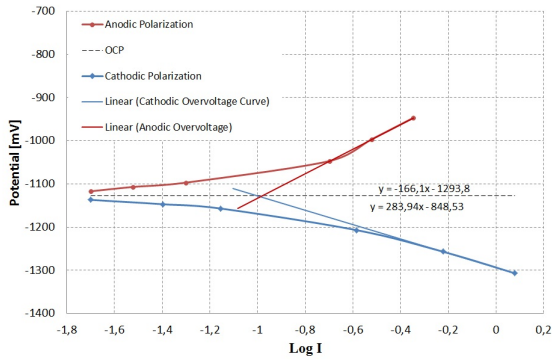
**Figure E.8:** Polarization Curve of thermally sprayed aluminium with no internal heating,, obtained 04.02.14
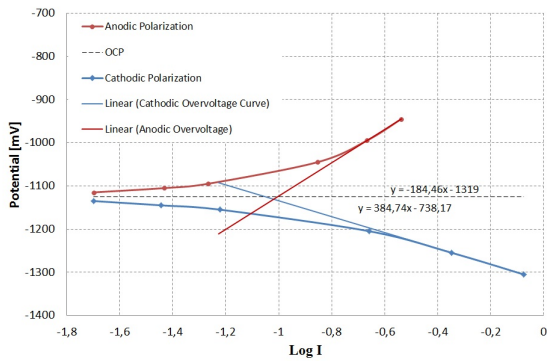


**Figure E.9:** Polarization Curve of thermally sprayed aluminium with no internal heating,, obtained 11.02.14
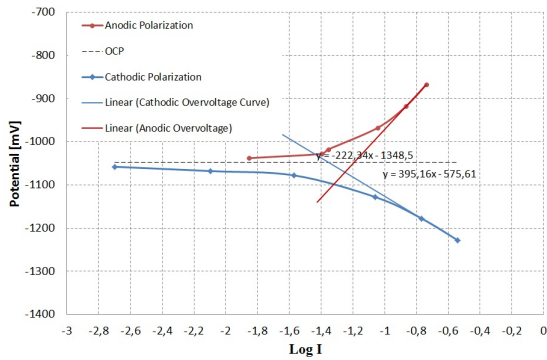


**Figure E.10:** Polarization Curve of thermally sprayed aluminium with no internal heating, obtained 25.03.14
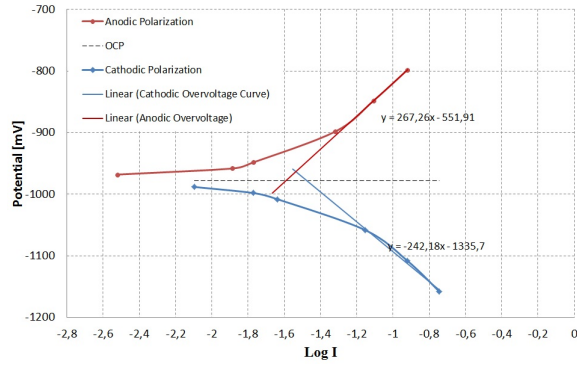
**Figure E.11:** Polarization Curve of thermally sprayed aluminium with no internal heating, obtained 01.04.14
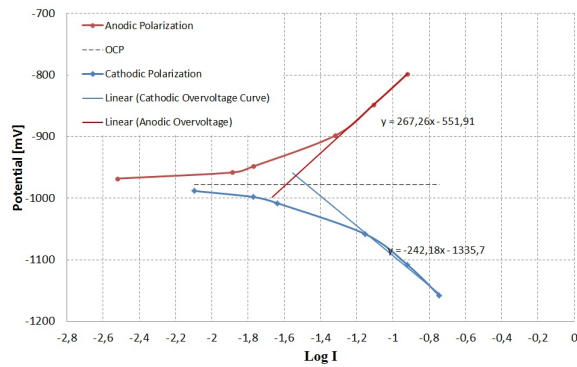


**Figure E.12:** Polarization Curve of thermally sprayed aluminium with no internal heating, obtained 15.04.14

# E.2 Polarization Curves 30 ° C Internal Temperature
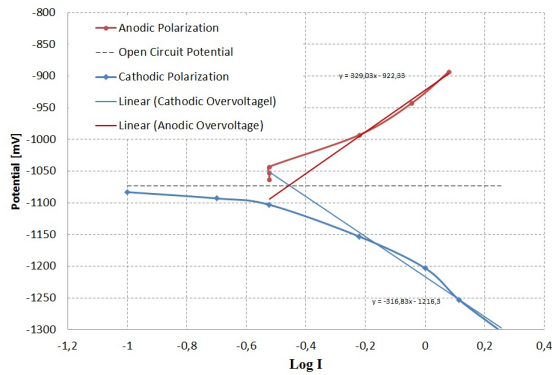


**Figure E.13:** Polarization Curve of thermally sprayed aluminium with an internal temperature of 30 °C, obtained 06.11.13
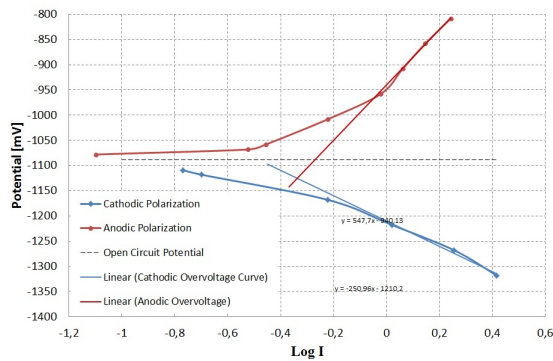


**Figure E.14:** Polarization Curve of thermally sprayed aluminium with an internal temperature 30 °C, obtained 09.11.13
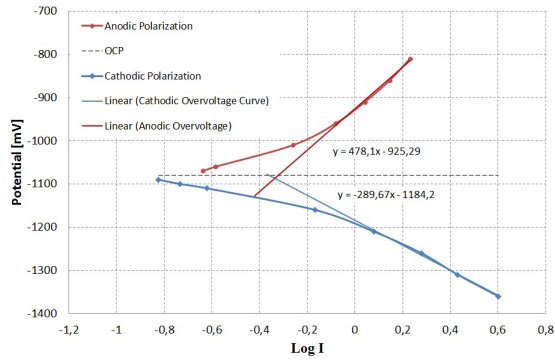
**Figure E.15:** Polarization Curve of thermally sprayed aluminium with an internal temperature 30 °C, obtained 11.11.13
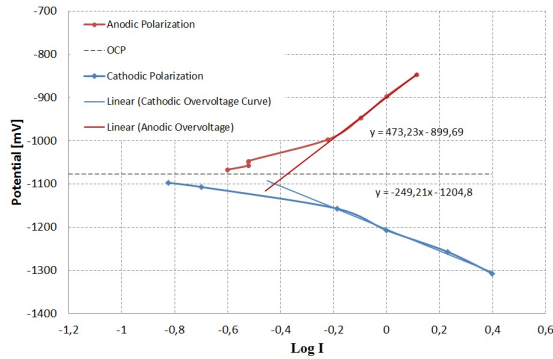


**Figure E.16:** Polarization Curve of thermally sprayed aluminium with an internal temperature 30 °C, obtained 14.11.13
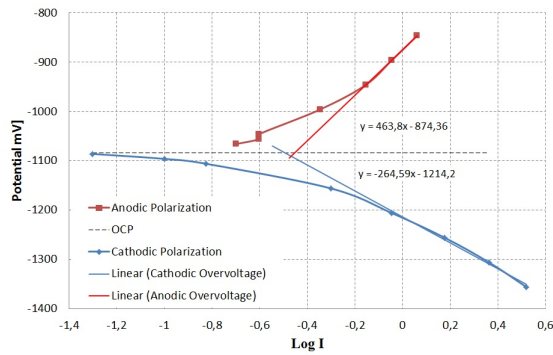


**Figure E.17:** Polarization Curve of thermally sprayed aluminium with an internal temperature 30 °C, obtained 18.11.13
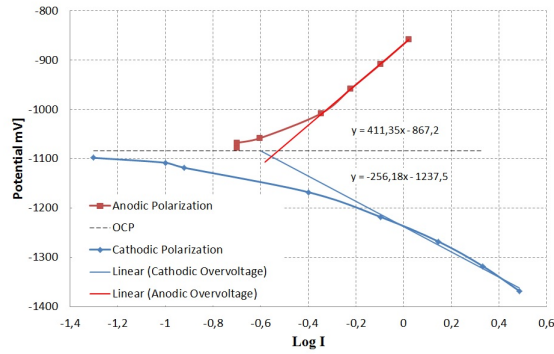
**Figure E.18:** Polarization Curve of thermally sprayed aluminium with an internal temperature 30 °C, obtained 21.11.13
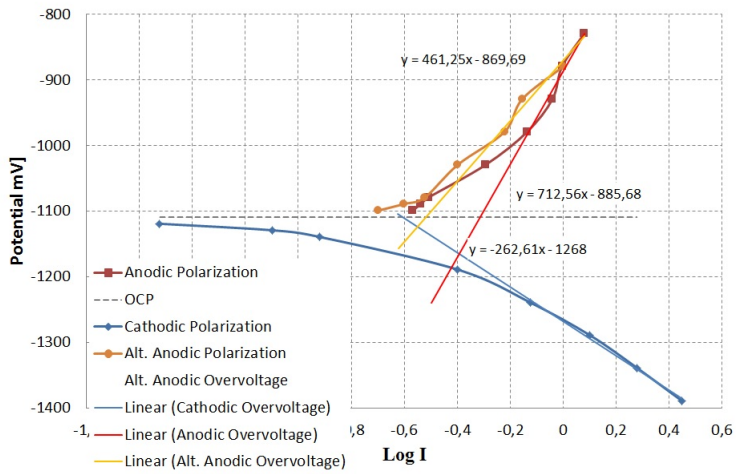


**Figure E.19:** Polarization Curve of thermally sprayed aluminium with an internal temperature 30 °C, obtained 25.11.13

# E.3 Polarization Curves 40 ° C Internal Temperature
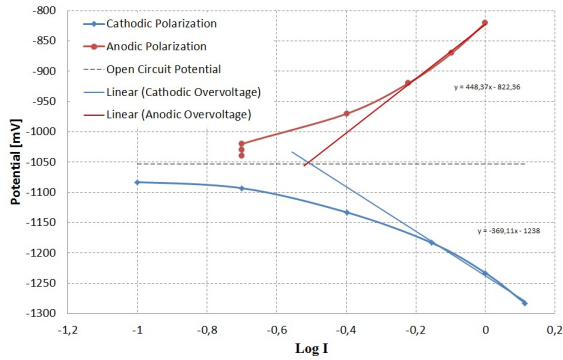


**Figure E.20:** Polarization Curve of thermally sprayed aluminium with an internal temperature 40 °C, obtained 06.11.13
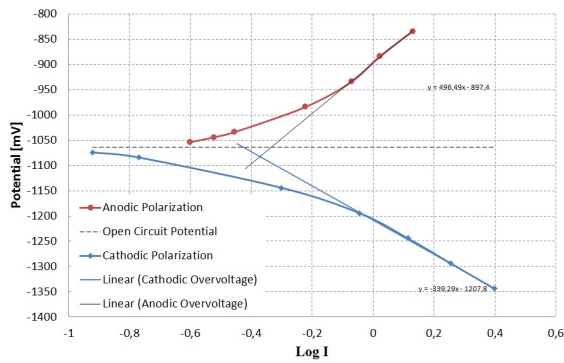


**Figure E.21:** Polarization Curve of thermally sprayed aluminium with an internal temperature 40 °C, obtained 09.11.13
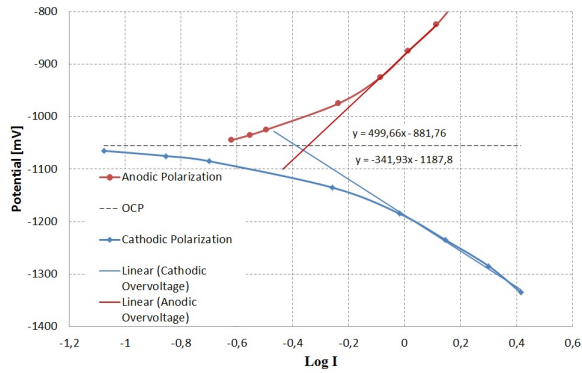
**Figure E.22:** Polarization Curve of thermally sprayed aluminium with an internal temperature 40 °C, obtained 11.11.13
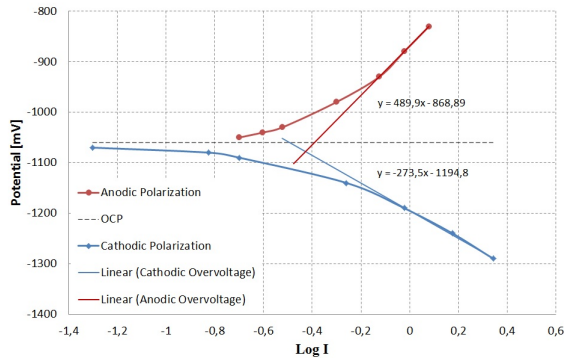


**Figure E.23:** Polarization Curve of thermally sprayed aluminium with an internal temperature 40 °C, obtained 14.11.13
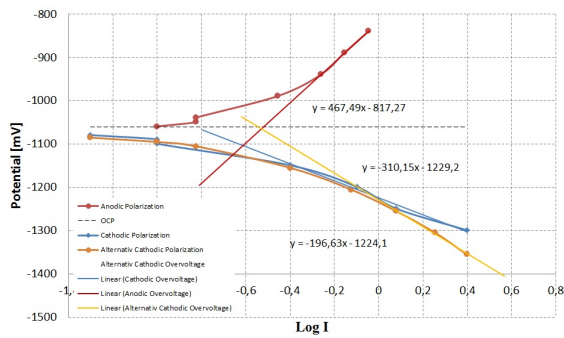


**Figure E.24:** Polarization Curve of thermally sprayed aluminium with an internal temperature 40 °C, obtained 18.11.13
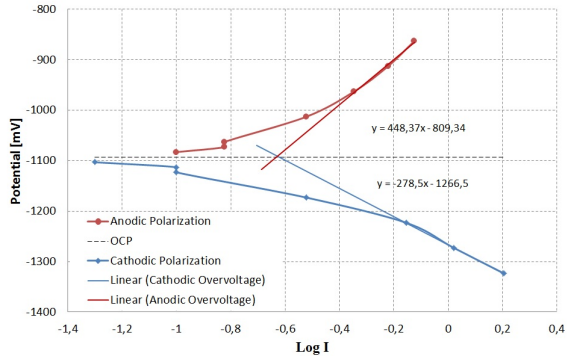
**Figure E.25:** Polarization Curve of thermally sprayed aluminium with an internal temperature 40 °C, obtained 21.11.13
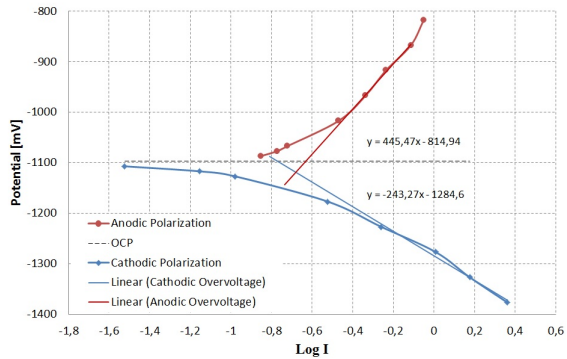


**Figure E.26:** Polarization Curve of thermally sprayed aluminium with an internal temperature 40 °C, obtained 25.11.13
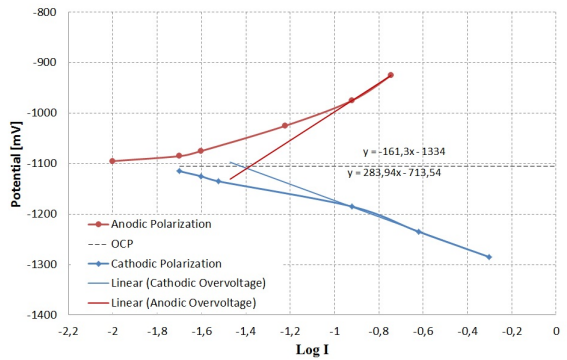


**Figure E.27:** Polarization Curve of thermally sprayed aluminium with an internal temperature 40 °C, obtained 04.02.14
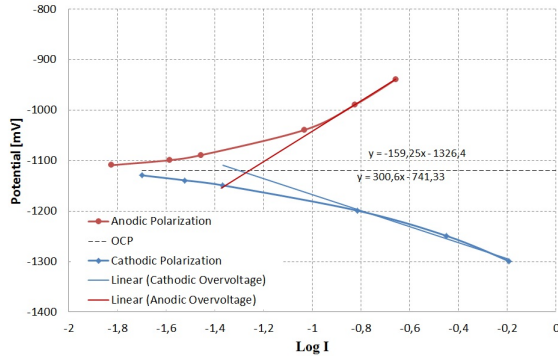
**Figure E.28:** Polarization Curve of thermally sprayed aluminium with an internal temperature 40 °C, obtained 11.02.14
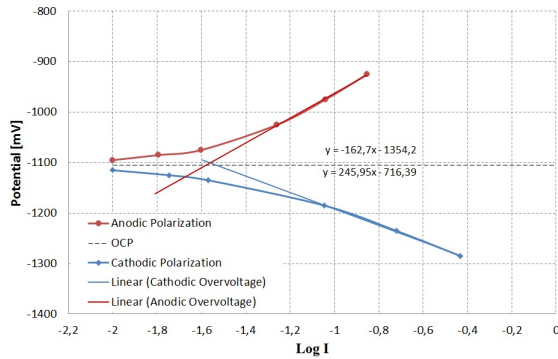


**Figure E.29:** Polarization Curve of thermally sprayed aluminium with an internal temperature 40 °C, obtained 18.02.14
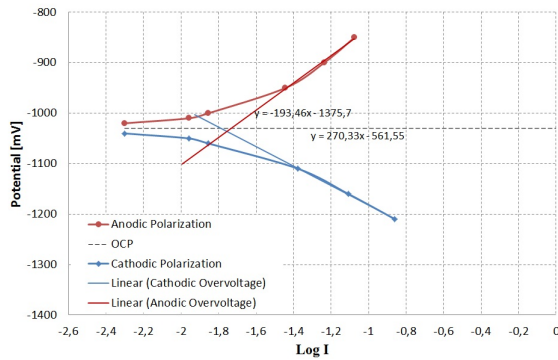


**Figure E.30:** Polarization Curve of thermally sprayed aluminium with an internal temperature 40 °C, obtained 25.03.14
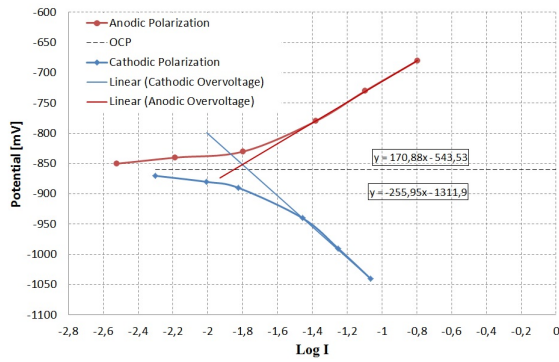
**Figure E.31:** Polarization Curve of thermally sprayed aluminium with an internal temperature 40 °C, obtained 01.04.14
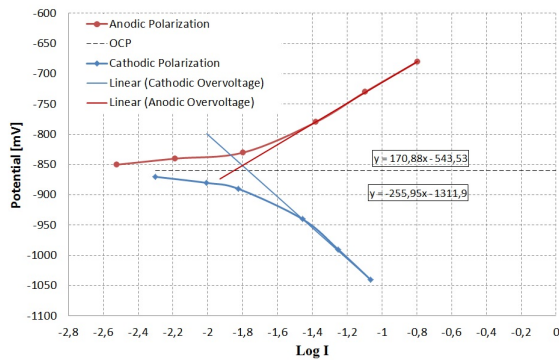


**Figure E.32:** Polarization Curve of thermally sprayed aluminium with an internal temperature 40 °C, obtained 15.04.14

# E.4 Polarization Curves 50 °C Internal Temperature
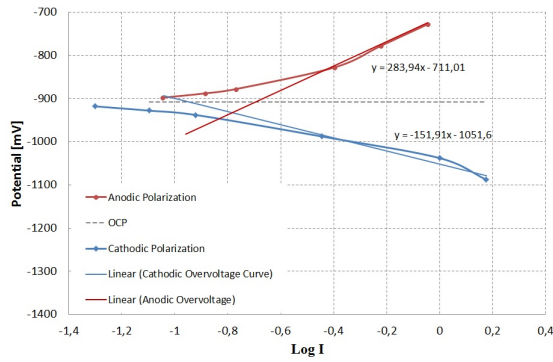


**Figure E.33:** Polarization Curve of thermally sprayed aluminium with an internal temperature 50 °C, obtained 25.03.14
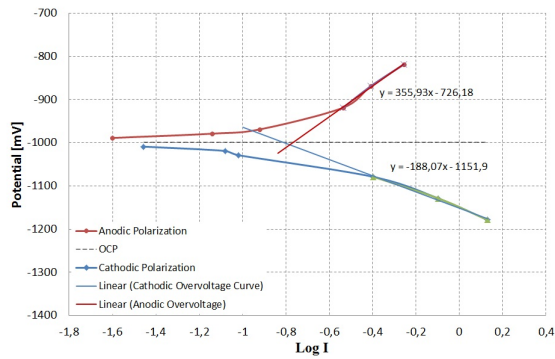


**Figure E.34:** Polarization Curve of thermally sprayed aluminium with an internal temperature 50 °C, obtained 01.04.14
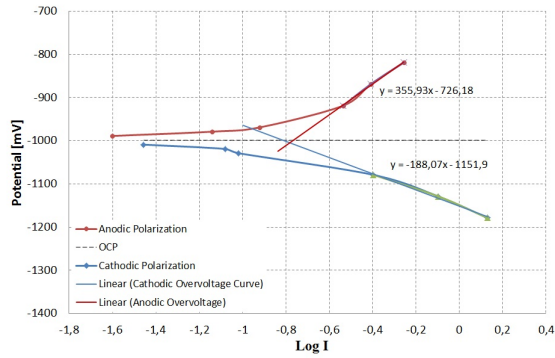
**Figure E.35:** Polarization Curve of thermally sprayed aluminium with an internal temperature 50 °C, obtained 15.04.14
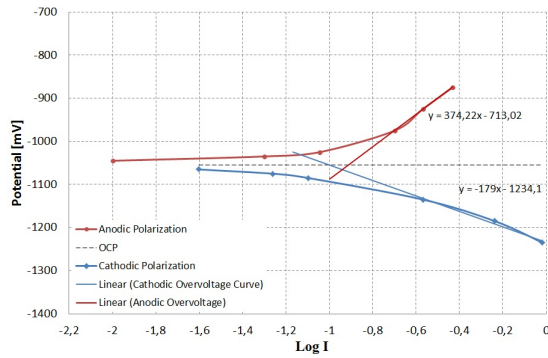


**Figure E.36:** Polarization Curve of thermally sprayed aluminium with an internal temperature 50 °C, obtained 22.04.14
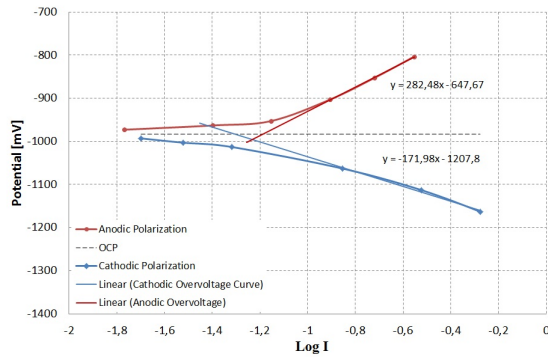


**Figure E.37:** Polarization Curve of thermally sprayed aluminium with an internal temperature 50 °C, obtained 29.04.14
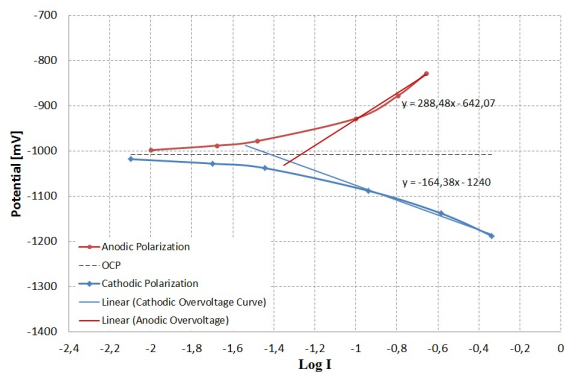
**Figure E.38:** Polarization Curve of thermally sprayed aluminium with an internal temperature 50 °C, obtained 06.05.14
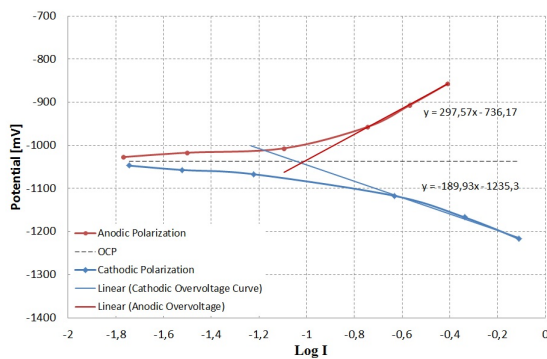


**Figure E.39:** Polarization Curve of thermally sprayed aluminium with an internal temperature 50 °C, obtained 13.05.14

# E.5    Polarization Curves 70 °C Internal Temperature
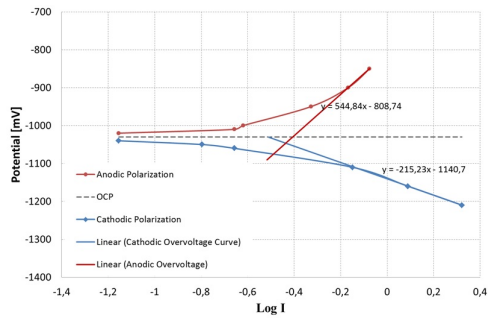


**Figure E.40:** Polarization Curve of thermally sprayed aluminium with an internal temperature 70 °C, obtained 18.03.14
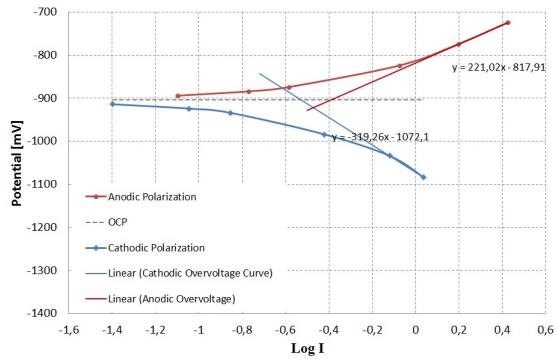


**Figure E.41:** Polarization Curve of thermally sprayed aluminium with an internal temperature 70 °C, obtained 25.03.14
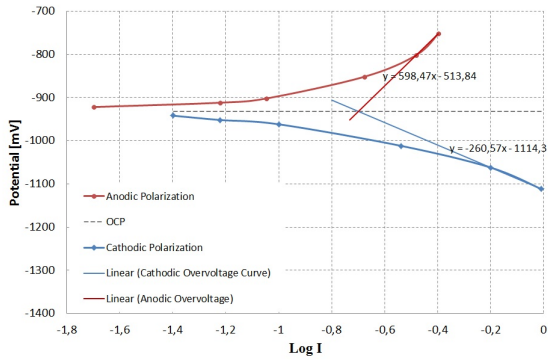
**Figure E.42:** Polarization Curve of thermally sprayed aluminium with an internal temperature 70 °C, obtained 01.04.14
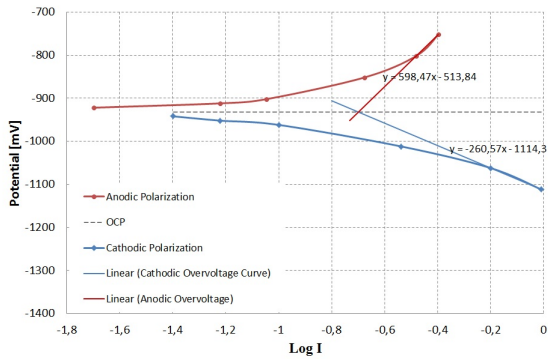


**Figure E.43:** Polarization Curve of thermally sprayed aluminium with an internal temperature 70 °C, obtained 15.04.14
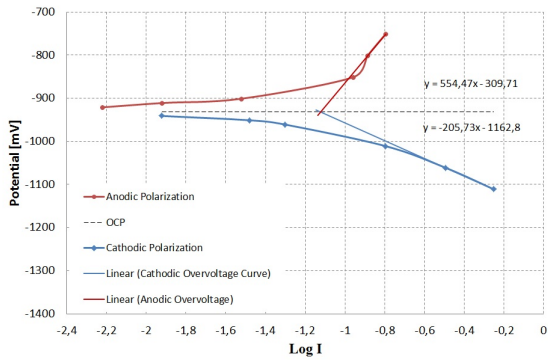


**Figure E.44:** Polarization Curve of thermally sprayed aluminium with an internal temperature 70 °C, obtained 22.04.14
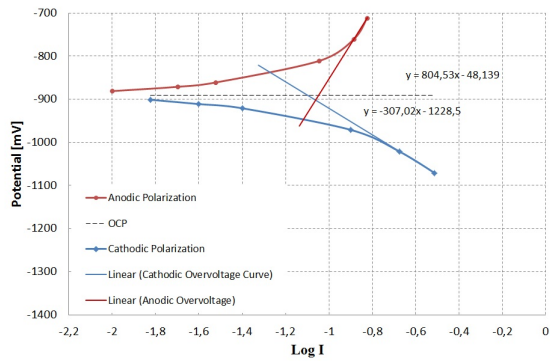
**Figure E.45:** Polarization Curve of thermally sprayed aluminium with an internal temperature 70 °C, obtained 29.04.14
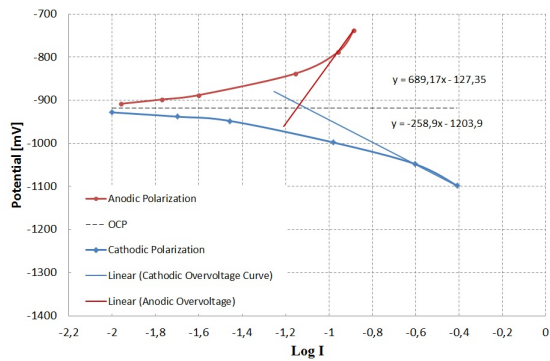


**Figure E.46:** Polarization Curve of thermally sprayed aluminium with an internal temperature 70 °C, obtained 06.05.14
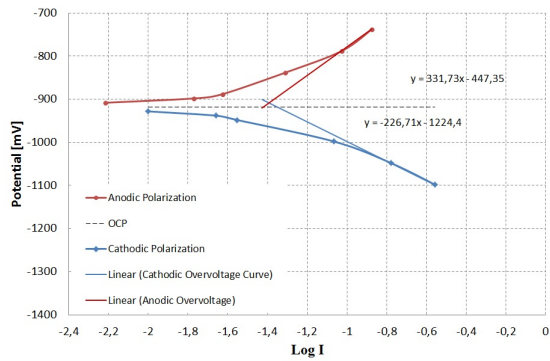


**Figure E.47:** Polarization Curve of thermally sprayed aluminium with an internal temperature 70 °C, obtained 13.05.14

# E.6 Polarization Curves 90 °C Internal Temperature
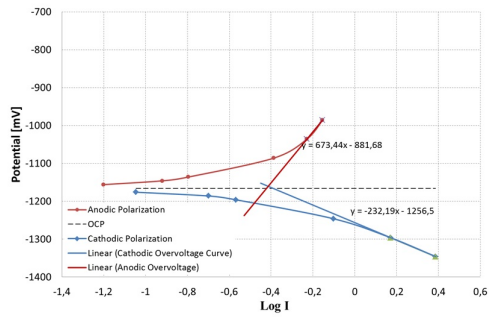


**Figure E.48:** Polarization Curve of thermally sprayed aluminium with an internal temperature 90 °C, obtained 18.03.14
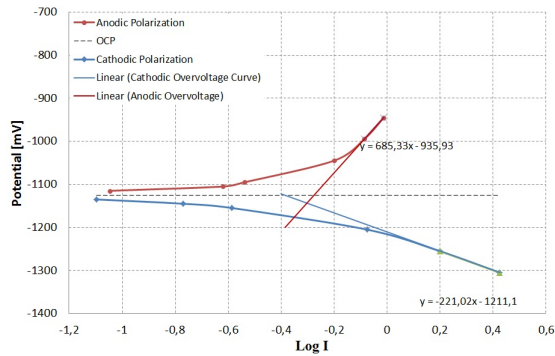


**Figure E.49:** Polarization Curve of thermally sprayed aluminium with an internal temperature 90 °C, obtained 25.03.14
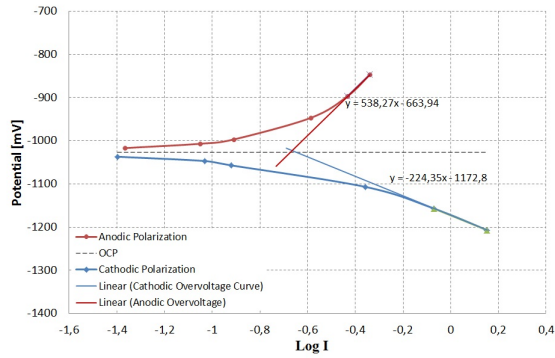
**Figure E.50:** Polarization Curve of thermally sprayed aluminium with an internal temperature 90 °C, obtained 01.04.14
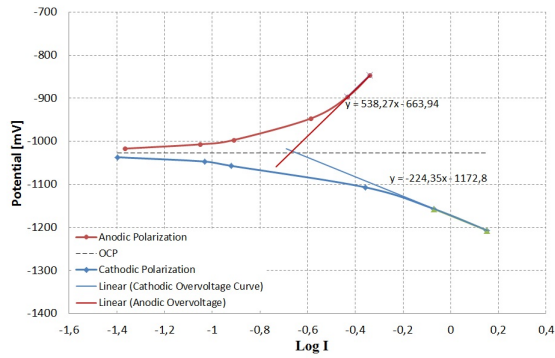


**Figure E.51:** Polarization Curve of thermally sprayed aluminium with an internal temperature 90 °C, obtained 15.04.14
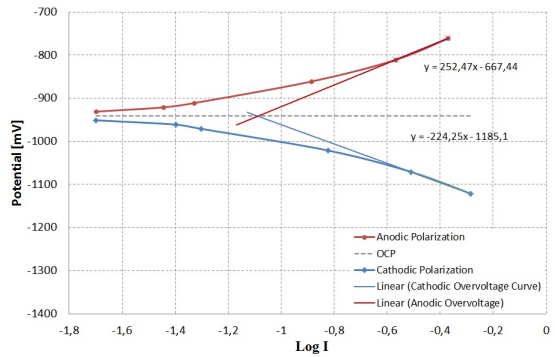


**Figure E.52:** Polarization Curve of thermally sprayed aluminium with an internal temperature 90 °C, obtained 22.04.14
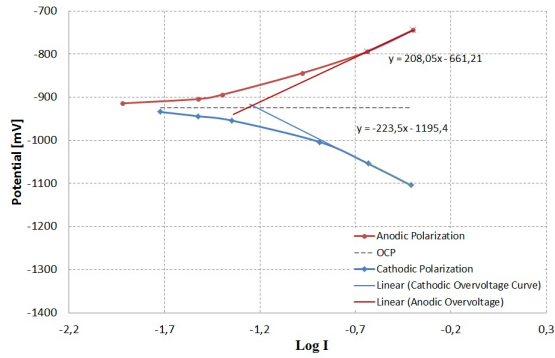
**Figure E.53:** Polarization Curve of thermally sprayed aluminium with an internal temperature 90 °C, obtained 29.04.14
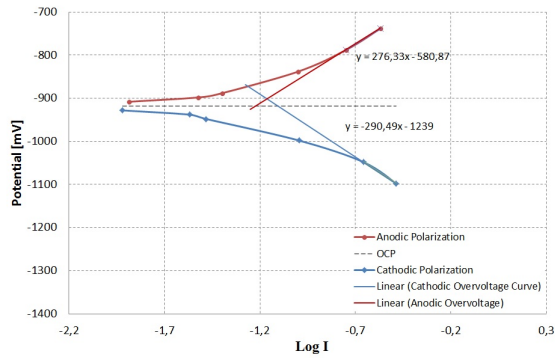


**Figure E.54:** Polarization Curve of thermally sprayed aluminium with an internal temperature 90 °C, obtained 06.05.14
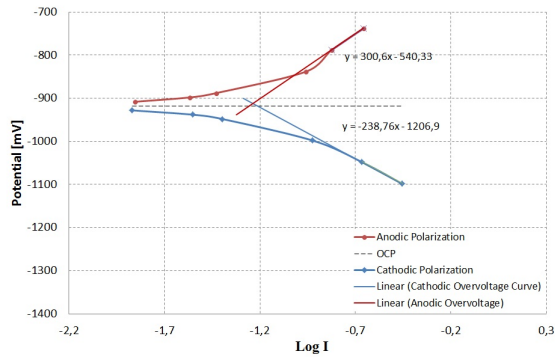


**Figure E.55:** Polarization Curve of thermally sprayed aluminium with an internal temperature 90 °C, obtained 13.05.14

# Appendix F

# Electrochemical Results

## F.1 No Internal Heating
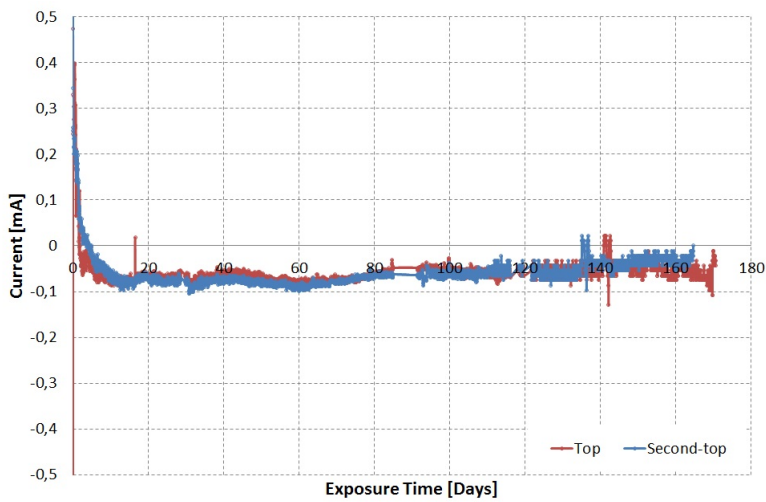


**Figure F.1:** Current between the anodes and the TSA coating for the spool with no internal heating.
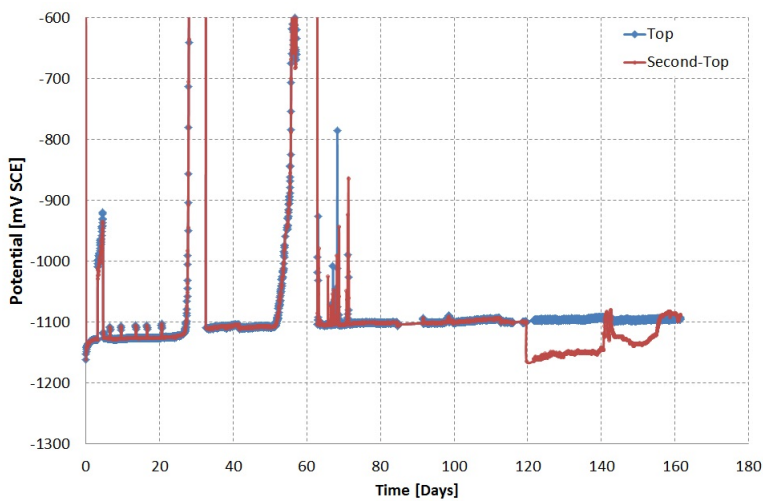
**Figure F.2:** The potential of TSA connected to an anode for the spool with no internal heating.
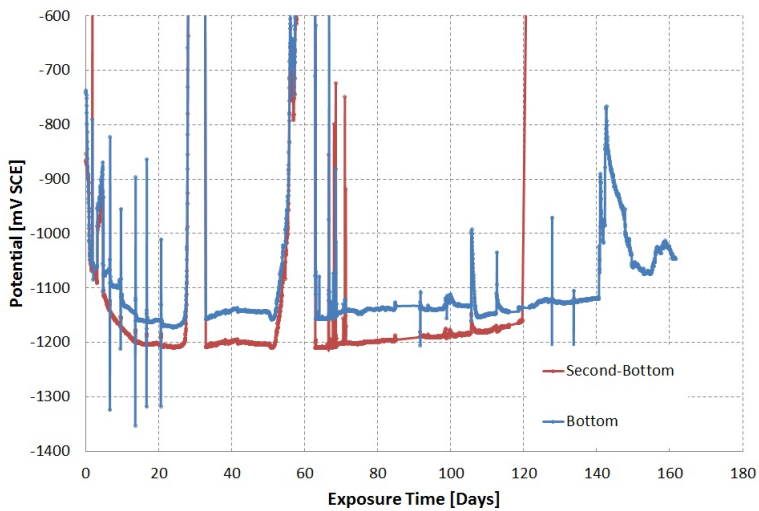


**Figure F.3:** The corrosion potential of TSA freely corroding with no internal heating.

# F.2 30 °C internal temperature
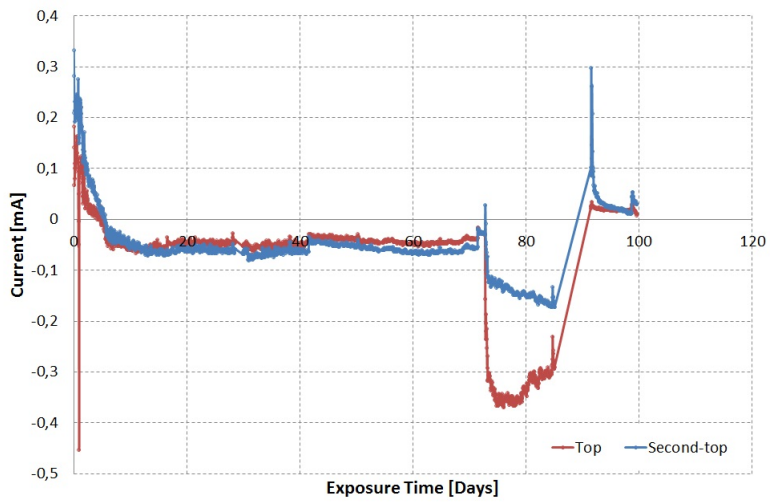


**Figure F.4:** Current between the anodes and the TSA coating for the spool with 30 °C internal temperature.
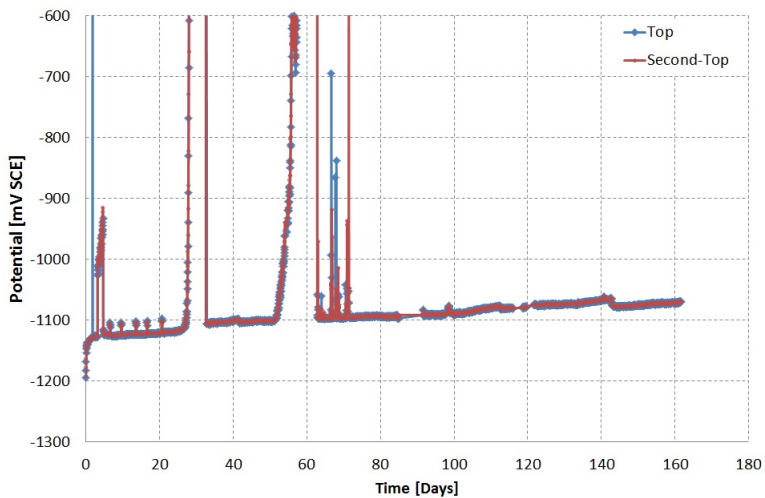
**Figure F.5:** The potential of TSA connected to an anode for the spool with 30 °C internal temperature.
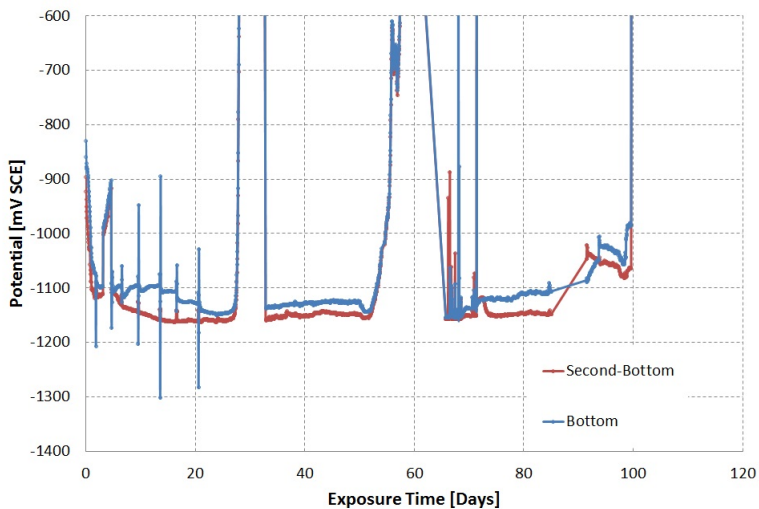


**Figure F.6:** The corrosion potential of TSA freely corroding with 30 °C internal temperature.

## F.3  40 °C internal temperature
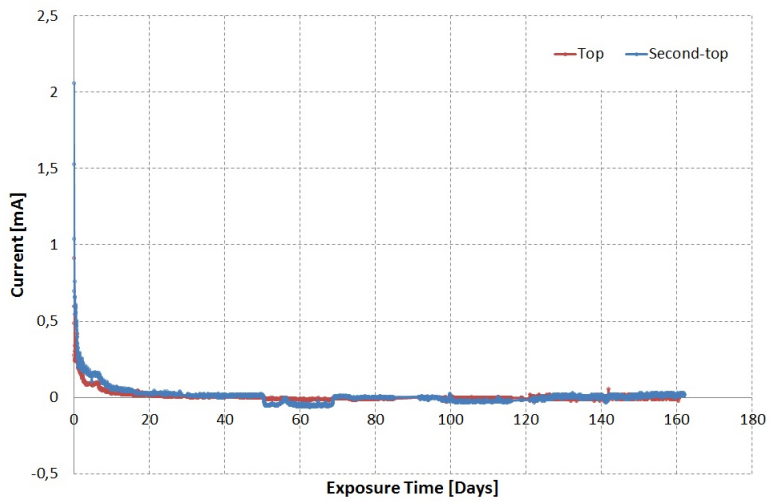


**Figure F.7:** Current between the anodes and the TSA coating for the spool with 40 °C internal temperature.
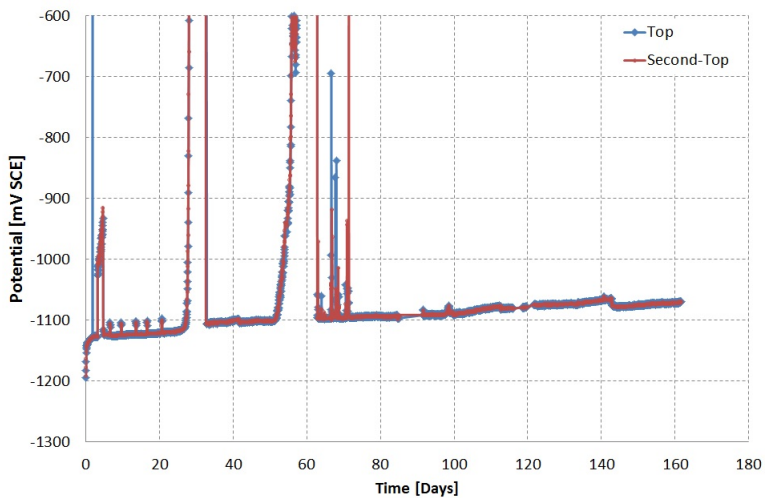
**Figure F.8:** The potential of TSA connected to an anode for the spool with 40 °C internal temperature.
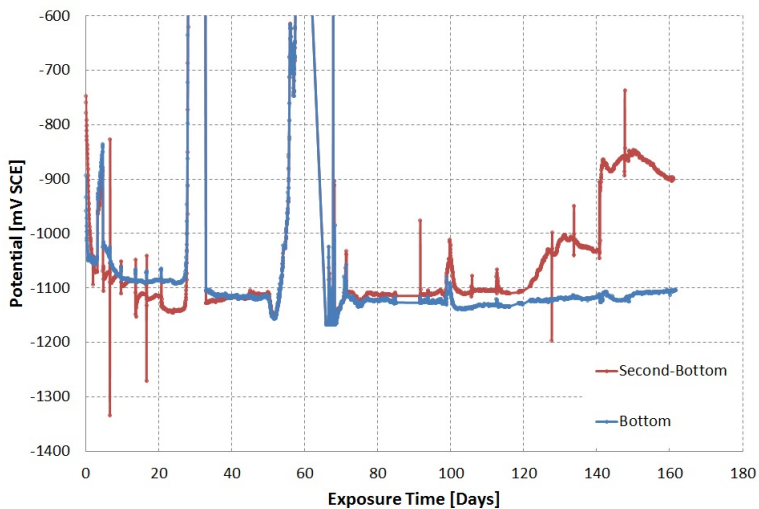


**Figure F.9:** The corrosion potential of TSA freely corroding with 40 °C internal temperature.

XL

## F.4   50 °C internal temperature
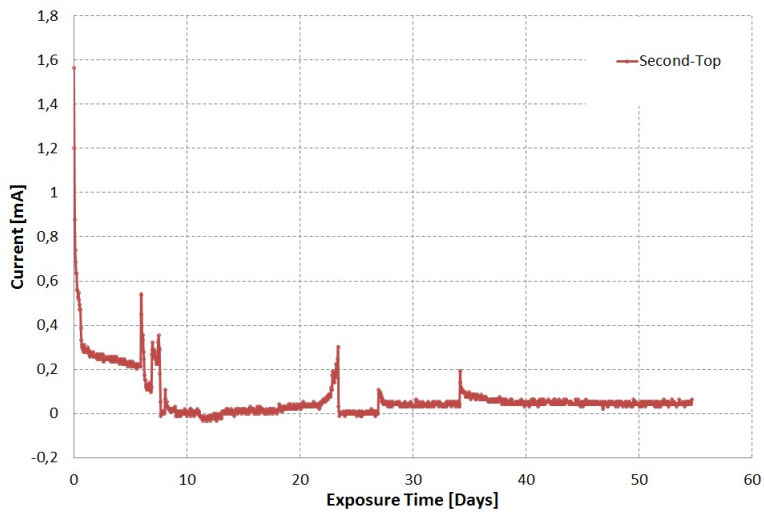


**Figure F.10:** Current between the anodes and the TSA coating for the spool with 50 °C internal temperature.
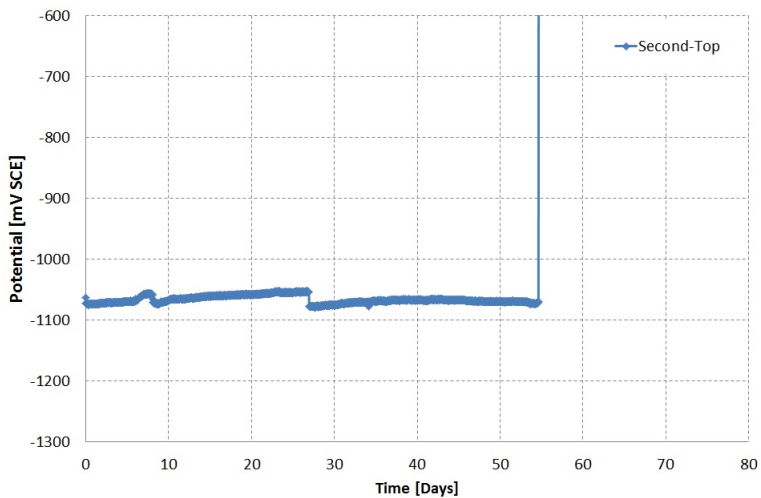
**Figure F.11:** The potential of TSA connected to an anode for the spool with 50 °C internal temperature.
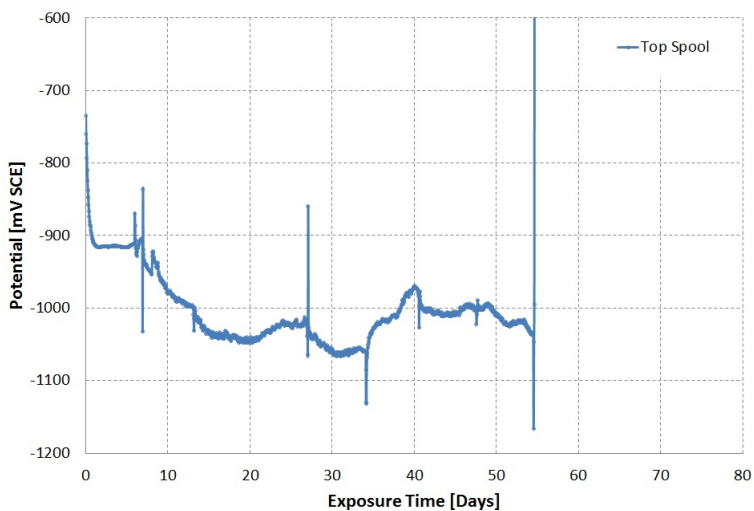


**Figure F.12:** The corrosion potential of TSA freely corroding with 50 °C internal temperature.

# F.5  70 °C internal temperature
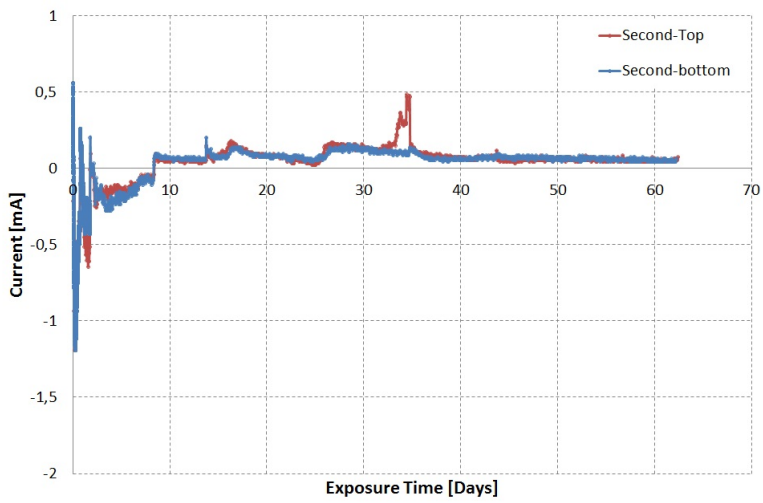


**Figure F.13:** Current between the anodes and the TSA coating for the spool with 70 °C internal temperature.
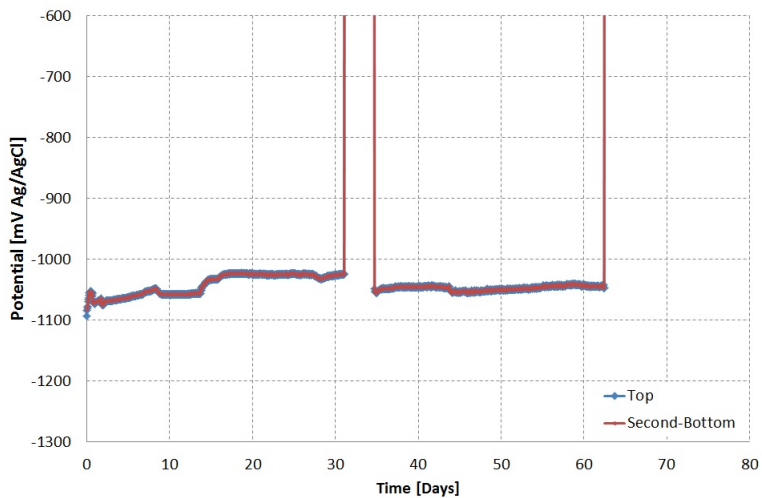
**Figure F.14:** The potential of TSA connected to an anode for the spool with 70 $^\circ$C internal temperature.
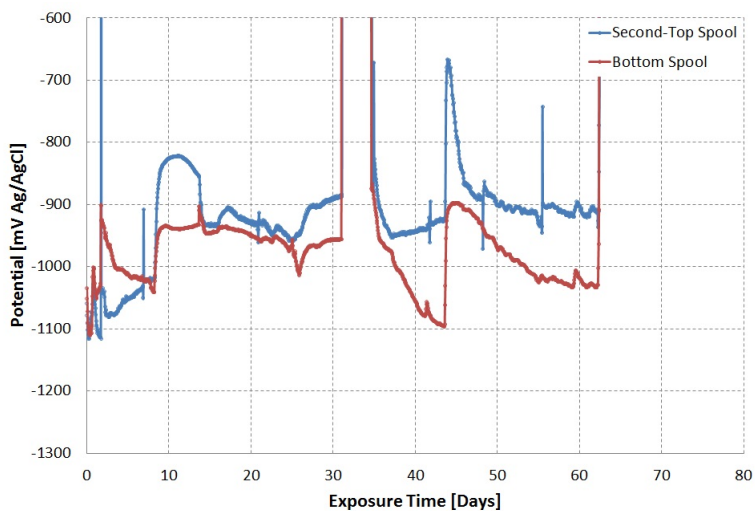


**Figure F.15:** The corrosion potential of TSA freely corroding with 70 $^\circ$C internal temperature.

# F.6   90 °C internal temperature
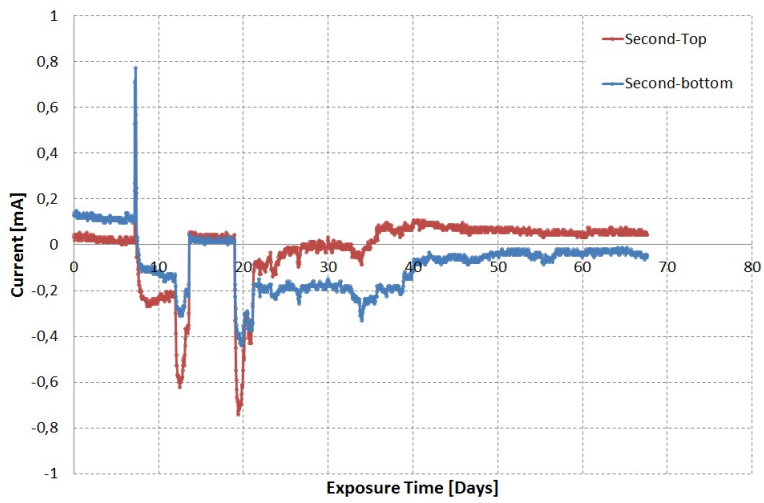


**Figure F.16:** Current between the anodes and the TSA coating for the spool with 90 °C internal temperature.
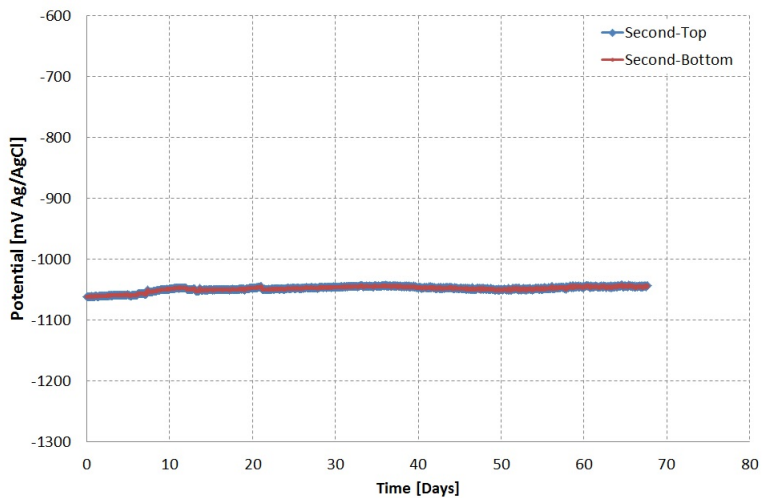
**Figure F.17:** The potential of TSA connected to an anode for the spool with 90 °C internal temperature.
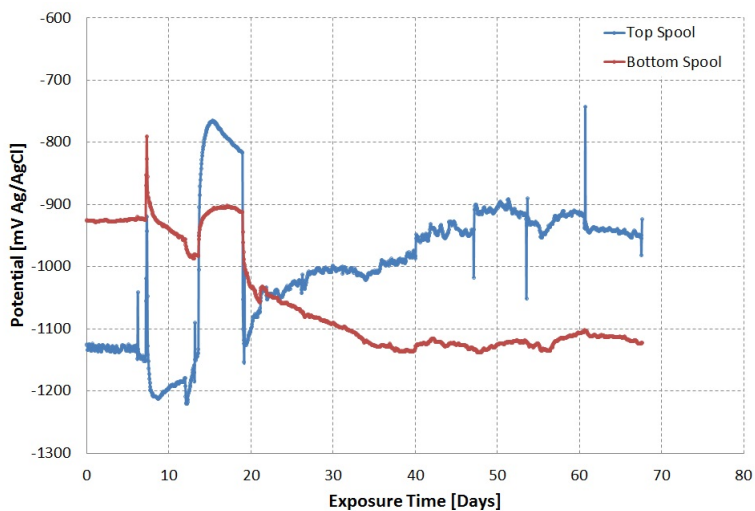


**Figure F.18:** The corrosion potential of TSA freely corroding with 90 °C internal temperature.

# Appendix G

# Cleanliness Grades and Requirements

**Table G.1:** Cleanliness grades and requirements

| Sa 1 | Light blast-cleaning | When viewed without magnification, the surface shall be free from visible oil, grease and dirt, and from poorly adhering mill scale, rust, paint coatings and foreign matter (see Note 1 to 3.1). See photographs B Sa 1, C Sa 1 and D Sa 1. |
|---|---|---|
| Sa 2 | Thorough blast-cleaning | When viewed without magnification, the surface shall be free from visible oil, grease and dirt, and from most of the mill scale, rust, paint coatings and foreign matter. Any residual contamination shall be firmly adhering (see Note 2 to 3.1). See photographs B Sa 2, C Sa 2 and D Sa 2. |
| Sa 2½ | Very thorough blast-cleaning | When viewed without magnification, the surface shall be free from visible oil, grease and dirt, and from mill scale, rust, paint coatings and foreign matter. Any remaining traces of contamination shall show only as slight stains in the form of spots or stripes. See photographs  A Sa 2½,  B Sa 2½,  C Sa 2½  and D Sa 2½. |
| Sa 3 | Blast-cleaning to visually clean steel | When viewed without magnification, the surface shall be free from visible oil, grease and dirt, and shall be free from mill scale, rust, paint coatings and foreign matter. It shall have a uniform metallic colour. See photographs A Sa 3, B Sa 3, C Sa 3 and D Sa 3. |

# Appendix H

# EDS Spectrums

## H.1 EDS Spectrum for the Coating Characterization
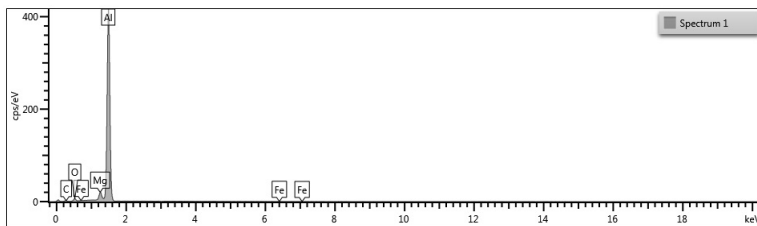


**Figure H.1:** EDS spectrum 1 for the sample not exposed to seawater.
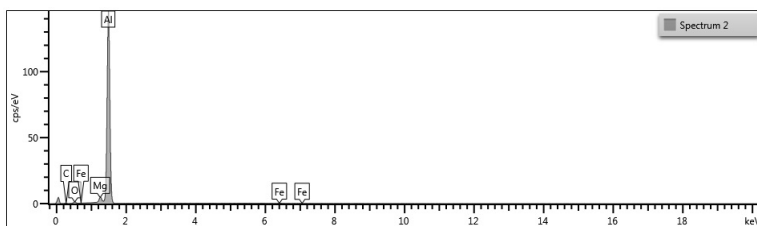


**Figure H.2:** EDS spectrum 2 for the sample not exposed to seawater.
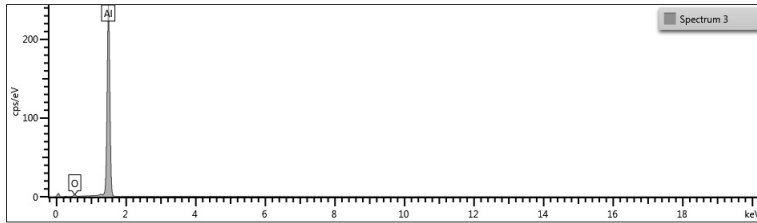
**Figure H.3:** EDS spectrum 3 for the sample not exposed to seawater.
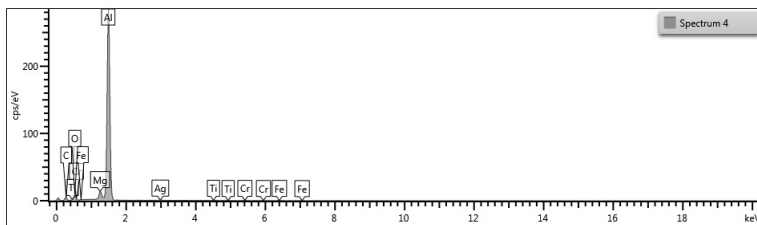


**Figure H.4:** EDS spectrum 4 for the sample not exposed to seawater.
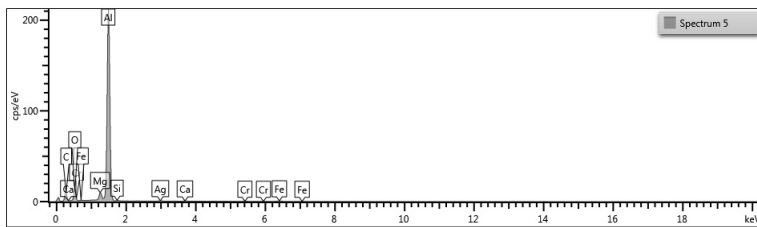


**Figure H.5:** EDS spectrum 5 for the sample not exposed to seawater.
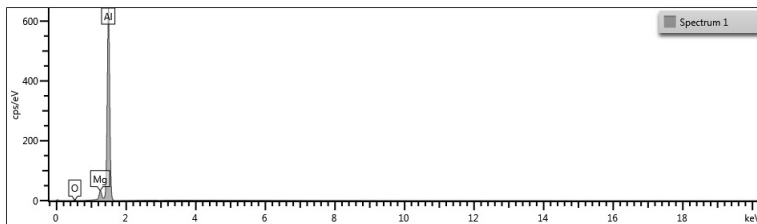


**Figure H.6:** EDS spectrum 1 for the sample with the surface polished.
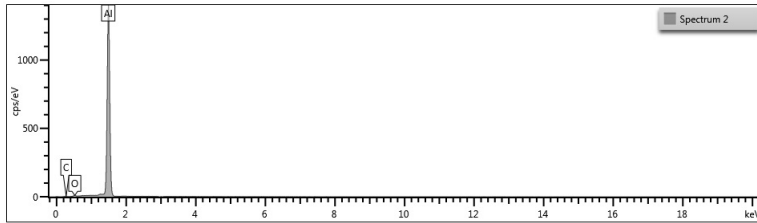
**Figure H.7:** EDS spectrum 2 for the sample with the surface polished.
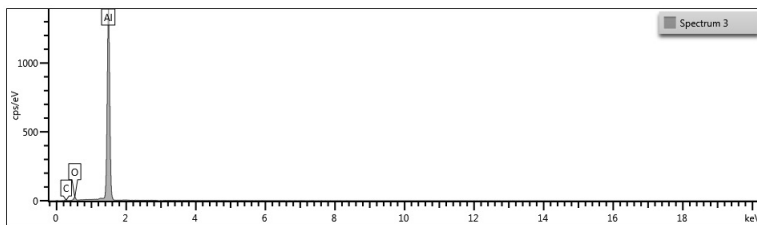


**Figure H.8:** EDS spectrum 3 for the sample with the surface polished.
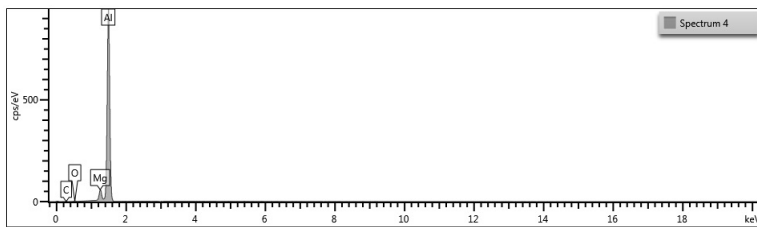


**Figure H.9:** EDS spectrum 4 for the sample with the surface polished.
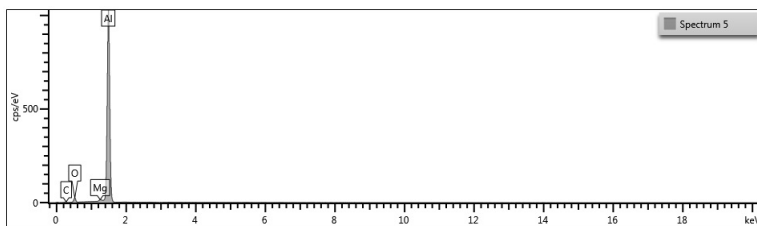


**Figure H.10:** EDS spectrum 5 for the sample with the surface polished.

## H.2 EDS Spectrum for No Internal Heating
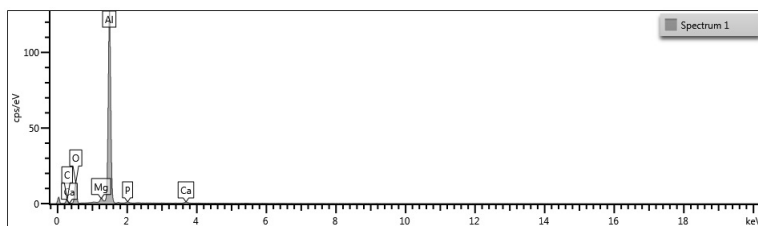


**Figure H.11:** EDS spectrum 1 for the sample with no internal heating connected to an anode.
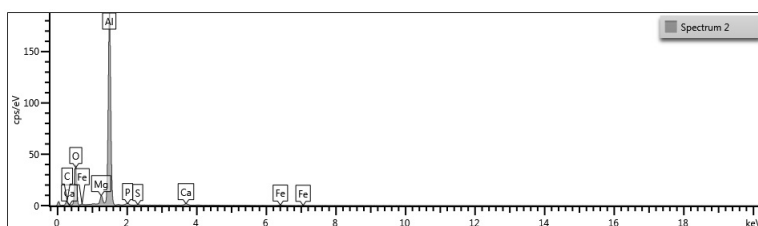


**Figure H.12:** EDS spectrum 2 for the sample with no internal heating connected to an anode.
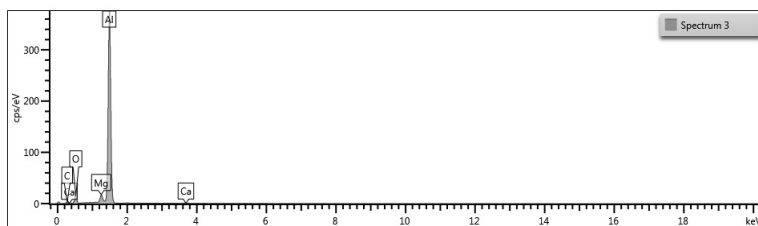


**Figure H.13:** EDS spectrum 3 for the sample with no internal heating connected to an anode.
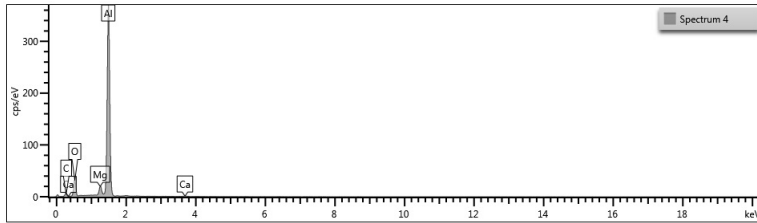
**Figure H.14:** EDS spectrum 4 for the sample with no internal heating connected to an anode.
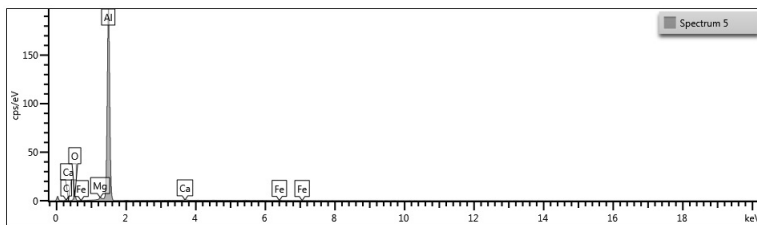


**Figure H.15:** EDS spectrum 5 for the sample with no internal heating connected to an anode.
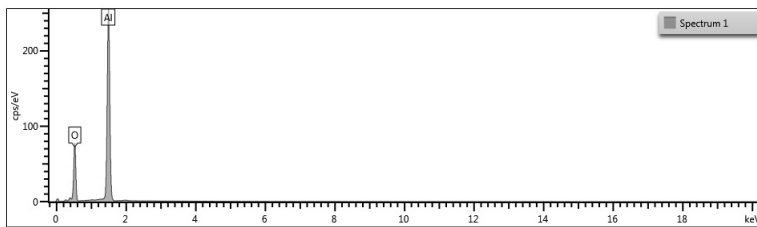


**Figure H.16:** EDS spectrum 1 for the sample with no internal heating freely corroding.
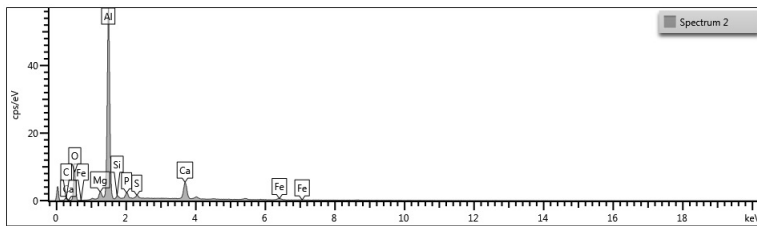


**Figure H.17:** EDS spectrum 2 for the sample with no internal heating freely corroding.
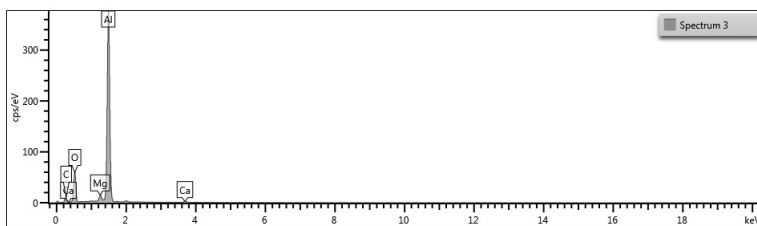
**Figure H.18:** EDS spectrum 3 for the sample with no internal heating freely corroding.
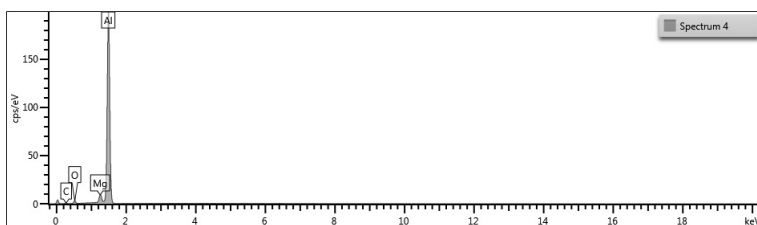


**Figure H.19:** EDS spectrum 4 for the sample with no internal heating freely corroding.
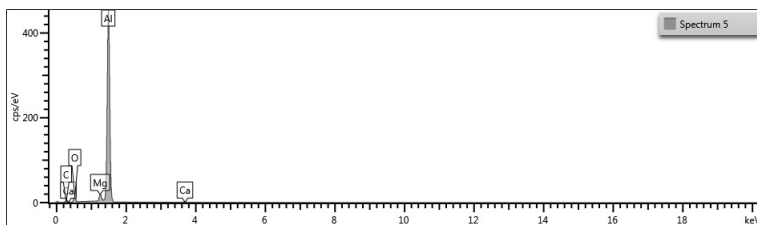


**Figure H.20:** EDS spectrum 5 for the sample with no internal heating freely corroding.
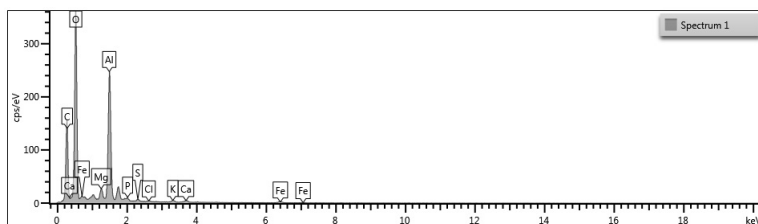
# H.3 EDS Spectrum 30 °C Internal Temperature
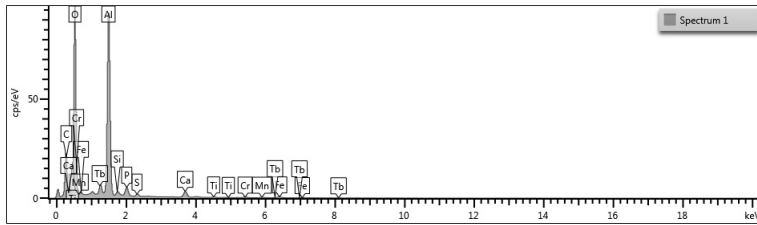


**Figure H.21:** EDS spectrum 1 for the sample with 30 °C internal temperature connected to an anode.
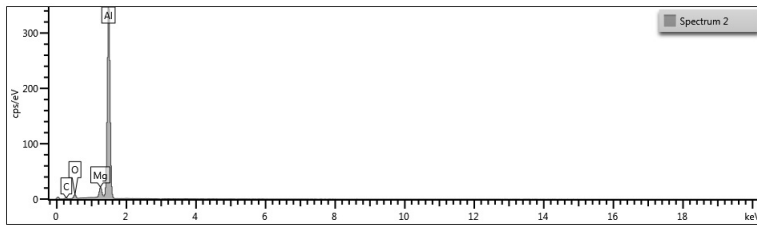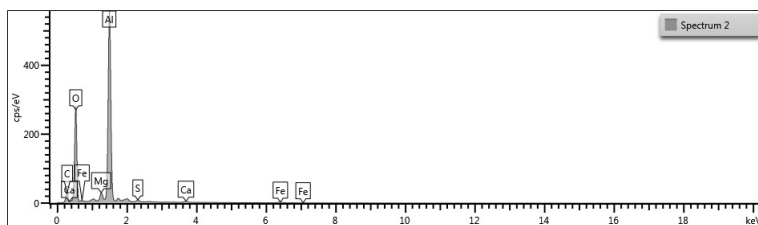


**Figure H.22:** EDS spectrum 2 for the sample with 30 °C internal temperature connected to an anode.
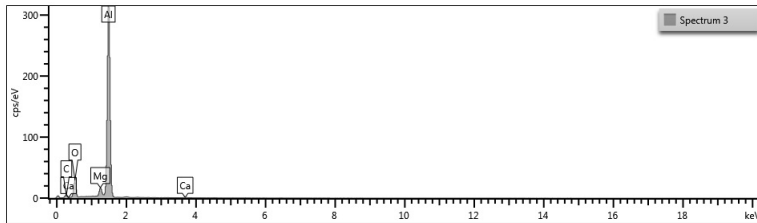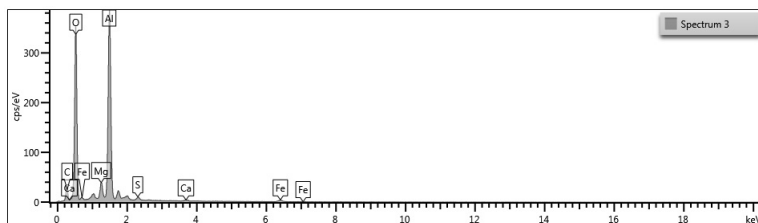


**Figure H.23:** EDS spectrum 3 for the sample with 30 °C internal temperature connected to an anode.
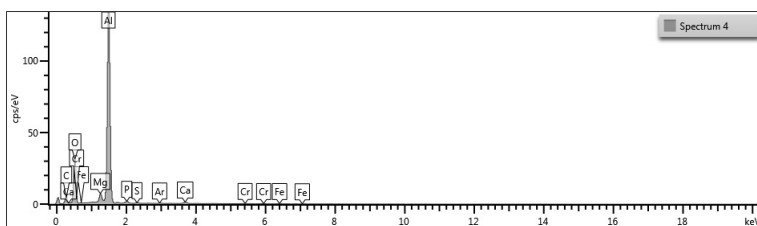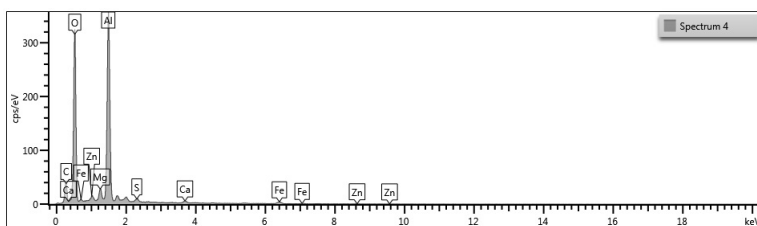
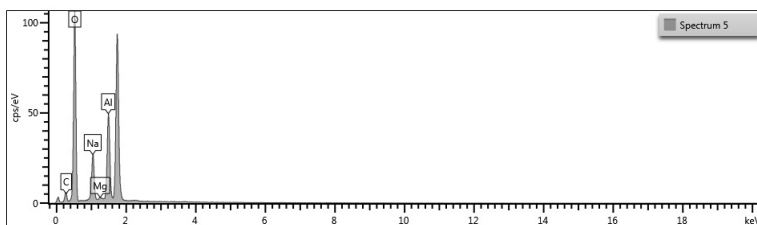**Figure H.24:** EDS spectrum 4 for the sample with 30 °C internal temperature connected to an anode.
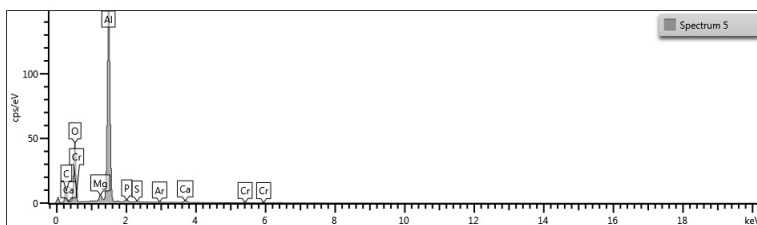


**Figure H.25:** EDS spectrum 5 for the sample with 30 °C internal temperature connected to an anode.
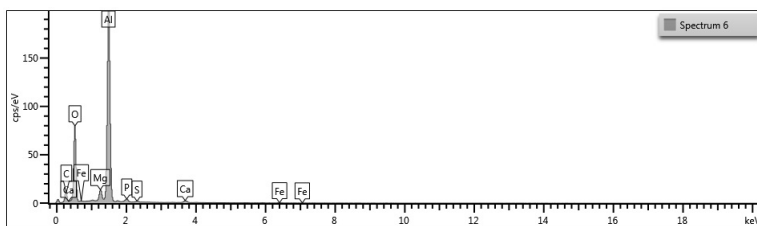


**Figure H.26:** EDS spectrum 6 for the sample with 30 °C internal temperature connected to an anode.
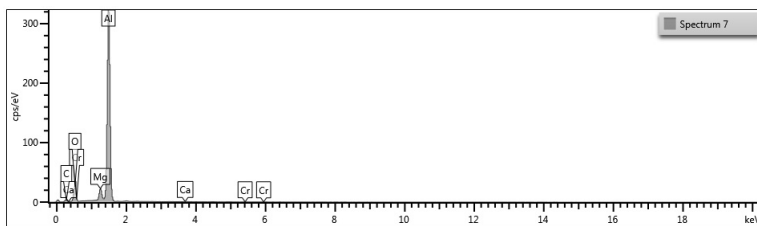


**Figure H.27:** EDS spectrum 7 for the sample with 30 °C internal temperature connected to an anode.
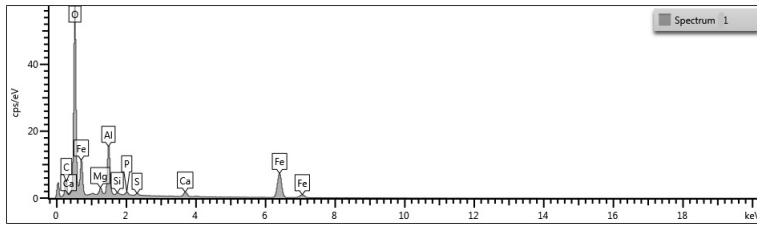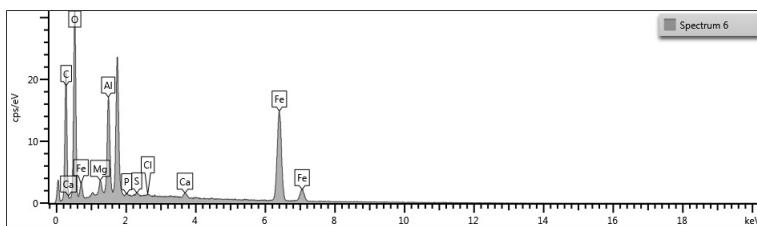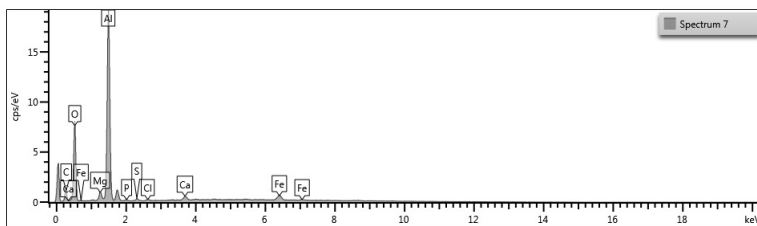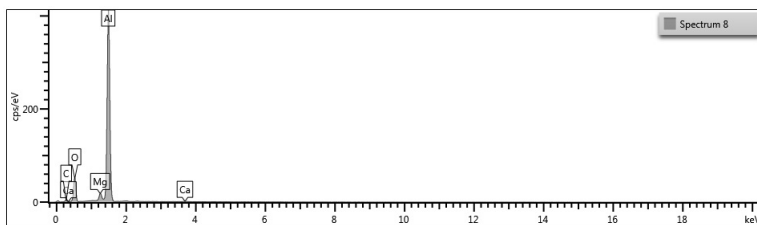
**Figure H.28:** EDS spectrum 1 for the sample with 30 °C internal temperature freely corroding.
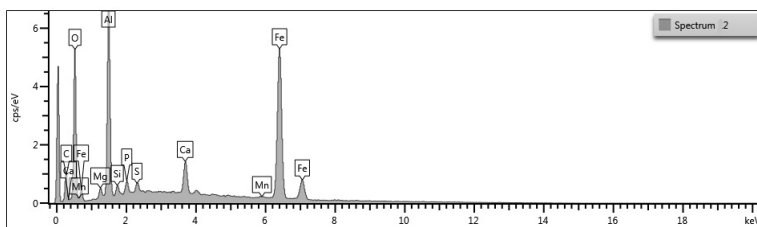


**Figure H.29:** EDS spectrum 2 for the sample with 30 °C internal temperature freely corroding.
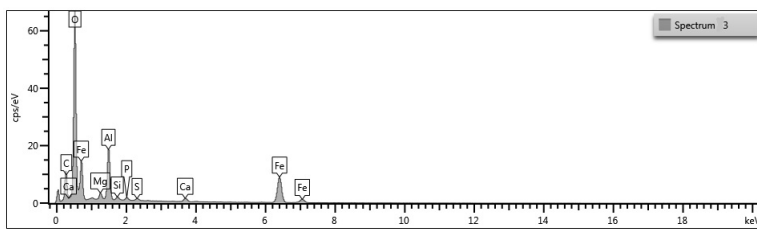


**Figure H.30:** EDS spectrum 3 for the sample with 30 °C internal temperature freely corroding.
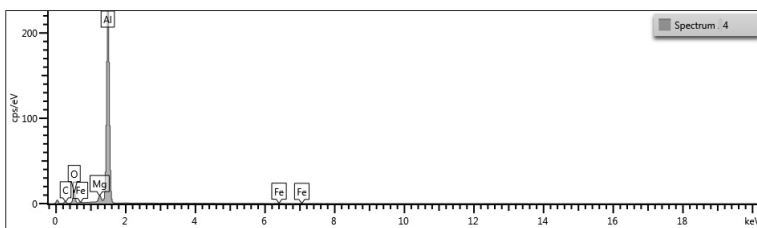


**Figure H.31:** EDS spectrum 4 for the sample with 30 °C internal temperature freely corroding.
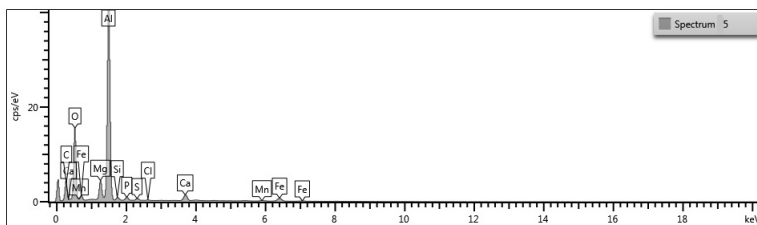
**Figure H.32:** EDS spectrum 5 for the sample with 30 °C internal temperature freely corroding.

# H.4    EDS Spectrum 40 °C Internal Temperature
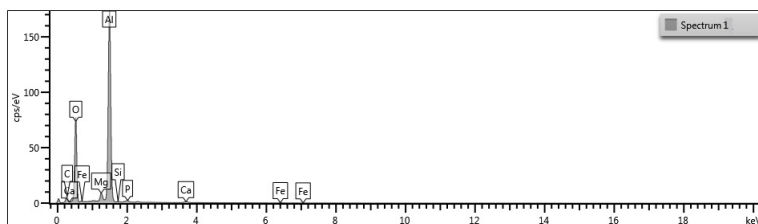


**Figure H.33:** EDS spectrum 1 for the sample with 40 °C internal temperature connected to an anode.
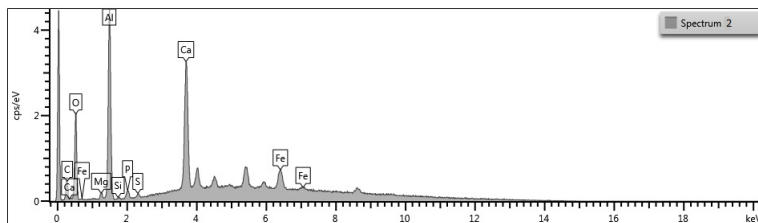


**Figure H.34:** EDS spectrum 2 for the sample with 40 °C internal temperature connected to an anode.
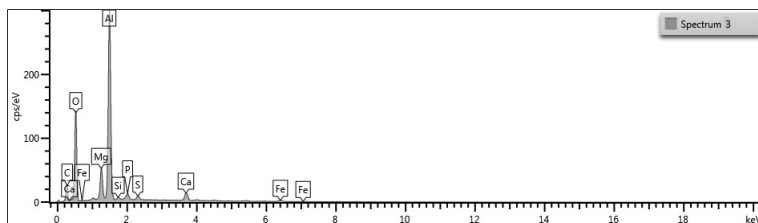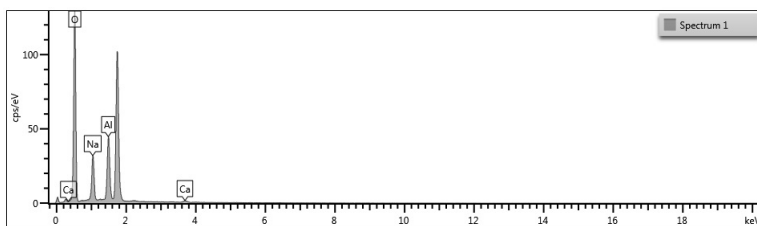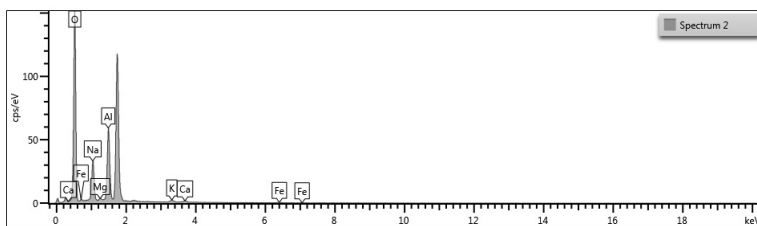


**Figure H.35:** EDS spectrum 3 for the sample with 40 °C internal temperature connected to an anode.
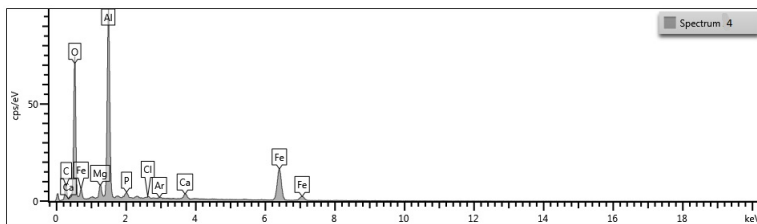
**Figure H.36:** EDS spectrum 4 for the sample with 40 °C internal temperature connected to an anode.
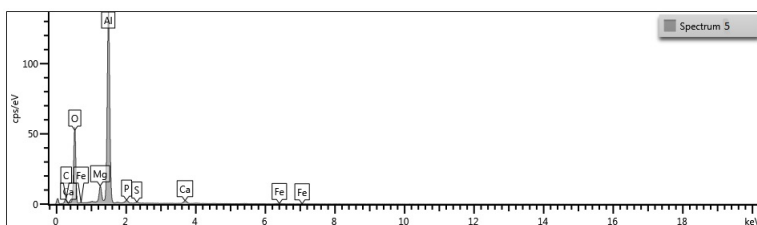


**Figure H.37:** EDS spectrum 5 for the sample with 40 °C internal temperature connected to an anode.
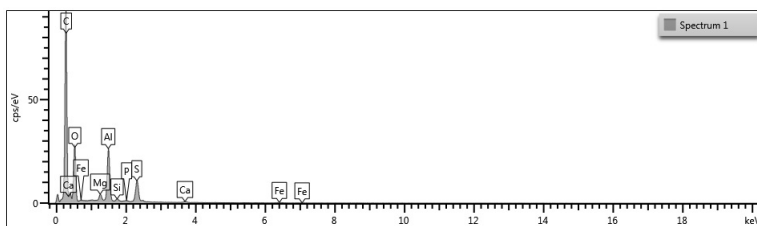


**Figure H.38:** EDS spectrum 1 for the sample with 40 °C internal temperature freely corroding.
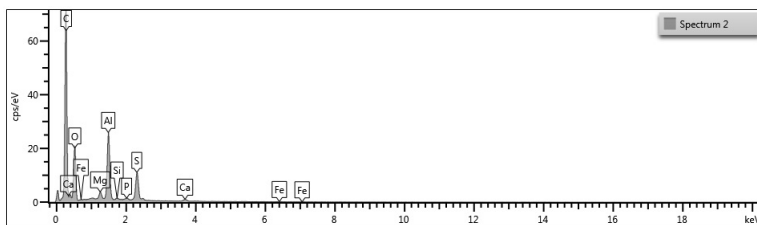


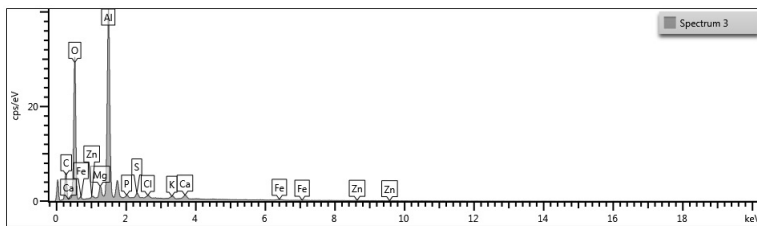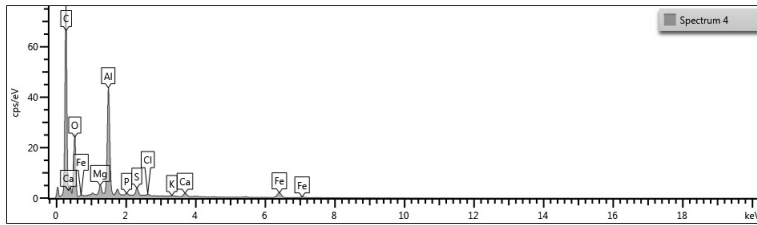**Figure H.39:** EDS spectrum 2 for the sample with 40 °C internal temperature freely corroding.
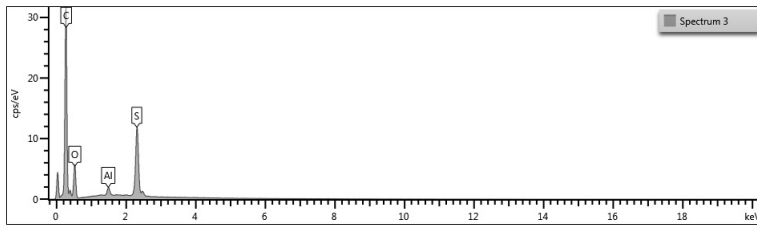
**Figure H.40:** EDS spectrum 3 for the sample with 40 °C internal temperature freely corroding.
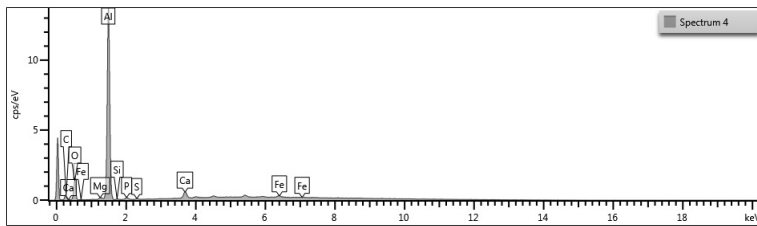


**Figure H.41:** EDS spectrum 4 for the sample with 40 °C internal temperature freely corroding.
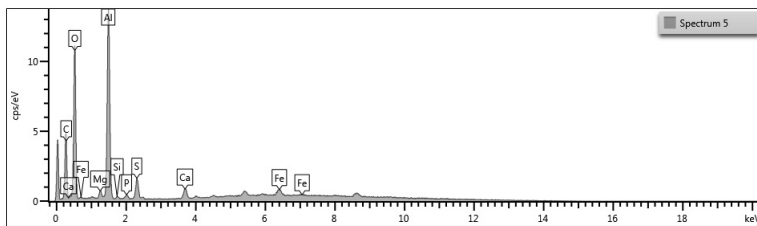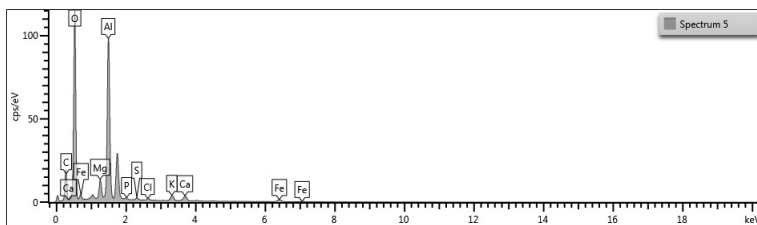


**Figure H.42:** EDS spectrum 5 for the sample with 40 °C internal temperature freely corroding.
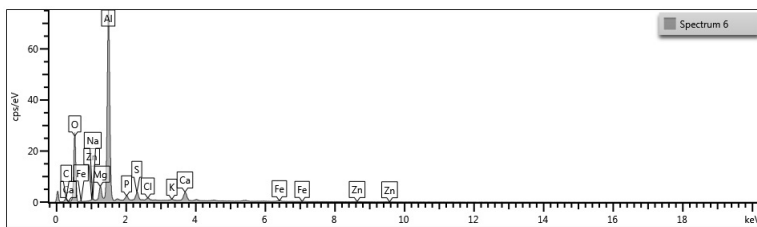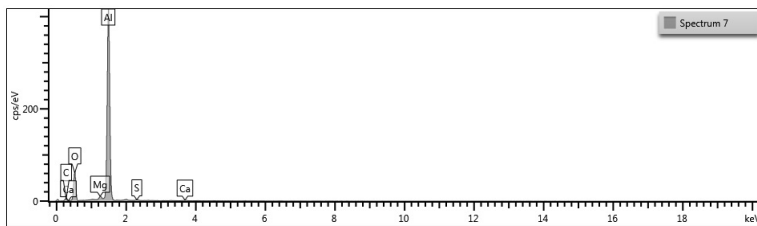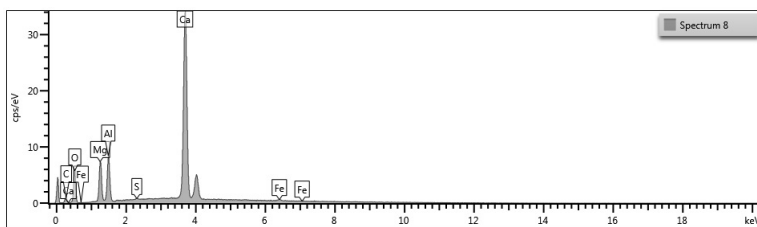
## H.5 EDS Spectrum 50 °C Internal Temperature



**Figure H.43:** EDS spectrum 1 for the sample with 50 °C internal temperature connected to an anode.



**Figure H.44:** EDS spectrum 2 for the sample with 50 °C internal temperature connected to an anode.



**Figure H.45:** EDS spectrum 3 for the sample with 50 °C internal temperature connected to an anode.

**Figure H.46:** EDS spectrum 4 for the sample with 50 °C internal temperature connected to an anode.



**Figure H.47:** EDS spectrum 5 for the sample with 50 °C internal temperature connected to an anode.



**Figure H.48:** EDS spectrum 6 for the sample with 50 °C internal temperature connected to an anode.
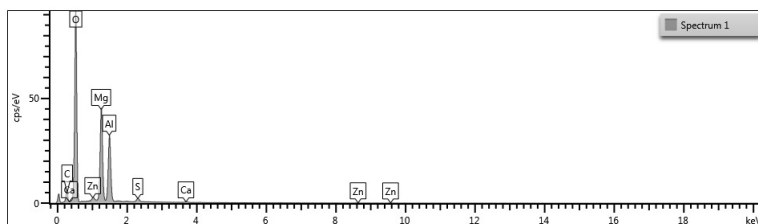


**Figure H.49:** EDS spectrum 7 for the sample with 50 °C internal temperature connected to an anode.
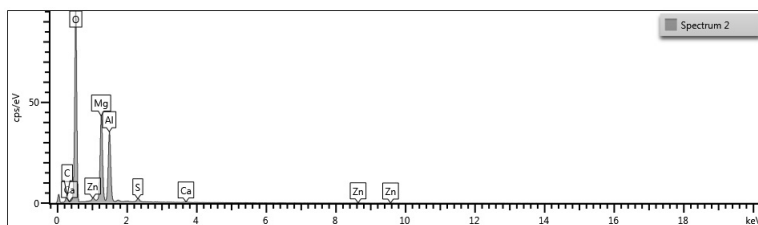
**Figure H.50:** EDS spectrum 8 for the sample with 50 °C internal temperature connected to an anode.
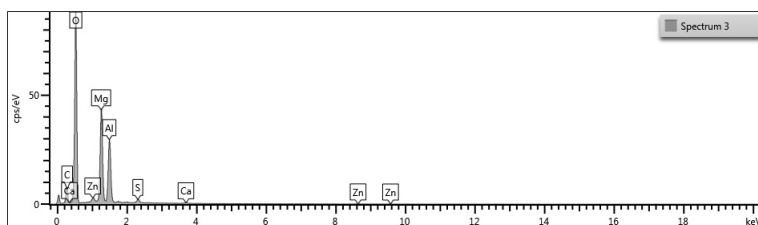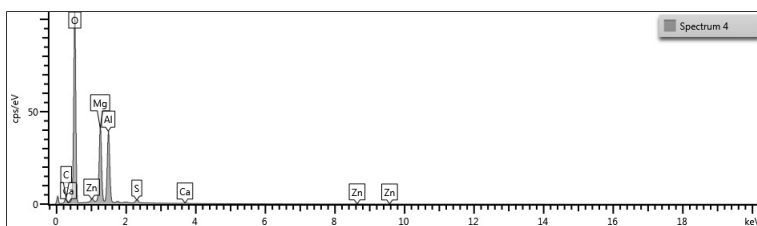


**Figure H.51:** EDS spectrum 1 for the sample with 50 °C internal temperature freely corroding.



**Figure H.52:** EDS spectrum 2 for the sample with 50 °C internal temperature freely corroding.



**Figure H.53:** EDS spectrum 3 for the sample with 50 °C internal temperature freely corroding.

**Figure H.54:** EDS spectrum 4 for the sample with 50 °C internal temperature freely corroding.



**Figure H.55:** EDS spectrum 5 for the sample with 50 °C internal temperature freely corroding.



**Figure H.56:** EDS spectrum 6 for the sample with 50 °C internal temperature freely corroding.



**Figure H.57:** EDS spectrum 7 for the sample with 50 °C internal temperature freely corroding.

**Figure H.58:** EDS spectrum 8 for the sample with 50 °C internal temperature freely corroding.

# H.6    EDS Spectrum 70 °C Internal Temperature



**Figure H.59:** EDS spectrum 1 for the sample with 70 °C internal temperature connected to an anode.



**Figure H.60:** EDS spectrum 2 for the sample with 70 °C internal temperature connected to an anode.
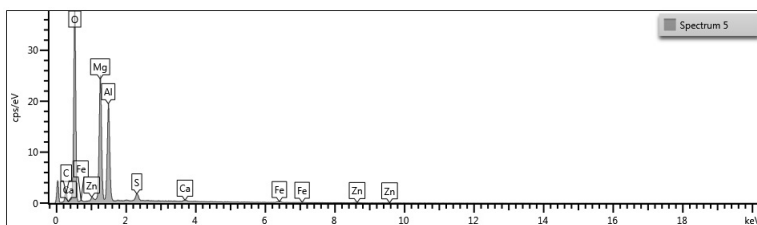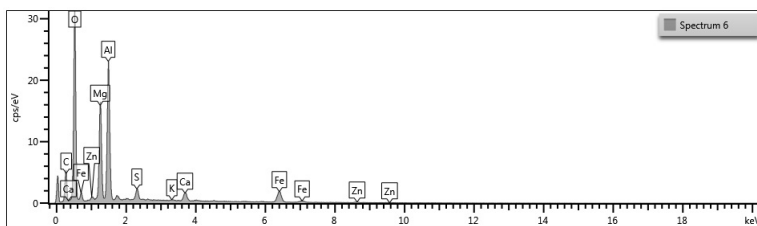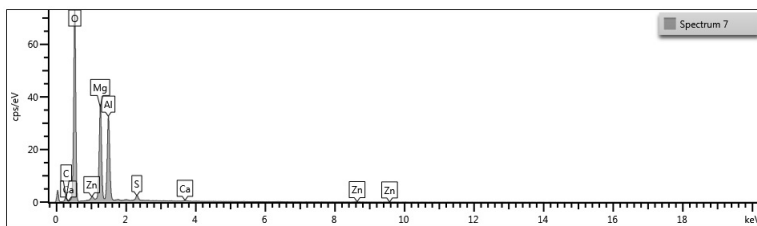


**Figure H.61:** EDS spectrum 3 for the sample with 70 °C internal temperature connected to an anode.

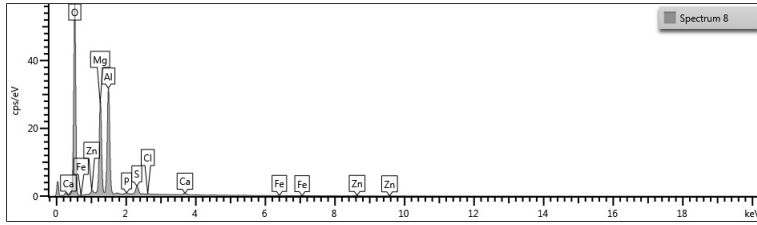**Figure H.62:** EDS spectrum 4 for the sample with 70 °C internal temperature connected to an anode.



**Figure H.63:** EDS spectrum 5 for the sample with 70 °C internal temperature connected to an anode.



**Figure H.64:** EDS spectrum 6 for the sample with 70 °C internal temperature connected to an anode.



**Figure H.65:** EDS spectrum 7 for the sample with 70 °C internal temperature connected to an anode.

**Figure H.66:** EDS spectrum 8 for the sample with 70 °C internal temperature connected to an anode.
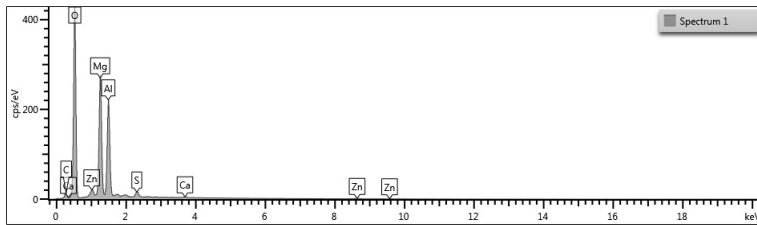


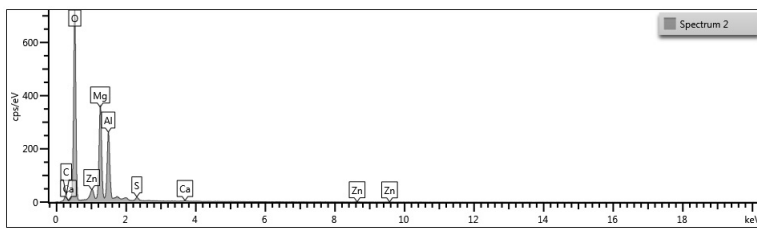**Figure H.67:** EDS spectrum 1 for the sample with 70 °C internal temperature freely corroding.



**Figure H.68:** EDS spectrum 2 for the sample with 70 °C internal temperature freely corroding.
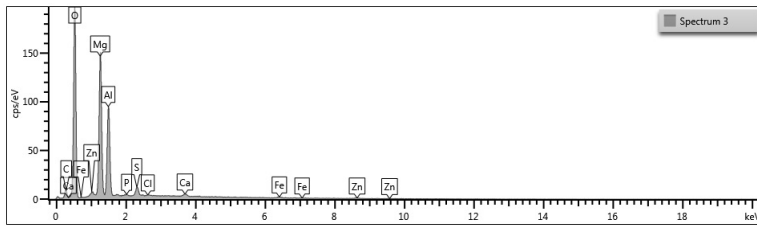


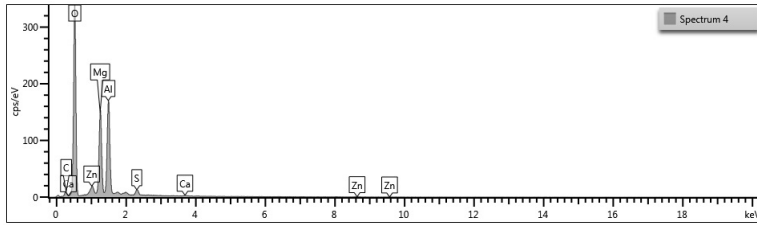**Figure H.69:** EDS spectrum 3 for the sample with 70 °C internal temperature freely corroding.

**Figure H.70:** EDS spectrum 4 for the sample with 70 °C internal temperature freely corroding.
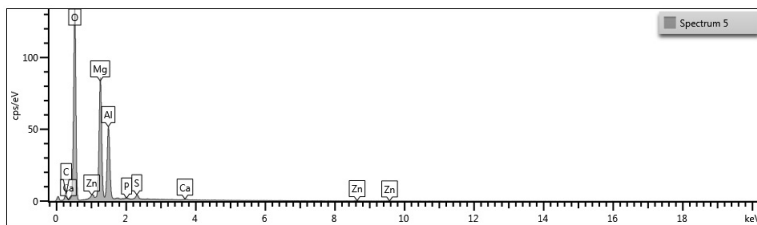


**Figure H.71:** EDS spectrum 5 for the sample with 70 °C internal temperature freely corroding.
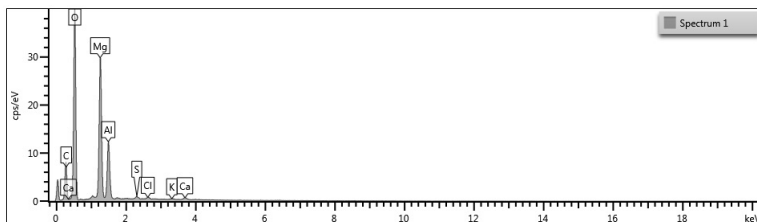
# H.7   EDS Spectrum 90 °C Internal Temperature



**Figure H.72:** EDS spectrum 1 for the sample with 90 °C internal temperature connected to an anode.
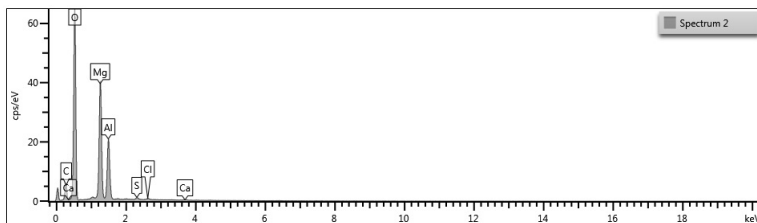


**Figure H.73:** EDS spectrum 2 for the sample with 90 °C internal temperature connected to an anode.



**Figure H.74:** EDS spectrum 3 for the sample with 90 °C internal temperature connected to an anode.

**Figure H.75:** EDS spectrum 4 for the sample with 90 °C internal temperature connected to an anode.



**Figure H.76:** EDS spectrum 5 for the sample with 90 °C internal temperature connected to an anode.



**Figure H.77:** EDS spectrum 6 for the sample with 90 °C internal temperature connected to an anode.
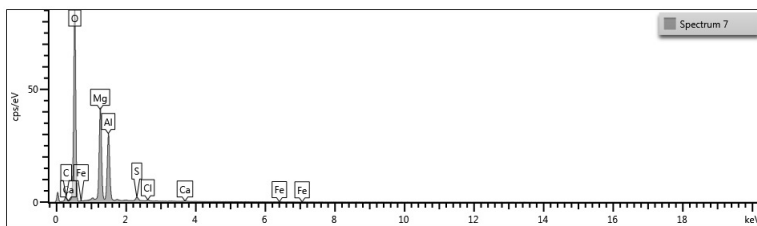


**Figure H.78:** EDS spectrum 7 for the sample with 90 °C internal temperature connected to an anode.
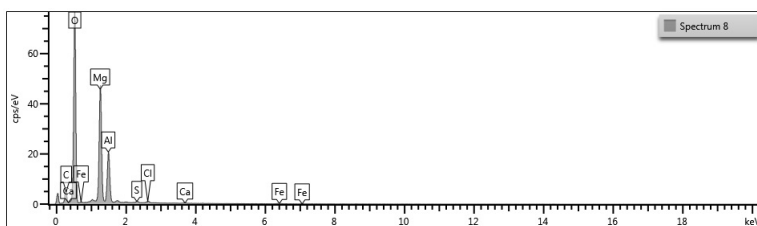
**Figure H.79:** EDS spectrum 8 for the sample with 90 °C internal temperature connected to an anode.
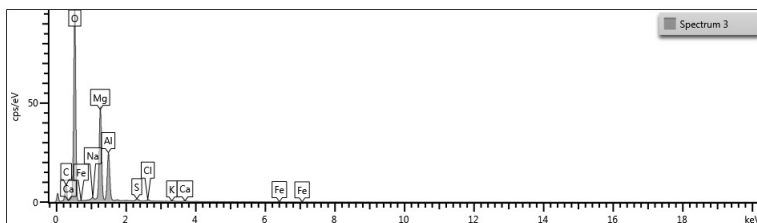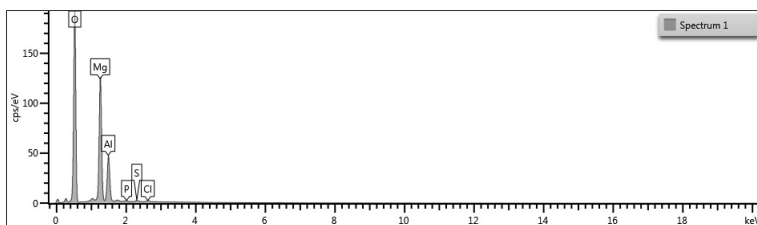


**Figure H.80:** EDS spectrum 1 for the sample with 90 °C internal temperature connected to an anode.
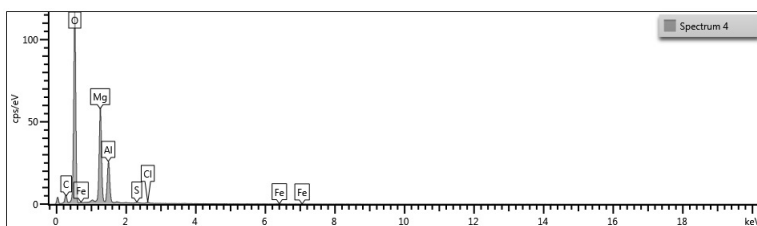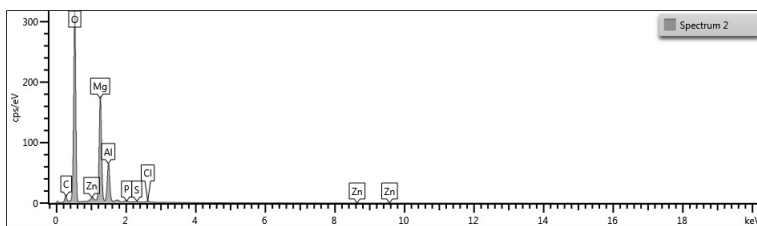


**Figure H.81:** EDS spectrum 2 for the sample with 90 °C internal temperature connected to an anode.
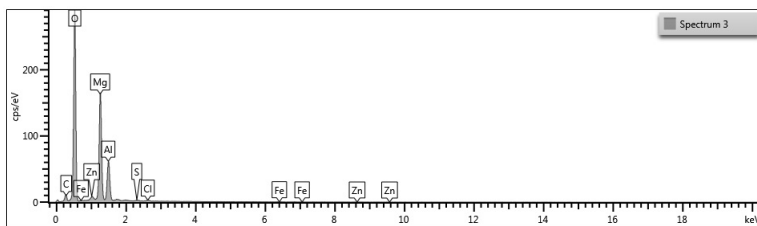


**Figure H.82:** EDS spectrum 3 for the sample with 90 °C internal temperature connected to an anode.
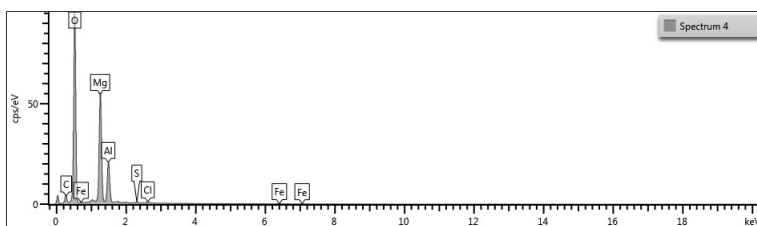
**Figure H.83:** EDS spectrum 4 for the sample with 90 °C internal temperature connected to an anode.
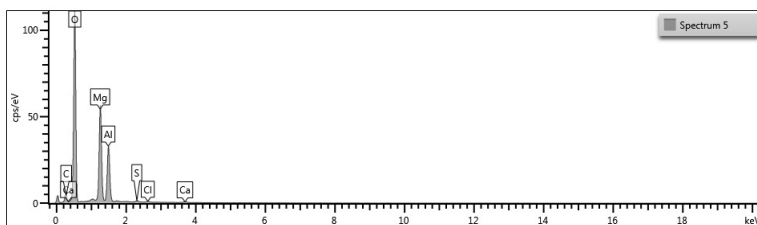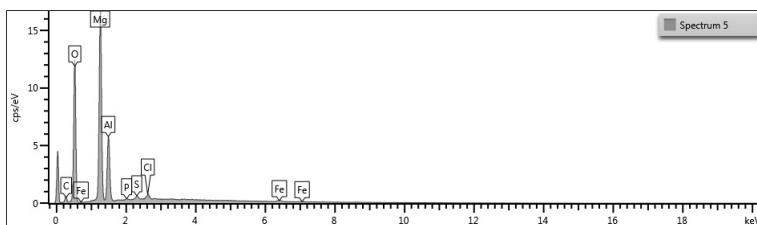


**Figure H.84:** EDS spectrum 5 for the sample with 90 °C internal temperature connected to an anode.
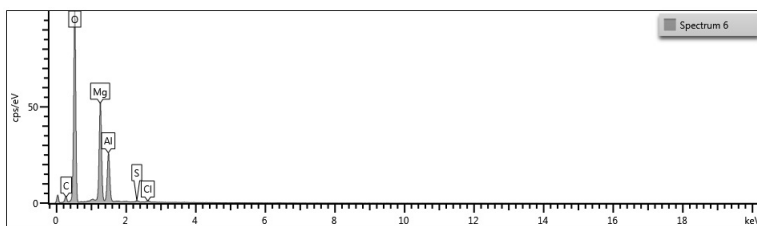


**Figure H.85:** EDS spectrum 6 for the sample with 90 °C internal temperature connected to an anode.



**Figure H.86:** EDS spectrum 7 for the sample with 90 °C internal temperature connected to an anode.

**Figure H.87:** EDS spectrum 8 for the sample with 90 °C internal temperature connected to an anode.
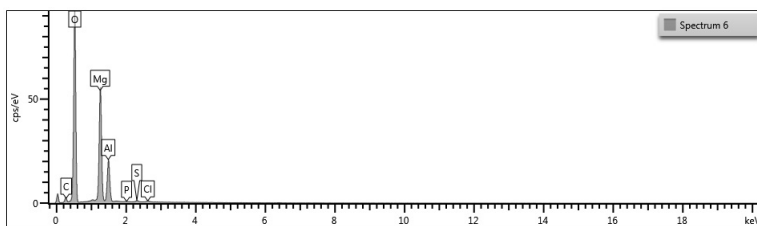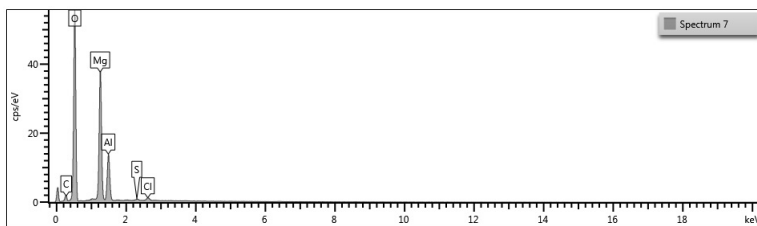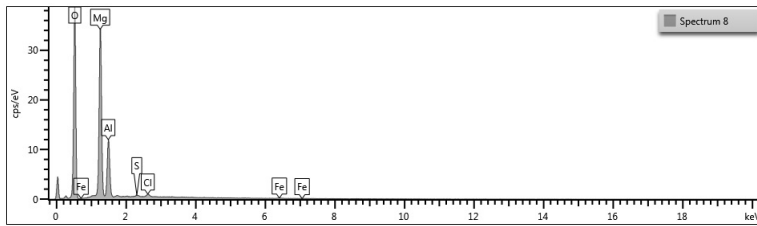
# Appendix I

# Risk Assessment

| NTNU | | | | Utarbeidet av | Nummer | Dato |
|---|---|---|---|---|---|---|
| | | | | HMS-avd. | HMSRV2601 | 22.03.2011 |
| | | Kartlegging av risikofylt aktivitet | | Godkjent av | | Erstatter |
| HMS | | | | Rektor | | 01.12.2006 |

**Enhet: IPM**

**Linjeleder: Torgeir Welo**

**Deltakere ved kartleggingen (m/ funksjon): Håvard Wilson, Student**
*(Ansv. veileder, student, evt. medveiledere, evt. andre m. kompetanse)*

**Kort beskrivelse av hovedaktivitet/hovedprosess:** Masteroppgave student Håvard Wilson. Termisk sprøytet aluminium for subsea varmeveksler overflater

**Er oppgaven rent teoretisk?** (JA/NEI): **Nei**     «JA» betyr at veileder innestår for at oppgaven ikke inneholder noen aktiviteter som krever risikovurdering. Dersom «JA»: Beskriv kort aktiviteten i kartleggingskjemaet under. Risikovurdering trenger ikke å fylles ut.

**Dato: 15.01.14**

**Signaturer:**     Ansvarlig veileder:     Student: Håvard Wilson

| ID nr. | Aktivitet/prosess | Ansvarlig | Eksisterende dokumentasjon | Eksisterende sikringstiltak | Lov, forskrift o.l. | Kommentar |
|---|---|---|---|---|---|---|
| 1 | Oppstart nye forsøk | Håvard | NTNU-Interne dokument HMS-utfordringer Arbeidsplass-Ergonomi | Verneustyr, brannslukkings aparat | Forskrift om organisering, ledelse og medvirkning. Kap. 15 – bruk av personlig verneustyr. | |
| 2 | Håndtere prøveoppsett (Rengjøre anode, justere ledning ol.) | Håvard | NTNU-Interne dokument HMS-utfordringer Varmtarbeid, støy | Verneustyr, brannslukkings aparat | Forskrift om utførelse av arbeid, bruk av arbeidsutstyr. Kap 5. Varmtarbeid | |
| 3 | Kjøre forsøk | Håvard | NTNU-Interne dokument HMS-utfordringer Varmtarbeid, støy | Verneustyr, brannslukkings aparat | Forskrift om tiltak og grenseverdier. Kap. 2 Støy | |
| 4 | Avslutte forsøk | Håvard | NTNU-Interne dokument HMS-utfordringer Elektrisk anlegg og ustyr | Verneustyr, brannslukkings aparat | Forskrift om utførelse av arbeid Kap. 14 | |
| | | | | | | |
| | | | | | | |
| | | | | | | |

**Enhet: IPM**

**Dato: 15.01.14**

**Linjeleder: Torgeir Welo**

**Deltakere ved kartleggingen (m/ funksjon): Håvard Wilson, Student**
(Ansv. Veileder, student, evt. medveiledere, evt. andre m. kompetanse)

**Risikovurderingen gjelder hovedaktivitet:** Masteroppgave student Håvard Wilson. Termisk sprøytet aluminium for subsea varmeveksler overflater

**Signaturer:** Ansvarlig veileder: _(signatur)_    Student: _Håvard Wilson_

| ID nr | Aktivitet fra kartleggings-skjemaet | Mulig uønsket hendelse/ belastning | Vurdering av sannsyn-lighet (1-5) | Vurdering av konsekvens: | | | | Risiko-Verdi (menn-eske) | Kommentarer/status Forslag til tiltak |
|---|---|---|---|---|---|---|---|---|---|
| | | | | Menneske (A-E) | Ytre miljø (A-E) | Øk/ materiel l (A-E) | Om-dømme (A-E) | | |
| 1 | Oppstart nye forsøk | Søle/komme i kontakt med varm olje | 3 | C | A | B | B | 4B | Verneustyr: Labfrakk, hansker |
| | | Kuttskader på skarpekante | 3 | B | A | A | A | 3B | Verneustyr: Hansker |
| | | Klemmeskade | 3 | A | A | A | A | 3A | |
| | | Støy- belastning, fra div ustyr på lab | 4 | A | A | A | A | 4A | Verneustyr: Hørselsvern |
| 2 | Håndtere prøveoppsett (Rengjøre anode, justere ledning ol.) | Velte tank med prøver | 3 | - | A | D | C | - | |
| | | Velte prøver i tanken | 3 | - | A | C | B | - | |
| 3 | Kjøre forsøk | Oversvømmelse av av sjøvann inn i prøver | 3 | - | - | C | B | - | Designe oppsett hvor dette ikke er mulig |
| | | Brann i elektriskustyr | 1 | D | B | C | B | 1D | Oppbevare slukkeustyr i nærheten |
| 4 | Avslutte forsøk | Skade prøver ved demontering | 2 | - | - | C | - | - | |
| | | Søle/komme i kontakt med varm olje | 3 | C | A | B | B | 4B | Verneustyr: Labfrakk, hansker |

# NTNU

**HMS**

# Risikovurdering

| Utarbeidet av | Nummer | Dato |
|---|---|---|
| HMS-avd. | HMSRV2601 | 22.03.2011 |
| Godkjent av | | Erstatter |
| Rektor | | 01.12.2006 |

# Risikovurdering

## Sannsynlighet vurderes etter følgende kriterier:

| Svært liten 1 | Liten 2 | Middels 3 | Stor 4 | Svært stor 5 |
|---|---|---|---|---|
| 1 gang pr 50 år eller sjeldnere | 1 gang pr 10 år eller sjeldnere | 1 gang pr år eller sjeldnere | 1 gang pr måned eller sjeldnere | Skjer ukentlig |

## Konsekvens vurderes etter følgende kriterier:

| Gradering | Menneske | Ytre miljø Vann, jord og luft | Øk/materiell | Omdømme |
|---|---|---|---|---|
| E Svært Alvorlig | Død | Svært langvarig og ikke reversibel skade | Drifts- eller aktivitetsstans >1 år. | Troverdighet og respekt betydelig og varig svekket |
| D Alvorlig | Alvorlig personskade. Mulig uførhet. | Langvarig skade. Lang restitusjonstid | Driftsstans > ½ år Aktivitetsstans i opp til 1 år | Troverdighet og respekt betydelig svekket |
| C Moderat | Alvorlig personskade. | Mindre skade og lang restitusjonstid | Drifts- eller aktivitetsstans < 1 mnd | Troverdighet og respekt svekket |
| B Liten | Skade som krever medisinsk behandling | Mindre skade og kort restitusjonstid | Drifts- eller aktivitetsstans < 1 uke | Negativ påvirkning på troverdighet og respekt |
| A Svært liten | Skade som krever førstehjelp | Ubetydelig skade og kort restitusjonstid | Drifts- eller aktivitetsstans < 1 dag | Liten påvirkning på troverdighet og respekt |

**Risikoverdi = Sannsynlighet x Konsekvens**
Beregn risikoverdi for Menneske. Enheten vurderer selv om de i tillegg vil beregne risikoverdi for Ytre miljø, Økonomi/materiell og Omdømme. I så fall beregnes disse hver for seg.

**Til kolonnen "Kommentarer/status, forslag til forebyggende og korrigerende tiltak":**
Tiltak kan påvirke både sannsynlighet og konsekvens. Prioriter tiltak som kan forhindre at hendelsen inntreffer, dvs. sannsynlighetsreduserende tiltak foran skjerpet beredskap, dvs. konsekvensreduserende tiltak.

| NTNU | | | utarbeidet av | Nummer | Dato |
|---|---|---|---|---|---|
| | | Risikomatrise | HMS-avd. | HMSRV2604 | 08.03.2010 |
| ◻ | | | godkjent av | Erstatter | 09.02.2010 |
| HMS/KS | | | Rektor | | |

# MATRISE FOR RISIKOVURDERINGER ved NTNU

| KONSEKVENS | | Svært liten | Liten | Middels | Stor | Svært stor |
|---|---|---|---|---|---|---|
| | Svært alvorlig | E1 | E2 | E3 | E4 | E5 |
| | Alvorlig | D1 | D2 | D3 | D4 | D5 |
| | Moderat | C1 | C2 | C3 | C4 | C5 |
| | Liten | B1 | B2 | B3 | B4 | B5 |
| | Svært liten | A1 | A2 | A3 | A4 | A5 |
| | | Svært liten | Liten | Middels | Stor | Svært stor |
| | | SANNSYNLIGHET | | | | |

**Prinsipp over akseptkriterium. Forklaring av fargene som er brukt i risikomatrisen.**

| Farge | | Beskrivelse |
|---|---|---|
| Rød | | Uakseptabel risiko. Tiltak skal gjennomføres for å redusere risikoen. |
| Gul | | Vurderingsområde. Tiltak skal vurderes. |
| Grønn | | Akseptabel risiko. Tiltak kan vurderes ut fra andre hensyn. |